AN AUTONOMOUS LONG-TERM FAST REACTOR SYSTEM

AND THE PRINCIPAL DESIGN LIMITATIONS OF THE CONCEPT

A Dissertation

by

GALINA VALERYEVNA TSVETKOVA

Submitted to the Office of Graduate Studies of
Texas A&M University
in partial fulfillment of the requirements for the degree of

DOCTOR OF PHILOSOPHY

December 2003

Major Subject: Nuclear Engineering

AN AUTONOMOUS LONG-TERM FAST REACTOR SYSTEM

AND THE PRINCIPAL DESIGN LIMITATIONS OF THE CONCEPT

A Dissertation

by

GALINA VALERYEVNA TSVETKOVA

Submitted to Texas A&M University
in partial fulfillment of the requirements
for the degree of

DOCTOR OF PHILOSOPHY

Approved as to style and content by:

Kenneth L. Peddicord (Chair of Committee)	Yassin A. Hassan (Member)
G. Donald Allen (Member)	Paul Nelson (Member)
	William E. Burchill (Head of Department)

December 2003

Major Subject: Nuclear Engineering

ABSTRACT

An Autonomous Long-Term Fast Reactor System

and the Principal Design Limitations of the Concept. (December 2003)

Galina Valeryevna Tsvetkova, Dipl., Moscow State Engineering Physics Institute,Russia

Chair of Advisory Committee: Dr. Kenneth L. Peddicord

The objectives of this dissertation were to find a principal domain of promising and technologically feasible reactor physics characteristics for a multi-purpose, modular-sized, lead-cooled, fast neutron spectrum reactor fueled with an advanced uranium-transuranic-nitride fuel and to determine the principal limitations for the design of an autonomous long-term multi-purpose fast reactor (ALM-FR) within the principal reactor physics characteristic domain. The objectives were accomplished by producing a conceptual design for an ALM-FR and by analysis of the potential ALM-FR performance characteristics.

The ALM-FR design developed in this dissertation is based on the concept of a secure transportable autonomous reactor for hydrogen production (STAR-H2) and represents further refinement of the STAR-H2 concept towards an economical, proliferation-resistant, sustainable, multi-purpose nuclear energy system. The development of the ALM-FR design has been performed considering this reactor within the frame of the concept of a self-consistent nuclear energy system (SCNES) that satisfies virtually all of the requirements for future nuclear energy systems: efficient energy production, safety, self-feeding, non-proliferation, and radionuclide burning.

The analysis takes into consideration a wide range of reactor design aspects including selection of technologically feasible fuels and structural materials, core configuration optimization, dynamics and safety of long-term operation on one fuel loading, and nuclear material non-proliferation. Plutonium and higher actinides are considered as essential components of an advanced fuel that maintains long-term operation. Flexibility of the ALM-FR with respect to fuel compositions is demonstrated acknowledging the principal limitations of the long-term burning of plutonium and higher actinides. To ensure consistency and accuracy, the modeling has been performed using state-of-the-art computer codes developed at Argonne National Laboratory.

As a result of the computational analysis performed in this work, the ALM-FR design provides for the possibility of continuous operation during about 40 years on one fuel loading containing mixture of depleted uranium with plutonium and higher actinides. All reactor physics characteristics of the ALM-FR are kept within technological limits ensuring safety of ultra-long autonomous operation. The results obtained provide for identification of physical features of the ALM-FR that significantly influence flexibility of the design and its applications. The special emphasis is given to existing limitations on the utilization of higher actinides as a fuel component.

"Every day you may make progress. Every step may be fruitful. Yet, there will stretch out before you an ever-lengthening, ever-ascending, ever-improving path. You know you will never get to the end of the journey. But this, so far from discouraging, only adds to the joy and glory of the climb".

Sir Winston Churchill (1874 - 1965).

ACKNOWLEDGMENTS

I would like to express my deepest thanks to my advisor, Dr. Kenneth L. Peddicord, for his encouragement, provided opportunities and for the unique atmosphere of scientific freedom he established. I would further like to thank Drs. G. Donald Allen, Yassin A. Hassan, and Paul Nelson for serving on my committee and providing insight.

I acknowledge the financial support of my research, which resulted in this dissertation, by the US Department of Energy as part of the collaborative Nuclear Energy Research Initiative (NERI) STAR-H2 project between Argonne National Laboratory and Texas A&M University. I am grateful for the technical advice received in consultations and discussions with Drs. David C. Wade, John A. Stillman, W. S. Yang, and Jim J. Sienicki of Argonne National Laboratory on the various aspects of the STAR-H2 design and fast reactor modeling.

I would like to express my gratitude to Drs. Marvin L. Adams, Dmitriy Y. Anistratov, Frederick R. Best, Ron R. Hart, Yassin A. Hassan, Paul Nelson, Alexander G. Parlos, W. Dan Reece, and Alan E. Waltar of the Department of Nuclear Engineering, and to Drs. G. Donald Allen and Joseph E. Pasciak of the Department of Mathematics, Texas A&M University, for their contributions to my scientific education. I would like to thank all of my colleagues at the Department of Nuclear Engineering, Texas A&M University, who have contributed to the realization of this dissertation.

Finally, I would like to extend my warmest appreciation to my family. Without the love, understanding, support, and tolerance of my parents and my husband, Pavel, this work would not have been possible and would have never been completed.

NOMENCLATURE

ADS	Accelerator-Driven System
ALM-FR	Autonomous Long-term Multi-purpose Fast Reactor
BWR	Boiling Water Reactor
BOC	Beginning Of Cycle
BOL	Beginning Of Life
1D, 2D, 3D	One Dimensional, Two Dimensional, Three Dimensional
DOE	US Department of Energy
ENHS	Encapsulated Nuclear Heat Source
EOC	End Of Cycle
EOL	End Of Life
HEU	Highly Enriched Uranium
HM	Heavy Metal composition
HTGR	High Temperature Gas-cooled Reactor
LEU	Low-Enriched Uranium
LM	Liquid Metal
LMFBR	Liquid Metal-cooled Fast Breeder Reactor
LWR	Light Water Reactor
MA	Minor Actinides
MOX	Mixed OXide
MSR	Molten-Salt Reactors
NERI	Nuclear Energy Research Initiative

PWR	Pressurized Water Reactor
RGPu	Reactor-Grade Plutonium
SCNES	Self-Consistent Nuclear Energy System
STAR	Secure Transportable Autonomous Reactor
STAR-H2	Secure Transportable Autonomous Reactor for Hydrogen production
STAR-LM	Secure Transportable Autonomous Reactor with Liquid Metal coolant
TRU	Trans-Uranium Composition
WGPu	Weapon-Grade Plutonium

TABLE OF CONTENTS

LIST OF FIGURES

FIGURE Page

FIGURE Page

LIST OF TABLES

CHAPTER I

INTRODUCTION

Because of the growing world's power needs, new systems for energy production are being discussed worldwide. The major task for energy research and development is to find environmentally and economically acceptable ways to make a transition away from the scarce primary fuels like natural gas and petroleum. Despite the great promise of solar, geothermal, and fusion power, only nuclear fission energy and coal can be relied upon to make the above mentioned transition possible and to supply energy in the quantities needed.[1] Furthermore, only a technology which is based on a nuclear reactor offers a way for the conservation of the biosphere of the Earth, as it does not release green houses gasses. Nuclear power can in fact be considered as a unique energy source suitable for utilization even in countries with developing economies.

However, public acceptance of nuclear technology is an essential issue that complicates future development. In order to be accepted by the general public, a new nuclear reactor concept must demonstrate efficient energy production, system safety, proliferation resistance, the availability of a renewable fuel supply, and operation with minimized waste materials production.

Promising existing nuclear reactor concepts together with new ideas are being discussed worldwide. Many new studies are underway in order to identify prototypes that will be analyzed and developed further as Generation IV systems.[2-4] The focus is on designs demonstrating full inherent safety, competitive economics, and satisfactory

---

This dissertation follows the style and format of *Nuclear Science and Engineering*.

proliferation resistance.[5]

Several types of nuclear power reactors are potentially expected to play major roles in nuclear power generation of the 21st century - Pressurized Water Reactors (PWR), Boiling Water Reactors (BWR), High Temperature Gas-cooled Reactors (HTGR), Liquid Metal-cooled Fast Breeder Reactors (LMFBR), Molten-Salt Reactors (MSR) and, perhaps, some other recently suggested innovative systems. This dissertation is focused on a multi-purpose, modular-sized, lead-cooled, fast neutron spectrum reactor fueled with an advanced uranium-transuranic-nitride fuel. The developed design is based on the concept of a secure transportable autonomous reactor for hydrogen production (STAR-H2) and represents further refinement of the STAR-H2 concept towards an economical, proliferation-resistant, sustainable, multi-purpose nuclear energy system.

The design development of an autonomous long-term multi-purpose fast reactor (ALM-FR) has been performed considering the reactor within the frame of the concept of a self-consistent nuclear energy system (SCNES) that satisfies virtually all of the requirements for future nuclear energy systems: efficient energy production, safety, self-feeding, non-proliferation, and radionuclide burning. This chapter gives an overview of the SCNES concept. The objectives and outline of the dissertation are then presented in the context of the preceding overview.

I.A. Multi-Purpose Self-Consistent Nuclear Energy System

An expanded nuclear technology development presumes that this technology will be able to satisfy growing energy needs during many decades ahead. Although natural

resources of nuclear fuel components are also limited,[1,6] in contrast with the scarce primary fuels like natural gas and petroleum, nuclear technology carries the solution for the problem. New nuclear fuel components, plutonium and higher actinides, are produced during reactor operation. These new materials could be considered as components of advanced fuels. In order to have ability to utilize plutonium and higher actinides as components of an advanced actinide fuel, they have to be extracted from the unloaded spent fuel irradiated in existing conventional nuclear reactors.

In a reactor which operates for some time various isotopes of uranium, neptunium, plutonium, as well as of the heavier elements such as americium and curium may accumulate. In addition, the spent fuel will contain a large amount of various fission products. “Traditional” recycle approaches presume actinide recycle in the conventional closed fuel cycle by reprocessing of spent fuel from PWR’s and BWR’s. In this approach, recovered minor actinides (MA) (Np, Am, Cm) are treated and stored as a high level waste. They constitute the most undesirable long-term radiotoxicity. According to the study of the MA inventories in spent fuel of LWR’s, the drastic increase of Am and Cm inventories are observed after uranium fuel irradiation and the second recycling of MOX fuel.[1] Therefore, partitioning and transmutation of the recovered MA’s could significantly reduce the long-term radiotoxicity.[7] According to the global fuel cycle analysis, this approach is technologically complex but it seems to be an appropriate waste management strategy as it provides additional fuel supply and incinerates hazardous nuclides.[8,9]

It is anticipated that efficient utilization of plutonium and higher actinides in reactor systems will have positive impact on the global nuclear fuel cycle since it

provides the long-term utilization of MA's. Principal achievability of a deep burnup level in thermal and fast reactors fueled with plutonium and MA's has been demonstrated theoretically in several studies worldwide.[10] However, it has to be acknowledged that extraction of Pu and MA's, especially from MOX fuel, is technologically difficult and has some limitations from reprocessing point of view.[8,9] The nuclear fuel cycles used today are the result of four decades of technological development. Many decisions made at that time still affect the fuel cycle industry today. Consequently, expanded utilization of MA's as components for advanced actinide fuels will require significant improvements and advances in fuel cycle technologies.

Based on the inherent capabilities of fuel material breeding and waste material incineration, the SCNES concept has been suggested as a next step of the nuclear technology development.[11,12] As originally proposed, the "ultimate" SCNES should be composed of fast reactors, probably LMFBR's, and special facilities for fission product separation. To eliminate fission product separation, an additional fission source is required. Accelerator-driven systems (ADS) and fusion neutron sources are envisioned as the possible candidates. Since the "ultimate" SCNES is far away in the future, a multi-component predecessor has been suggested as an intermediate solution. Taking into account domination of LWR's worldwide, the multi-component pre-SCNES is represented by a virtual tandem of thermal reactors (PWR or BWR) and fast reactors (LMFBR). The accumulated MA's from spent fuel of LWR's can be separated and used as components for fuel loadings of LMFBR's. The LWR-LMFBR tandem system allows confining MA's within a closed fuel cycle. As a result, the long-term radiotoxicity problem due to MA's is suppressed. The following tandem system is a close-to-SCNES

example: 50 GW LWR with a breeding ratio of 0.6 and 50 GW LMFBR with a breeding ratio of 1.4.[11] Recognizing the ultimate importance of sustainable nuclear technology development and its inherent potential for unlimited self-feeding leading to self-consistency, many other concepts of a multi-component SCNES predecessor are under discussion worldwide.

Liquid-metal-cooled fast reactors are uniquely suitable for application as components of the SCNES predecessor. Their inherent low sensitivity to fission product poisoning and the possibility of designing a fast core with internal breeding are the unique features that allow achieving long-term operation with minimal or no reactivity loss. Therefore, the long-term breeding and burning of plutonium and higher actinides can be accomplished in LMFBR's, making these nuclear weapons and high level waste materials a very efficient advanced actinide fuel that is also completely artificial and can be easily reproduced maintaining unlimited self-feeding. Thus, LMFBR's possess many features of the "ultimate" SCNES.

The STAR-H2 concept is one of the promising LMFBR concepts that already offers many features of the "ultimate" SCNES and can be chosen at least as a basis component of the SCNES predecessor.[13,14] The postulated design targets of the STAR-H2 concept as a sustainable energy source are secure longevity, ecological compatibility, and social acceptability. It is a lead-cooled, fast spectrum, uranium-transuranic-nitride-fueled, modular fast reactor intended for the mid-end 21st century global economics, in which electricity and hydrogen are expected to serve as complementary energy carriers provided by nuclear energy as sustainable energy source. The STAR-H2 project is oriented for worldwide deployment and specifically addresses the needs of developing

countries for economical, proliferation-resistant, sustainable, multi-purpose energy system designed as a source of electricity and nuclear heat for hydrogen production.[14]

The work presented in this dissertation is focused on the ALM-FR design based on the STAR-H2 concept. The ALM-FR design differs from the original STAR-H2 concept by the postulated design requirement to provide fully autonomous, sustainable operation during the entire reactor lifetime instead of the STAR-H2 15-years refueling interval. The reactor lifetime long operation without refueling provides self-consistency in a single sealed reactor unit and allows to mitigate technical challenges associated with the STAR-H2 refueling operations. The ALM-FR design development and the targeted features of the ALM-FR design are aimed to achieve the ultra-long operation, which equals to the entire reactor lifetime, without need for intermediate core reloading or refueling. It is presumed that the design has to utilize the most advanced materials known and technologically available.

The dissertation presents a detailed analysis of the possibility of a long-term operation on one fuel loading through utilization of plutonium and higher actinides in the ALM-FR core. The analysis takes into consideration a wide range of reactor design aspects including selection of technologically feasible fuels and structural materials, core configuration optimization, dynamics and safety of long-term operation on one fuel loading, nuclear material non-proliferation. Flexibility of the ALM-FR with respect to fuel compositions is demonstrated acknowledging the principal limitations of the long-term burning of plutonium and higher actinides. The technological challenges and further research are outlined. The results allow the identification of physical features of the ALM-FR that significantly influence flexibility of the design and its applications.

I.B. Objectives of This Dissertation

The proposed innovative nuclear reactor is envisioned as an ALM-FR system that offers potential possibility for an autonomous long-term operation with minimized human action required. Plutonium and higher actinides are considered as essential components of an advanced fuel that maintain long-term operation on one fuel loading.

The objectives of this dissertation are to find a principal domain of promising and technologically feasible reactor physics characteristics for a multi-purpose, modular-sized, lead-cooled, fast neutron spectrum reactor fueled with an advanced uranium-transuranic-nitride fuel and to determine the principal limitations for the ALM-FR design within the found principal reactor physics characteristic domain. This comprises the conceptual development of an ALM-FR and an analysis of potential performance characteristics.

The emphasis is on a wide range of reactor design aspects including selection of technologically feasible fuels and structural materials, core configuration optimization, dynamics and safety of long-term operation on one fuel loading, nuclear material non-proliferation.

The general goals of the outlined research effort lead to several targets for the computational study:

- Global fuel cycle overview including waste management strategies under consideration worldwide and existing possibilities for actinide recycle and transmutation in the conventional closed fuel cycles.

- Conceptual development of an ALM-FR design that utilizes plutonium and higher actinides as advanced fuel components, and provides fully autonomous, sustainable operation during the entire reactor lifetime.
- Technological feasibility analysis of advanced actinide fuels and structural materials for the ALM-FR concept.
- Development of the general strategy of the ALM-FR design analysis and specific computational schemes that allow consistent modeling using sophisticated computer codes and modern nuclear data applicable for realistic representation of the processes governing ALM-FR performance.
- Reactor physics analysis of the ALM-FR configurations with different fuel compositions and structural materials, and configuration optimization of the ALM-FR core.
- Analysis of achievability of ultra-long operation utilizing plutonium and minor actinides in the ALM-FR core.
- Analysis of dynamics and safety characteristics of the ALM-FR design under conditions of long-term operation on one fuel loading.
- Analysis of the proliferation-resistance characteristics of the ALM-FR design under conditions of long-term operation on one fuel loading.
- Analysis of the engineering issues and principal limitations of the autonomous long-term operation utilizing plutonium and higher actinides.

The analysis of the ALM-FR performance should emphasize advantages of the concept and identify features that significantly influence flexibility of the design as an autonomous long-term reactor with plutonium and higher actinides as fuel components.

I.C. Outline of This Dissertation

This dissertation deals with innovative nuclear energy concepts, and more particularly, with a lead-cooled, fast spectrum, modular fast reactor that utilizes an advanced fuel containing plutonium and minor actinides. The emphasis is on the fully autonomous, sustainable operation during the entire reactor lifetime. The primary goal of the analysis is to determine feasibility of the ALM-FR concept and identify physical features of the ALM-FR that significantly influence flexibility of the design and its applications.

Computational analysis of the ALM-FR design is performed using modern state-of-the art computer codes and nuclear data developed at Argonne National Laboratory that allow realistic and comprehensive modeling of the important physical processes governing system behavior during long-term reactor operation. Results of the analysis describe a wide range of reactor design aspects including selection of technologically feasible fuels and structural materials, core configuration optimization, dynamics and safety of long-term operation on one fuel loading, nuclear material non-proliferation.

The research work described in this dissertation is focused on the following aspects of the ALM-FR concept:

- Conceptual development of an ALM-FR design and identification of its potential application areas;
- General strategy of the ALM-FR design development;
- Computational modeling of the ALM-FR design characteristics;
- Selection of reactor core materials for the ALM-FR design;

- Configuration optimization of the ALM-FR core;
- Dynamics and safety of the ALM-FR design;
- Plutonium and minor actinides in the ALM-FR as a possibility to maintain ultra-long operation;
- Proliferation-resistance of the ALM-FR design.

The dissertation is composed of eight chapters and two appendices that are outlined below.

Chapter I provides an overview of the multi-purpose SCNES concept and the nuclear technology development philosophy associated with it. It introduces both the original STAR-H2 concept and the ALM-FR design based on the STAR-H2 concept in the perspective of the SCNES.

Chapter II introduces and discusses the STAR concept, family of STAR power plant designs, and fundamental features that characterize the ALM-FR design and its potential application areas. Technological feasibility of advanced actinide fuels and structural materials for the ALM-FR concept is analyzed taking into account the current state of the nuclear technology worldwide.

Chapter III describes the general strategy of the ALM-FR design development as it has been applied in the research work described in this dissertation. It also describes the computational schemes and detailed 3D models of the ALM-FR. Descriptions are presented with special emphasis on the applied computer codes.

Chapter IV presents the reactor physics analysis of the ALM-FR configurations with different fuel compositions and structural materials. The obtained results have been used as a basis for selection of reactor core materials for the developed ALM-FR design.

Chapter V presents the results of the ALM-FR core configuration optimization analysis. The set of optimization studies have been performed in order to identify the reactor core configurations allowing autonomous long-term operation on one fuel loading.

Chapter VI presents analysis of dynamics and safety characteristics of the ALM-FR design under conditions of long-term operation on one fuel loading.

Chapter VII discusses achievability of ultra-long operation utilizing plutonium and minor actinides in the ALM-FR core. Proliferation-resistance characteristics of the ALM-FR design are examined under conditions of long-term operation on one fuel loading. Flexibility of the ALM-FR with respect to fuel compositions is demonstrated acknowledging the principal limitations of the long-term burning of plutonium and minor actinides. This chapter completes the computational analysis of the ALM-FR.

Chapter VIII presents the conclusions of the study. In this chapter, the determined principal domain of promising and technologically feasible ALM-FR characteristics is presented together with characteristics of the developed ALM-FR design. The summarizing discussion emphasizes limitations for the ALM-FR design within the found principal reactor physics characteristic domain. The results allow identification of physical features of the ALM-FR that significantly influence flexibility of the design and its applications. Special emphasis is given to existing limitations on utilization of higher actinides as a fuel component.

At the end of this dissertation, two appendices are included that provide specific details of the computational modeling.

CHAPTER II

AUTONOMOUS LONG-TERM MULTI-PURPOSE FAST REACTOR AND ITS POTENTIAL APPLICATION AREAS

Chapter II provides a general analysis of the STAR concept, the family of STAR power plant designs, and the fundamental features that characterize the ALM-FR design. It focuses on technological feasibility aspects and the potential application areas of ALM-FR's. Technological feasibility of advanced actinide fuels and structural materials for the ALM-FR concept is discussed taking into account the current state of the nuclear technology worldwide.

II.A. Concept of a Secure Transportable Autonomous Reactor

The electricity consumption share in the overall power balance is steadily growing worldwide and, according to IAEA predictions, will reach the level of about 40% by 2015.[15] The remaining power consumption is domestic and industrial heat, as well as transportation. It is expected that an increase in power consumption worldwide will be for the most part determined by developing countries. According to IAEA estimates, electric power consumption in Africa, Latin America, South East Asia, Middle East and South Asia will increase by 250-300% in 2000-2030.[15,16]

To maintain a sufficient supply, humankind has created large systems that form a partially globalized infrastructure for production and supply of electric power, mining and transportation of gas, oil and coal. These large systems are now the basis of

economy of developed countries in Northern America and in Europe.[16,17] Prices and volumes of mining, and the projected consumption levels of power resources are currently established worldwide on the basis of requirements and features of the existing large systems.[18] It is recognized that for developing countries it will be rather difficult, if not impossible, to build similar diversified power supply systems, especially in a view of the great amount of investments required by large power systems.[19]

Contributions of various power technologies to power production and the world power balance determine dynamics of basic power technologies. Forecasts usually assume conservatively that power generation will be doubled by the mid-21st century.[15,16,19] Fossil fuels (coal, oil, gas), nuclear energy and solar energy are considered as the main competing primary power resources.

Availability and accessibility of fuel resources and environmental impact determine dynamics of each of the power technologies and its role in the world power balance. Eventually this reduces to acceptability of one or another power resource in terms of economics.

Although a comparison of fossil fuel power resources, power consumption and its current and projected growth rates in the 21st century does not lead to an immediate concern, it is anticipated that depletion of oil and gas deposits will necessitate an increase in the use of coal even in the 21st century.[15,16,19] On the contrary, estimated deposits of nuclear fuel in the earth's crust and ocean waters, even based on conservative assumptions about possible extraction of these materials, suggest that the use of nuclear power on any scale will not encounter resource constraints over an observable period of time.[15,19]

Global warming is thought to be associated with the greenhouse effect due to discharge of combustion gases. This is one of the fundamental limitations on the growth of power production through burning of fossil fuels. Nuclear power does not directly contribute to the greenhouse effect and is characterized by technically feasible possibility to concentrate, localize and isolate the associated radioactive wastes. The overall mass of nuclear wastes is millions times lower than the mass of wastes produced from burning fossil fuels.[15,16]

Thus, virtually limitless nuclear fuel resources, high energy capacity, compactness of waste, environmental compatibility, availability of demonstrated technologies, safety and potential of economic competitiveness make nuclear power a favorite among the basic power technologies mentioned above. One of the greatest concerns associated with nuclear power is the hazard of nuclear weapon proliferation. To assure sustainable and expanding nuclear technology development worldwide, it is vitally important that the suggested new nuclear power systems, process flows, fuel cycle facilities, and fuel forms incorporate inherent non-proliferation features and eliminate the hazard of nuclear weapon proliferation.

The use of nuclear power creates new avenues for development of the power industry worldwide. Nuclear power systems can meet demands of the developing countries and regions that lack heavy-duty power grids, highly developed industrial infrastructure, and economic resources.

The Secure Transportable Autonomous Reactor (STAR) is a new nuclear reactor concept that has been proposed for meeting the needs of developing countries for small, economical nuclear power systems while at the same time addressing proliferation

concerns.[13,14,20] The STAR systems are based on the "safety-by-design" philosophy of nuclear reactor development, implementation and operation (inherent physical prevention of accidents from occurring rather than dealing with, by active or passive means, with their consequences). Candidate STAR plants must be inherently safe and must be able to operate autonomously with minimal reliance on active control for load adjustment and burnup reactivity compensation. The STAR approach for increasing capability of autonomous operation is founded on inherent mechanical, thermodynamic, and neutronics characteristics which are determined by the applied materials, their arrangement and the overall reactor system design.

The most important features of these systems are simplified active control and safety protection mechanisms; minimized reliance on on-site operating staff; and assurance of high levels of operational safety, reliability, and facility security. Due to the assumed orientation on operational environment of developing countries and remote unpopulated regions, the STAR designs should allow implementation of simplified control strategies based on the passive plant response and computer-based technologies for remote monitoring of operation and safeguard from centralized surveillance facilities.

Because of the features discussed above, the STAR systems have the following competitive advantages:

- Autonomous, self-regulated operation with prolonged refueling intervals;
- Absence of radioactive releases under any accidental situations;
- Minimized operating personnel and required support facilities;
- Modularity.

II.B. Family of STAR Power Plant Designs

As a result of the detailed analysis performed by the Generation IV International Forum, the six nuclear reactor designs have been identified as the most promising candidates to be considered and developed further as next-generation nuclear energy systems.[21] All of the suggested systems are evolutionary designs and are based on the preceding extensive research and development efforts worldwide.

It has been recognized that the sodium-cooled LMFBR system is the most developed design among the selected Generation IV systems due to extensive development and successful operation experience in Russia and in France. The supercritical water-cooled reactor system is an innovative LWR design based on the existing fossil power plant technology. The very high temperature gas-cooled reactor system is intended for economic hydrogen production and is entirely based on the extensively developed HTGR technology. The lead-cooled LMFBR offers achievability of a very fast neutron spectrum that is required for efficient actinide utilization. The concept is based on the sodium-cooled LMFBR technology and the existing experience with use of lead as a coolant. The molten-salt reactor and gas-cooled fast reactor designs have been selected for their very promising performance characteristics. However many significant aspects of both designs will have to be developed including the engineering system designs, processing technologies, and the fuel cycle technology.

Although all of the selected Generation IV systems have potential and can be developed as the STAR systems, the greatest promise have those concepts that have strong reactivity feedback effects, minimized reactivity losses due to burnup, and offer

possibility to maintain natural circulation of a primary coolant within a reactor core. As emphasized above, this dissertation is focused on the design development of the STAR system that is based on the lead-cooled LMFBR concept.

The lead-cooled LMFBR system is uniquely suitable for further consideration and development within the frame of the STAR concept. The inherent low sensitivity to fission product poisoning and possibility of designing a fast core with internal breeding are the unique features that allow achieving long-term operation with minimal or no reactivity loss. The following advantages of these reactor systems have to be emphasized as they represent features required within the frame of the STAR concept:

- High discharge burnup levels (up to 150,000MWd/tonne);
- Achievability of long refueling intervals;
- Self-regulation capability due to internal breeding;
- Inherent safety due to strong reactivity feedback effects.

Because of the very promising characteristics, several STAR systems have been suggested and are under development on the basis of lead-bismuth-cooled and lead-cooled LMFBR concepts. The family of STAR power plant designs consists of the following LMFBR systems:

- Encapsulated Nuclear Heat Source (ENHS);[13]
- Pb-Bi–cooled Secure Transportable Autonomous Reactor (STAR-LM);[22-24]
- Pb–cooled Secure Transportable Autonomous Reactor for Hydrogen Production (STAR-H2).[14,20]

This family of the LMFBR-based STAR power plants is characterized by the following common design development goals:

- Factory-fueled core cartridge designed for off-site pre-processing and post-processing;
- Full-cartridge refueling;
- Long-term full power operation without refueling and with near-zero burnup reactivity swing;
- Lead-bismuth or lead cooling;
- 100% natural circulation for primary heat removal;
- No mechanical connections to energy conversion components;
- Autonomous load following;
- Inherent safety;
- High energy-conversion efficiency;
- Transportability.

It is anticipated that inherent feedback mechanisms will provide self-regulation with respect to reactivity changes due to burnup effects and load variations. Natural circulation offers possibility to eliminate primary pumps. As indicated above, substantial flexibility exists in the form of fuel types, core configurations, reactor material selection, primary system layouts, heat transport design, and selection of secondary-side components. The small modular nuclear power plants are designed to use factory-fueled core cartridges delivered to a plant site form centralized regional processing centers.

This dissertation is focused on the further development of the STAR-H2 system that is a lead-cooled, fast neutron spectrum, 400MW_{th} modular-sized reactor delivering electricity and heat at ~800^{o}C core outlet temperature. Significant margins exist between lead-coolant operating temperature (~800°C), its boiling temperature (~1700°C), and its

freezing temperature (~327°C). The 400MW_{th} sizing retains natural circulation capability in a rail shippable reactor vessel size and assures passive decay heat removal capabilities.

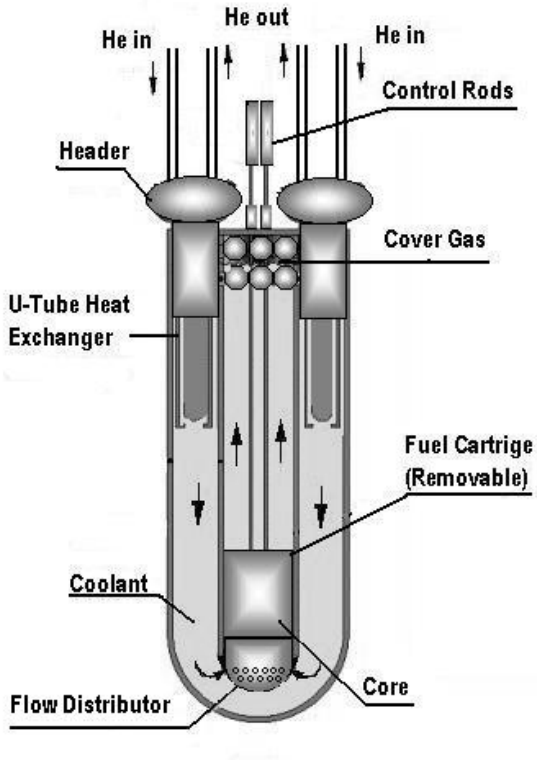

Fig. 1. Lead-cooled, fast neutron spectrum, 400MW_{th} STAR-H2 concept.

The principal STAR-H2 components and their arrangement are shown in Fig. 1. The coolant module consists of the reactor vessel with internal structures for positioning the core module and flow redistribution, U-tube lead-to-gas heat exchangers, top head penetrations for installing the core module and heat exchangers, and the auxiliary coolant purification system piping. The core module is a “flow-through” fuel cartridge

that is assembled at the factory, transported intact and installed into the coolant module at the client site. Following the core life, the used core cartridge module is removed from the vessel and is transported from the site to a secure reprocessing center.

The core cartridge module consists of the fueled core assembly, coolant inlet diffuser, steel reflector, and the core barrel. The components of the core cartridge module form the vertical natural circulation heat transport passage. Table I gives a summary of the main design characteristics of the STAR-H2 core I cartridge module.[14,20]

TABLE I

400MW_{th} STAR-H2 Core Cartridge Module Characteristics

Core Thermal Power (MW_{th})	400
Coolant	Pb
Core Diameter (m)	2.5
Active Core (Heated Zone) Height (m)	1.99
Fission Gas Plenum Height (m)	0.50
Fuel Pin Outer Diameter (cm)	1.905
Fuel Pin Triangular Pitch-to-Diameter Ratio	1.50
Cladding Thickness, (cm)	0.10
Fuel Material	(92%U-8%Pu)N
Fuel Smeared Density	0.78
Fuel Pellet Diameter (cm)	1.51
Cladding-Fuel Pellet Gap Thickness (cm)	0.0996
Gap Bond Material	Pb-Be
Number of Spacer Grids	3
Core-Wide Fuel Volume Fraction	0.252
Core-Wide Cladding Volume Fraction	0.0802
Core-Wide Bond Volume Fraction	0.0710
Core-Wide Coolant Volume Fraction	0.597
Core Fuel Mass (kg)	35300
Core Uranium Mass (kg)	33300
Core Flow Area (m^2)	2.93
Number of Fuel Pins	6940
Number of Support and Flow Distributor Plates Below Core	2
Plate Open Area Fraction	0.6
Core Coolant-to-Fuel Pin Volume Ratio	1.48
Core Specific Power of Uranium (KW/kg)	12.0
Core Power per Volume (MW/liter)	0.0409
Core Mean Heat Flux (MW/m^2)	0.483

The STAR-H2 core is a single fueled core assembly and it is not composed of removable traditional assemblies. Fuel pins are supported by grid spacers. The design characteristics of the fueled core assembly are determined by the requirements of inherent safety and criteria for achieving natural circulation heat removal and transport. Figure 2 shows components of the fueled core assembly and the corresponding axial dimensions.

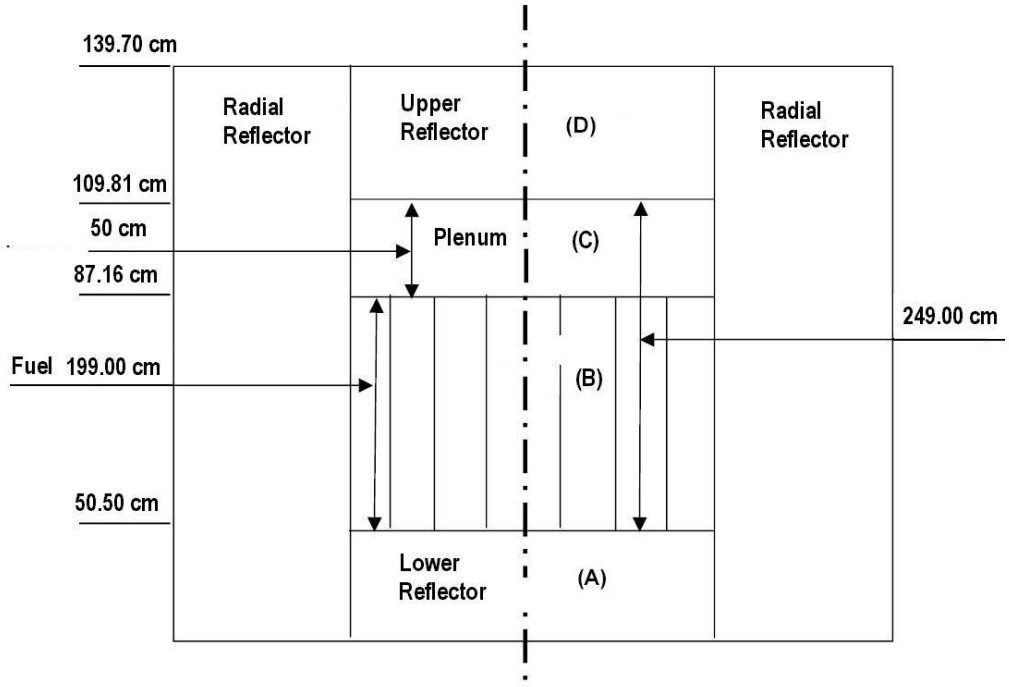

Fig. 2. Fueled core assembly of the STAR-H2 concept.

As is illustrated in Fig. 2, zone A and zone D are lower and upper reflectors formed by the surrounding lead coolant. Zone B consists of an array of fuel pins. Zone C is the fuel pin upper gas plenum. The radial reflector, which is shown in Fig. 2, is formed

by the ferritic-martensitic steel structure that surrounds the fuel pin array and prevents any access to the core internals.

The fuel pin array (zone B in Fig. 2) is formed by the non-removable hexagonal ductless fuel assemblies (pitch P1=~16.147cm, hexagon side a1=~9.3194cm). The assembly profile is schematically shown in Fig. 3.

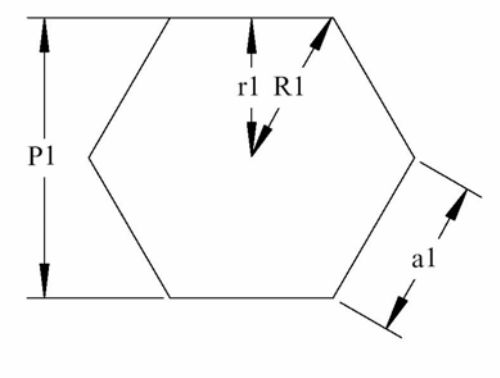

Fig. 3. Hexagonal ductless fuel assembly profile of the STAR-H2 concept.

Figure 4 shows characteristics of the triangular fuel pin lattice. It is anticipated that open pitch fuel pin lattice will help avoiding channel blockages.

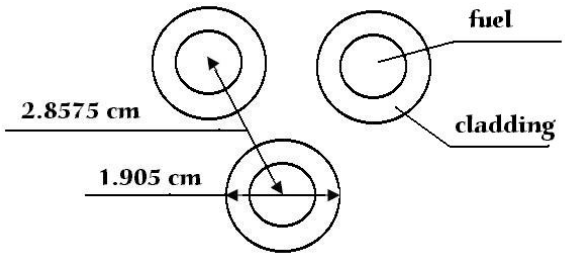

Fig. 4. Triangular fuel pin lattice of the STAR-H2 concept.

The reactor is thought to be operated on a 15-year whole core cassette-refueling interval using uranium (U) -transuranic (TRU) nitride fuel. The U-TRU-nitride fuel is compatible with lead and is expected to be pyro-recyclable and suitable for vibropac-remote fabrication. Chemical compatibility of U-TRU-nitride fuel and lead-coolant allows operation beyond cladding breach. The bond material is Pb-Bi fluid. The fuel pin design is illustrated in Fig. 5.

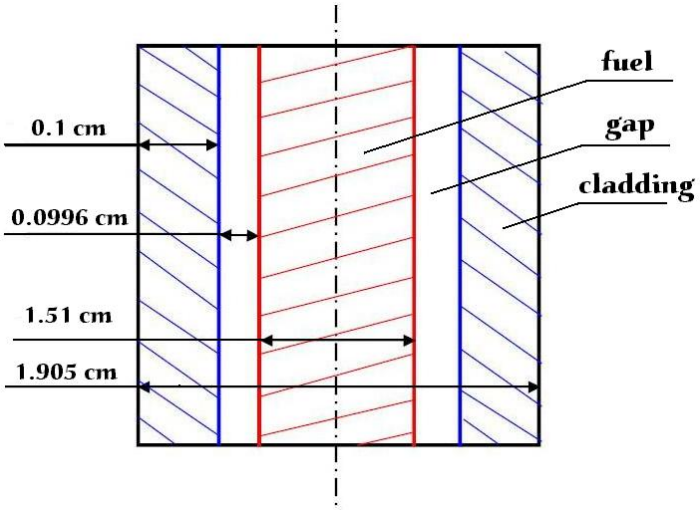

Fig. 5. Fuel pin of the STAR-H2 concept.

As is illustrated by the preceding discussion, the STAR-H2 system is radically simplified and is designed accounting for inherent safety and proliferation resistance. Once deployed, it is anticipated to run fissile self-sufficient with depleted (or natural) uranium feedstock. The initial fuel inventory is derived from LWR spent fuel at the regional fuel cycle center. In the very long term, a growing deployment of STAR-H2 power plants will draw initial fuel from excess fissile fuel production of LMFBR's.

II.C. Autonomous Long-Term Multi-Purpose Fast Reactor

In view of the fact that the STAR-H2 system is being developed targeting sustainability, longevity, eco-compatibility, and socio-acceptability, this system may already be considered as the one offering many features of the "ultimate" SCNES. It can be selected at least as a basis component of the SCNES predecessor.

In this dissertation, the ALM-FR design is considered as further refinement of the STAR-H2 system towards an economical, proliferation-resistant, sustainable, multi-purpose nuclear energy system. The main difference of the ALM-FR design from the original STAR-H2 system consists in the design requirement to provide fully autonomous, sustainable operation during the entire reactor lifetime while the STAR-H2 system is designed assuming 15-years refueling cycle.

The reactor lifetime-long operation without refueling allows achieving self-consistency in a single ALM-FR unit. The ALM-FR design can be considered as the "once-through-then-out" version or performance mode of the STAR-H2 system. It must be emphasized that the ALM-FR design will be able to demonstrate economic performance only if its operation lifetime is maximized matching the fuel lifetime with the entire reactor lifetime.

To achieve the reactor complete lifetime, fully autonomous, sustainable operation maintaining inherent safety and non-proliferation characteristics, the ALM-FR system should have the following design features and performance characteristics:

- Near-zero burnup reactivity swing with minimized spatial reactivity fluctuations is desirable during the entire operation;

- Fuel composition should be able to provide self-feeding without significant fissile material buildup at the end of reactor lifetime;
- The reactor core should be designed to provide strong reactivity feedback effects without significant deterioration and fluctuations during the entire operation;
- Reactor component materials should be able to withstand fast neutron radiation damage effects and should retain their design characteristics without significant performance deterioration during the entire operation;
- The reactor lifetime-long operation should be achieved by selecting the reactor component materials that are able to withstand high burnup levels and high fast neutron fluences.

II.D. Technological Feasibility of Advanced Actinide Fuels for the ALM-FR Concept

As it was mentioned above, the nuclear fuel components, such as plutonium and higher actinides, produced during reactor operation could be considered as components of advanced actinide fuels. In order to have ability to utilize plutonium and higher actinides as advanced actinide fuel components, they have to be extracted from a spent reactor fuel during its reprocessing and utilized in a new fresh fuel manufacturing process.[6-10]

Many technological problems and safety-related issues need to be taken into account with respect to a discharged spent fuel.[8,9] For example, the discharged spent fuel continues to emit heat due to fission products decay. Because of the decay heat and

strong radiation levels, the discharged fuel has to be stored in a cooling pond for a period up to 100 days to permit β- and γ- active nuclides to decay.[6,25]

Several solutions have been suggested and are under consideration for the final disposal of high-level and long-lived waste materials extracted from a spent reactor fuel. Two options of waste disposal are usually discussed. First one is extended storage and the other one is partitioning and transmutation of the long-lived radionuclides contained within the waste.[6,7] Partitioning and transmutation approach involves extraction of the long-lived radionuclides, which are then irradiated in nuclear reactors.

Fuel reprocessing is a very difficult and expensive process in comparison with conventional spent fuel storage.[7] The decision about whether to reprocess spent reactor fuel or store depends on the overall fuel utilization strategy adopted by nuclear energy industry in individual countries. The reprocessing of spent fuel from thermal reactors would be considered as the necessary step in a fast reactor program in order to produce the required initial plutonium inventory. The recovery of valuable fuel nuclides from spent reactor fuel is one of the most important components of sustainable nuclear technology development.

"Traditional" recycle approach considers fission products and actinides separately.[7,25] The recovered MA's are treated and stored as a high level waste because they constitute the most undesirable long-term radiotoxicity. Partitioning and transmutation of the recovered MA's could significantly reduce the long-term radiotoxicity.[7] According to the global fuel cycle analysis, this approach is technologically complex but it seems to be an appropriate waste management strategy as it provides additional fuel supply and incinerates hazardous nuclides.[8,9]

Neptunium and americium are the most attractive elements to be extracted from the spent reactor fuel because they are fissionable and can be utilized as advanced actinide fuel components. Some experience of their extraction and utilization has already been accumulated worldwide.[7]

Extracted neptunium is used for production of ^{238}Pu that is used for space power applications. Oak Ridge National Laboratory (ORNL) manages the U.S. Department of Energy (DOE) program for the production of ^{238}Pu, which can be used in radioisotope thermoelectric generators (RTG's). ^{237}Np serves as the feed material for the production of ^{238}Pu.[26] Americium is often used in domestic smoke detectors.

During the past decades an interest in partitioning and transmutation of the recovered MA's has been growing worldwide.[7] Recognizing the long-term radiotoxicity of the recovered MA's and their value as the nuclear fuel material, international research efforts are focused on waste management, disposal of high level waste, substantial reduction of the disposed radiotoxic inventory, and on utilization of the recovered MA's as part of advanced actinide fuels.

Japan has initiated the OMEGA program to study partitioning and transmutation options and their feasibility. The research is focused on nitride fuels with inert matrix and on pyro-processing technologies. The European Nuclear Energy Agency (NEA) is active participant of the OMEGA program. Several facilities have recently been built for processing of the recovered MA's. They have capabilities to handle isotopes of plutonium, americium, neptunium and curium.

One of the most important studies has recently been initiated at the Argonne National Laboratory in cooperation with the Idaho National Engineering and

Environmental Laboratory.[27] The initiated experimental program is aimed towards development of metallic alloys for use as transmutation fuels. Metallic alloys have high heavy metal atom density, relatively high thermal conductivity, favorable gas release behavior, and allow application of remote recycle processes. Because of the advantageous performance characteristics, the U.S. Advanced Fuel Cycle Program considers non-fertile and uranium-bearing metal fuels containing MA's for use as advanced actinide-transmutation fuels.

The program initiated at the Argonne National Laboratory addresses the fact that experimental irradiation performance data are very limited for any fuel form containing a significant fraction of MA's. The first irradiation tests of non-fertile high-actinide-content fuels, the AFC-1 experiment, are scheduled to begin in early 2003 in the Advanced Test Reactor (ATR).

The AFC-1 irradiation test matrix was designed to provide basic information on the irradiation behavior of high plutonium content fuel and the effect of MA’s on fuel behavior. Five different compounds of transuranic-zirconium-based alloy fuels and six plutonium-zirconium-nitride fuels containing americium and neptunium are fabricated and will be irradiated in the ATR.

Very substantial research effort is still required for development of advanced actinide fuels before their use in next generation reactors like the ALM-FR system, which is being conceptually analyzed in this dissertation. However, the already performed experimental studies clearly indicate technological feasibility of nuclear fuel compounds with high content of plutonium and MA’s.

II.E. Flexibility, Limitations and Potential Application Areas of the ALM-FR Design

The ALM-FR design is intended for a reactor lifetime-long autonomous operation as a dual-purpose nuclear energy system that provides electricity and a high temperature heat. It is presumed that the ALM-FR system will be used as a heat source in a newly developing concept of hydrogen-fueled electric power generation.

The ALM-FR design modularity gives a high degree of flexibility with respect to power level attained to satisfy energy needs of its clients. Production of oxygen and potable water is envisioned as intrinsic by-product of hydrogen generation process. As a result, the ALM-FR system should be able to satisfy needs of the developing countries and remote regions that lack heavy-duty power grids and developed industrial infrastructure but require comprehensive energy resources and potable water to ensure further economic growth and continuous social development.

It has to be mentioned that the combination of nuclear energy system and hydrogen production is not necessary, but it represents a feasible option to facilitate the emergence of a hydrogen economy. The current limited efforts and accomplishments on the further development of a new energy technology are the justifying reasons for consideration of a nuclear system like the ALM-FR design for hydrogen production and for viewing hydrogen as the promising and only alternative fuel to drive humankind forward.

Hydrogen is the truly ultimate source of clean energy. It is produced by water splitting using primary energy. When burned, hydrogen releases energy and turns into water again closing its transformation circle. To ensure survival of the Earth ecosystems

and humankind, the ultimate goal is to build a hydrogen energy system on a worldwide scale.

There are three possible methods for hydrogen production: thermo-chemical process, high temperature steam electrolysis, and methane reforming. Among these three methods, the last one is the most widely used method for hydrogen production. The United States already produces about 11 Megatons of hydrogen per year.[21] Almost 95% of this amount is produced from natural gas (methane). The methane reforming with the hydrogen production efficiency of 80% constitutes the most efficient process. However, natural gas is a premium fossil fuel, which means that it is much more expensive than water. At the same time, methane-reforming process yields about 74 Megatons of CO_2 in atmosphere per year.

The nuclear energy system as a heat source can significantly reduce emissions of carbon dioxide production – the key of greenhouse concern. A combination of a nuclear energy system with either thermo-chemical process or high temperature steam electrolysis process is very promising because both processes are more efficient at high temperatures, about 800^{o}C - 1050^{o}C or higher.

The efficiency of the high temperature steam electrolysis process is about 72%. The overall efficiency of the nuclear energy system for hydrogen production, which uses this process, would be about 36% that is lower than overall thermo-chemical process efficiency of 50%. The main advantage of the high temperature steam electrolysis process is that it provides oxygen and potable water as by-products of hydrogen production. The two thermo-chemical processes, which should be suitable for hydrogen production, are the iodine-sulfur (IS) and calcium- bromine (UT-3) processes. The main

problem with IS process is optimization of the system performance characterisitcs. The main problem with UT-3 cycle is high uncertainty of HBr water splitting. The main advantage of both processes is that they represent complete closed chemical cycles.[28]

The modularity of the ALM-FR design greatly simplifies optimization of the hydrogen production characteristics because it allows variation of the total plant power output. The discussed above design features assure inherent safety, ultra-long autonomous operation, and proliferation resistance. The elevated core temperature assumed as the ALM-FR design target makes this system specifically suitable for application as a heat source for hydrogen production. At the same time, the main limiting characteristics of the ALM-FR design result from its advantageous performance features.

Ultra-long operation with minimized reactivity swing due to burnup effects requires advanced actinide fuels or high Pu-content fuels. Despite of the inherent ALM-FR proliferation resistance, the need for advanced actinide loading or for high Pu-content loading creates significant proliferation concern and consequent limitation based on the nuclear non-proliferation safeguard regulations. As a result, the spectrum of possible fuel compositions for ALM-FR systems is constrained. Furthermore, the spent ALM-FR fuel must meet spent fuel standard requirements as well.

The reactor lifetime-long operation is also limited by fast fluences on the fuel and structural materials, whereas limitation on structural materials as a result of fast fluences is more critical limiting factor. The targeted high temperature required for efficient hydrogen production results in the additional limitations on possible choices for

structural material candidates and coolant selection. Extensive studies of advanced high temperature materials are needed.

Elevated temperature operation, high levels of burnup and compatibility with liquid lead coolant provide justification for selection of nitride fuel. To minimize reactivity loss during reactor operation and to reduce the formation of radioactive ^{14}C from (n,p) reaction on ^{14}N -component of nitride fuel, the nitride fuel composition has to be 90-99% enriched with ^{15}N. Production of the 99%-^{15}N-enriched fuel is still a very expensive process and it is not yet fully developed technology.

The coupling of nuclear systems with chemical plant for hydrogen production into an integrated ALM-FR design creates new safety issues that must be addressed as well. The dynamics and safety characteristics of the ALM-FR system require detailed studies to assure performance reliability and "inherent safety-by-design" throughout the entire ultra-long operation.

Therefore, application of the ALM-FR design for hydrogen production requires extensive studies of an integrated system performance, safety characteristics of the ALM-FR system and its subsystems for storage and delivery of hydrogen, hydrogen utilization safety, and wide variety of economics regulatory aspects.

CHAPTER III

ALM-FR DESIGN DEVELOPMENT

This chapter describes the general strategy of the ALM-FR design development as it has been applied in the research work described in this dissertation. It discusses the computational schemes, models, and computer codes that have been used to analyze the ALM-FR design characteristics. Descriptions of the computational schemes and detailed 3D models of the ALM-FR are presented with special emphasis on the applied computer codes.

III.A. General Strategy of the ALM-FR Design Development

As discussed in the preceding chapters, the ALM-FR system is intended for lifetime autonomous operation as a dual-purpose nuclear energy system that provides electricity and high temperature heat. It is presumed that the ALM-FR system will be used as a heat source in the newly developing concept of hydrogen-fueled electric power generation. Since thermo-chemical cycles have been selected as appropriate for nuclear hydrogen production, the ALM-FR core must be able to provide outlet coolant temperatures about 800^{o}C or higher to maintain high cycle efficiencies.

A complex integrated scheme of the ALM-FR design development is shown in Fig. 6. The analysis procedure addresses the need for proper selection of new high temperature materials that should assure material compatibility and provide attainability of the design-targeted ALM-FR system performance characteristics.

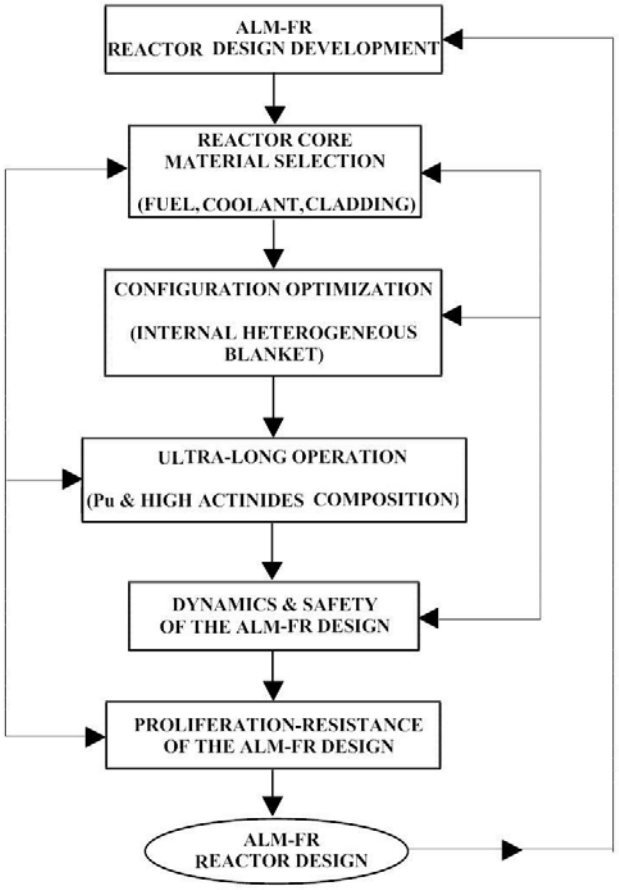

Fig. 6. General strategy of the ALM-FR design development.

The final material selection is based on physical properties of the candidate materials, their anticipated inter-compatibility in the ALM-FR system, and on the detailed reactor physics analysis that takes into account a wide variety of performance characteristics including overall reactivity swing, achievable burnup level, attainable fast fluence and material limits, power peaking and its dynamics during reactor operation, temperature reactivity coefficients, and kinetics parameters. The applied detailed 3D model of the ALM-FR system considers spatial locations of each fuel element bundle

during the entire reactor operation. To increase discharge burnup levels and decrease fluence-to-burnup ratios, material selection is followed by optimization of the ALM-FR configuration.

Reactor physics characteristics of the final optimized ALM-FR configuration are analyzed considering the entire reactor lifetime-long operation. Different fuel compositions have been examined with respect to achievability of ultra-long operation, inherent safety characteristics and nuclear non-proliferation aspects.

As illustrated in Fig. 6, the ALM-FR design development is an extensive iterative process because of complex interactions and interdependence between various characteristics of the ALM-FR system. In this dissertation, special effort has been made in order to obtain the final optimized ALM-FR design with balanced performance characteristics and to identify domain of their possible variation and the resulting design flexibility. The results describe performance of the ALM-FR system and allow conclusions regarding the concept's technological feasibility and possible directions for further analysis, development, and deployment.

III.B. Applied Computer Codes

In this dissertation, design development and analysis of the ALM-FR system characteristics are based on the computational modeling that utilizes the capabilities of the following subject-specific computer code systems:

- DIF3D 8.0/VARIANT 8.0 (A code system for using variational nodal methods and finite difference methods to solve neutron diffusion and

transport theory problems of fast spectrum nuclear reactor physics and design-oriented modeling);[29-35]

- VARI3D (A generalized perturbation theory code for calculations of the effects of alternations in microscopic cross sections and material densities on reactivity and reaction rate ratios);[36]
- REBUS-3/VARIANT 8.0 (A code system for analysis of fast reactor fuel cycles);[37-39]
- MC^2-2 (A transport theory code to calculate fast neutron spectra and multigroup cross sections).[40-42]

DIF3D 8.0/VARIANT 8.0 is a versatile computer code system for multi-group, three-dimensional, whole core neutronics calculations. It provides detailed 3D flux and power density distributions by mesh cell and regional-wise balance integrals. DIF3D solves the multi-group steady-state diffusion equation in 3- dimensional geometries. DIF3D allows modeling Cartesian, curvilinear, and hexagonal core geometries by finite difference and nodal approaches. The following problems can be specified to solve: eigenvalue, adjoint, fixed source, criticality. A variant of the Chebyshev semi-iterative acceleration is available.

In the finite-difference option, the mesh-centered form of the finite-difference equations is applied. The problem domain is subdivided into a regular array of mesh cells, such as all material interfaces lie on mesh cell surfaces. The mesh cell scheme of the DIF3D 8.0/VARIANT 8.0 finite-difference diffusion calculations is shown in Fig. 7. Within each cell, the material properties are assumed homogeneous and time

independent. Flux ϕ and surface-normal component of the net current J_n are continuous across the cell interface R_S:

$$\phi_k^g(R_S) = \phi_l^g(R_S)\,, \tag{1}$$

$$J_n^k(R_S) = J_n^l(R_S)\,. \tag{2}$$

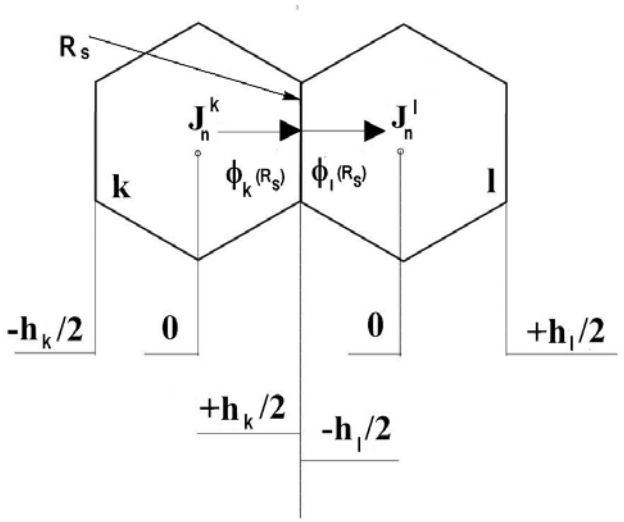

Fig. 7. Mesh cell scheme of the DIF3D 8.0/VARIANT 8.0 finite-difference diffusion calculations.

Although three-dimensional calculations of the neutron flux distribution within a reactor core may be performed by direct numerical solution of the diffusion equations, this procedure is computationally expensive. To reduce computational time DIF3D 8.0/VARIANT 8.0 uses the nodal procedure that consists of the following steps:

- Decomposition of the reactor core into large sub-zones or node cells in which each node cell is characterized by uniform material composition and flux distribution;

- Determination of the coupling coefficients characterizing interactions between individual node cells;
- Determination of the nodal flux distribution:

$$\bar{\phi} = K \cdot \bar{S}\,,\ K = k_{nn`}\,, \tag{3}$$

where $\bar{\phi}$ is the nodal flux, K is the nodal transfer matrix, $\bar{S}$ is the nodal source, and $k_{nn`}$ is a probability of a neutron to be born in cell $n`$ and diffuse into cell n.

In this scheme, nodes are coupled by requiring the surface averaged partial currents to be continuous across the nodal surface as shown in Fig. 8:

$$\bar{J}_l^{in}(-\frac{h_l}{2}) = \bar{J}_k^{out}(+\frac{h_k}{2})\,, \tag{4}$$

where k and l are neighboring nodes. The nodal equations are derived using higher order polynomial approximations.

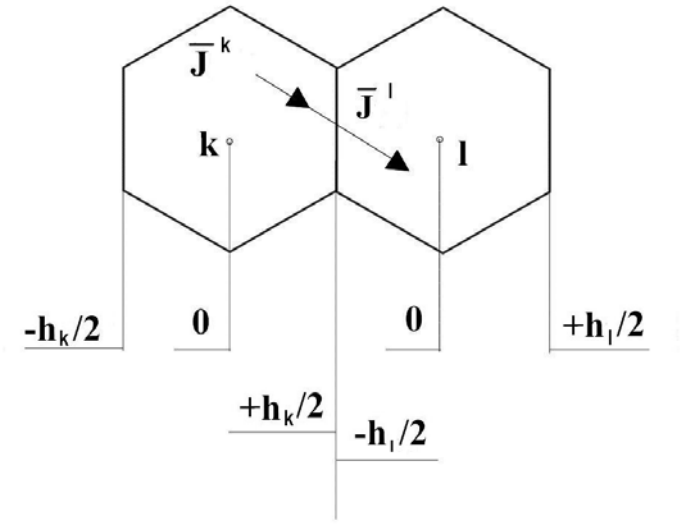

Fig. 8. Nodal mesh cell coupling.

In this dissertation, DIF3D 8.0/VARIANT 8.0 has been applied for calculations of effective multiplication factors, flux, and power distributions. The flux and adjoint distributions are used for calculations of reactivity coefficients and kinetics parameters with VARI3D. VARI3D is a computer code system, which is developed at Argonne National Laboratory for perturbation theory calculations. It utilizes DIF3D 8.0/VARIANT 8.0 to find multigroup flux and adjoint solutions. The first order option for unperturbed adjoint solution and exact solution option for perturbed adjoint are utilized. It computes regional sensitivity of reaction rates to cross section and density variations. Several options are also available for leakage term treatment.

REBUS-3/VARIANT 8.0 is a reactor design and fuel cycle analysis code system that applies DIF3D 8.0/VARIANT 8.0 for criticality calculations at each fuel depletion time-step. As a result, REBUS-3/VARIANT 8.0 allows to calculate region-wise 3D nuclide chain transformations for both equilibrium and non-equilibrium cycle problems.

Equilibrium or infinite time model describes a system that operates under fixed fuel management. It is characterized by an infinite number of burnup cycles with fixed fuel management scheme after each cycle assuming that discharged fuel is processed externally. A non-equilibrium model describes the direct explicit cycle-by cycle operation of the reactor system taking into account specific fuel management strategies after each cycle. An equilibrium cycle approximation provides the required initial fuel characteristics and the detailed information about reactor operation. In this dissertation, this approach has been used to compare performance of the different ALM-FR core configurations.

REBUS-3 can adjust the fuel enrichment, the burn time, and the control poison required for sustaining criticality conditions. Also the code can adjust discharge fuel burnup or to find the desired multiplication factor at specified burnups. The following types of problems can be specified:

- Adjustment of total burn cycle time to achieve a specified burnup by the end of fuel life-time;
- Adjustment of the fresh fuel enrichment to achieve a specified multiplication factor at the specified burning time;
- Adjustment of the control poison density at each time point to achieve a specified multiplication factor at the specified burning time.

The REBUS-3 system has two major segments: the neutronics code and the fuel cycle code. Each of these two segments is formed into separate modules and hence is compatible with execution. The REBUS-3 system comprises not only these two major segments, but also a number of other modules, which perform cross-section homogenization, dataset conversion, input processing and others. Since there is no geometric information inherent to the REBUS fuel cycle model, any neutronics code or module may be used such as one-, two-, or three-dimensional diffusion or transport theory to provide the region average fluxes to fuel cycle modules as long as the interface datasets are compatible. REBUS-3 has available various neutronics solution algorithms such as finite difference, spatial flux synthesis, nodal diffusion theory, variational nodal transport, discrete ordinate transport methods.

The fuel cycle model in REBUS-3 system can be subdivided into two cycles: in-core cycle, ex-core cycle. The in-core cycle considers the location of each discrete fuel

bundle or composition in space over the residence time of the reactor. The tree-level indexing system is used to identify and locate each of the fuel bundles in the reactor core: material type, stage, and region. The space-dependant group fluxes are used in the isotopic transmutation or burnup equations. A region may be as small as one neutronics mesh cell. If several different fuel bundles are placed in the same region, their compositions will be homogenized into a single-region composition.

The external cycle models the actual events following the discharge of fuel from the reactor such as cooling, delivery to a reprocessing plant, refabrication with reprocessing and external feed supplies, preloading storage and reactor charge.

The input data for REBUS-3 are of two types: a binary cross-section dataset and an input data file. The cross-section file contains the microscopic cross-sections in the ISOTXS format. It is also possible to provide the cross sections data by BCD card and include them in the input data stream. REBUS-3 permits variation of microscopic capture and fission cross-sections during depletion calculations. It is assumed that the microscopic (n,g) and (n,f) cross sections can be correlated with the atomic density of specific isotopes – base isotopes. Specified burnup dependant isotopes can be correlated with the atomic densities of base isotopes and their cross-sections of particular energy group can be expressed mathematically based on this dependence. For example, cross-sections of ^{239}Pu might be related to the atomic density of ^{235}U. All burnup dependant isotopes in a given region of the system must refer to the same reference base isotope. But different reference base isotopes can be used for different regions.

The multigroup cross-section libraries for calculations with REBUS-3 and DIF3D have been prepared with MC^2-2 on the basis of ENDF-VI data. This code has

been developed at Argonne National Laboratory for needs in fast reactor calculations. MC^2-2 has capability to collapse the basic ENDF data into multi-group cross section libraries in ISOTXS format suitable for DIF3D and REBUS-3. In MC^2-2 four different slowing down formulations are used:

- Multi-group calculations;
- Continuous slowing down calculations with Goertzel-Greling or Improved Goertzel-Greuling moderating parameters;
- Hyper-fine-group integral transport calculations.

Resolved and unresolved resonance cross sections are calculated taking into account self-shielding, broadening and overlap effects. The resulting composition-, temperature- and region- dependant microscopic cross sections can be used for diffusion or transport theory calculations for a fast reactor core. Resulting MC^2-2 library includes ultra fine group smooth data with broad resonance and other files with detailed anisotropy, inelastic scattering and etc.

Several major limitations of the multigroup cross section libraries prepared with MC^2-2 have to be emphasized, because they affect accuracy of the obtained ALM-FR performance characteristics:

- Resulting multigroup cross sections depend on composition and temperature;
- Spectral effects of neutron leakage are not explicitly taken into account by infinite medium calculations;
- Extensively applied narrow resonance approximation introduces errors if resonance effects extend beyond a certain ultra-fine group;

- Higher order scattering matrices cannot be generated;
- No thermal energy range treatment.

MC^2-2 code system and SDX (Standard Code Description) processing codes have been used for generation region-dependent 21-group cross sections on ENDF/B-V.2 basic data. Combination of MC^2-2 and SDX allow utilization of single MC^2-2 base library for range of isotope enrichments. SDX provides re-inclusion of the actinide resonances for specific compositions of interest. It also provides unit cell calculations to take into account heterogeneity effects.

III.C. ALM-FR Modeling

The ALM-FR design development and analysis of its performance characteristics are based on the computational modeling with MC^2-2, REBUS-3/VARIANT 8.0, DIF3D 8.0/VARIANT 8.0, and VARI3D that represent the code and data system, which has been developed, validated and extensively used for fast reactor calculations at the Argonne National Laboratory. To a great extent, the accuracy of the results and conclusions depends on the available flexibility and inherent limitations of these code systems and on the adequacy of the applied ALM-FR model to represent phenomena governing performance characteristics of the ALM-FR system during its reactor lifetime-long operation. The long-term development and validation of the applied code systems and their extensive application for fast reactor studies at Argonne National Laboratory provide sufficient degree of confidence that the results of this dissertation adequately represent the ALM-FR system performance.

The applied model of the ALM-FR system and its performance is developed assuming applicability of the equilibrium cycle problem. It uses the burnup-dependent nuclide composition, which is characterized by burnup-dependent nuclide densities and burnup-independent multi-group cross sections. The ALM-FR modeling is based on the following assumptions:

- Constant reactor power level is assumed for the entire operation;
- Criticality calculations are performed at the beginning-of-life (BOL), at the end-of-life (EOL) and at several discrete burnup points during reactor operation to ensure that the burnup-dependent nuclide composition and the ALM-FR performance characteristics are properly calculated taking into account neutron flux variation with burnup;
- Region-wise averaged multi-group fluxes and nuclide compositions are used to calculate reaction rates for the REBUS-3 depletion equations;
- All materials in a given region are assumed to be irradiated in the same neutron flux;
- Multi-group cross sections are burnup-independent; they are externally pre-calculated with MC^2-2 for several operating temperatures.

The developed 3D model of the ALM-FR fueled core assembly is given in Fig. 9. The ALM-FR core model has several macro-regions, which represent fuel element array, gas plenums, grids, reflectors, and coolant pool.

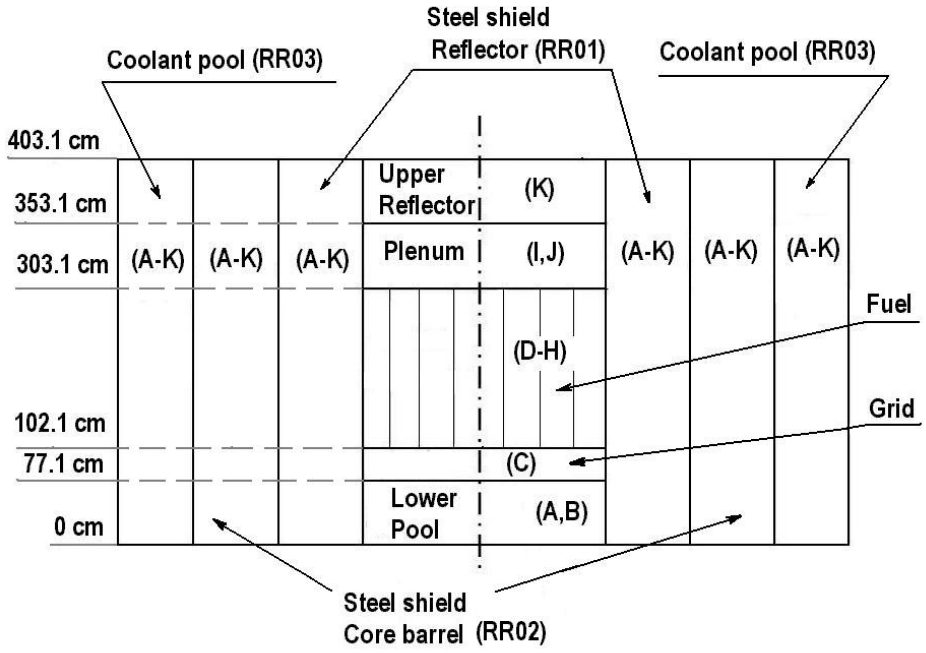

Fig. 9. 3D model of the ALM-FR fueled core assembly.

For detailed 3D modeling, the central fuel element macro-region consists of a number of hexagonal homogenized sub-regions describing ductless fuel assemblies. Each hexagonal sub-region represents a model zone and has five axial zones. Zone boundaries correspond to the model mesh.

The calculations have been performed using the imposed zone structure that is shown in Fig. 10. The core map is divided into five regions depending on the initial fuel enrichment: ICORE – inner core driver region, MCORE- medium core driver region, OCORE – outer core driver region, IBLKT - inner core blanket region, OBLKT – outer core blanket region. The total core region, TCORE, includes all listed fuel regions. The description of the developed ALM-FR core model with the complete list of the assigned

zone numbers and the region names for different core configurations is given in Appendix A.

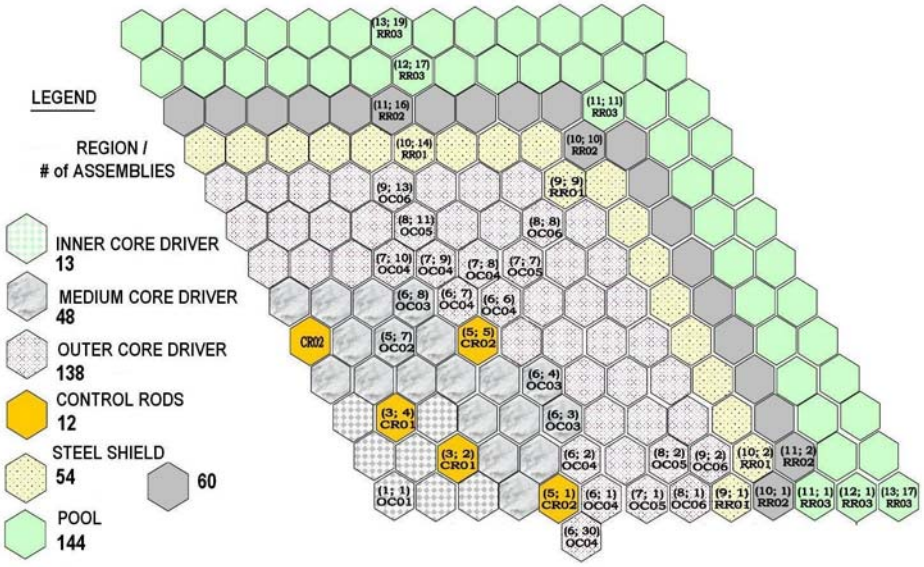

Fig. 10. 1/3 core model layout for the ALM-FR configuration without internal heterogeneous blanket.

The REBUS-3 modeling takes into account the spatial locations of each discrete fuel element bundle during the reactor operation. Since reactor lifetime-long operation is targeted by the ALM-FR design, it is assumed that fuel element bundles are not reloaded or relocated. The REBUS-3 burnup calculations are performed for the 1/3-part of the symmetrical ALM-FR core as shown in Fig. 10.

The fuel cycle model utilizes a three-level indexing scheme, (l, τ, r), to assign and identify the location of each fuel element bundle: l - material type, τ - stage, r – region. Table II illustrates the applied ALM-FR model nomenclature.

TABLE II

ALM-FR Model Nomenclature

L	Number of different material types in the reactor
K	Number of different regions in the reactor
$r_1, r_2 \ldots r_K$	Reactor regions
l	Material type
S	Stage
τ	The stage number
V_l	Volume of material l
V_r	The total volume of region r

Material type index (l) and stage index (τ) are used to calculate reactor operation characteristics. Each material type is characterized by the initial composition and by the volume of each constituent (fuel, cladding, bond, coolant, reflector, plenum). The region index (r) determines the physical location of the fuel element bundle, control rods or other materials. The stage number is determined by the number of burn cycles which fuel spends in the core. The associated region number and the associated stage number describe the material location.

Therefore, the atom density vector for a single composition for material type l and stage τ, which is associated with time t, can be expressed as:

$$\overrightarrow{n_{l,\tau}}(t) = [n_{l,\tau,1}(t), n_{l,\tau,2}(t).....n_{l,\tau,I}(t)], \tag{5}$$

and the complete set of equations to determine the atom density vector can be written as following:

$$\frac{\partial}{dt}\overrightarrow{n_{r,\tau}}(t) = A_{l,\tau}[\phi(t)]\overrightarrow{n_{r,\tau}}(t), \tag{6}$$

where $l=1...L_{l;}$, $\tau=1...S$, *and* $A_{l,\tau}[\phi(t)]$ is the appropriate burnup matrix. The homogenized density vectors are determined for all regions using the absolute atom density vectors defined and computed according to Eq. (5) and Eq. (6):

$$\overrightarrow{n_r}(t) = \frac{1}{V_r}\sum_{l,\tau}\overrightarrow{n_{l,\tau}}(t)\cdot V_l\,. \tag{7}$$

The neutron flux $\phi(t)$ is the solution of the static criticality problem that can formally be written as a system of homogeneous non-linear equations:

$$F[\phi(t), \overrightarrow{n_{r1}}(t), \overrightarrow{n_{r2}}(t).....\overrightarrow{n_{rK}}(t)] = 0\,. \tag{8}$$

Analogously to Eq. (6), the equilibrium cycle problem can formally be stated as the following set of generalized equations:

- Relationship between the fresh material (charge) density vector $\vec{n}$ and discharge vector n:

$$n = B(T, E, \vec{n})\vec{n}\,, \tag{9}$$

- Cyclic mode with burnup constraint:

$$b_0 = b(T, E, \vec{n})\,, \tag{10}$$

- New charge material vector production from reprocessing (unconstrained equilibrium mode):

$$\vec{n} = Q_r(n)n + Q_f(n)n_f\,, \tag{11}$$

- Equilibrium mode:

$$k_0 = k(\alpha T, E, \vec{n})\,, \tag{12}$$

where b_0 is a desired burnup, k_0 is a desired value of unpoisoned multiplication factor, α is a specific fraction of the burn cycle time, T is a burn time, E is an enrichment, $\vec{n}$ is a charge density vector, $B_{l,\tau}(E,E,\vec{n})$ is a transformation (transmutation) matrix.

Assigning the desired burnup b_0 and the desired unpoisoned multiplication factor k_0 to be obtained at the specified fraction α of the burn cycle T, the required initial enrichment E and the charge density vector $\vec{n}$ can be found by the iteration procedure based on Eq. (9) – Eq. (12). If the discharge density vector is the same after every burn step, the reactor is in a cyclic mode. This mode is described by Eq. (9). The cyclic mode is only related to the in-core cycle and is completely independent from the external fuel cycle.

The pair of Eq. (9) and Eq. (10) describes a reactor in a cyclic mode that is constrained by the assigned burnup level. If iterative parameters satisfy Eq. (9), Eq. (10) and Eq. (11), the entire fuel cycle including its external part is in the unconstrained equilibrium mode. To be in unconstrained equilibrium mode, a reactor has to be in cyclic mode as well.

If Eq. (9) – Eq. (12) are satisfied for a given configuration, the system is in its final equilibrium mode characterized by the required equilibrium enrichment E. The unconstrained equilibrium mode and the final equilibrium mode are related to the entire fuel cycle including its internal and external parts.

The solution strategy for the considered equilibrium cycle problem is illustrated in Fig. 11. During the iteration process, an unconstrained equilibrium mode can be found for a system with initial enrichment vector E_0,. At the next step, the reactor operation

time $T=T(E)$ and the charge density vector $\vec{n}(E)$ are determined. The enrichment E is then adjusted, if necessary, to obtain the desired multiplication factor k_0.

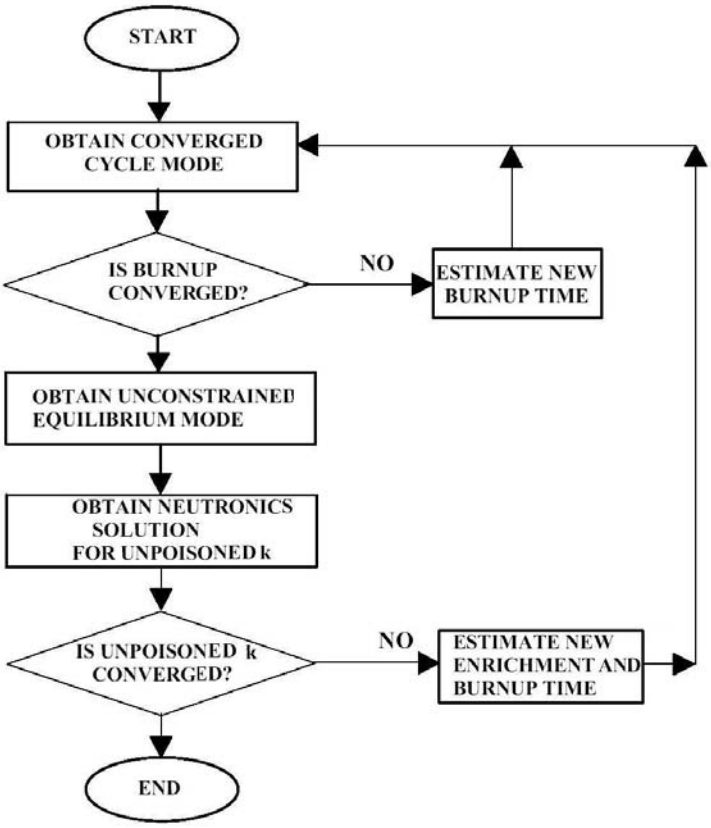

Fig. 11. Equilibrium cycle modeling scheme.

The applied equilibrium cycle modeling parameters for the ALM-FR design calculations are summarized in Table III. As noted above, the DIF3D nodal calculations are performed for the 1/3 part of the ALM-FR core.

TABLE III

Parameters of the ALM-FR Equilibrium Cycle Modeling

Problem Type	Equilibrium Cycle
Cross Section Library	Pre-Calculated, Burnup-Independent
Convergence Criterion on Region Density	1.000e-03
Convergence Criterion on Cyclic Mode	1.000e-03
Convergence Criterion on Unconstrained Equilibrium	1.000E-04
Burnup Convergence Criterion	1.000E+00
Convergence Criterion on Charge Enrichment	1.000E-03
Maximum Number of Region Density Iterations	4
Maximum Number of Cyclic Mode Iterations	1
Number of Previous Burn Cycles	0
Shutdown Time between Burn Cycles (days)	1.095e+03
Time at which Problem Begins (days)	0.000e+00
Number of Sub-Intervals for the Burn Cycle	3
Number of Fuel Management Operations	0
Desired Unpoisoned $k_{eff}(0)$	1.000e+00
Fraction of Burn Cycle Time for $k_{eff}(0)$	0.000e+00
Number of Hexagon Rings	13
Number of 60^{o} Sectors	2
Number of Hexagons in Plane	157
Number of Active Hexagons in Plane	157
Number of Axial Planes	18
Number of Hexagonal Nodes	2826
Number of Unique Node Types	97

For each of the considered configurations, the following performance characteristics are obtained as a result of the ALM-FR modeling with REBUS-3:

- Material (nuclide) mass flow characteristics;
- Peak and average discharge burnup levels;
- Peak fast fluences and peak burnup levels;
- Initial (charge) enrichment (fissile content) and the final (discharge) fissile content;
- k_{eff} at the EOL assuming that unpoisoned k_{eff} is equal to unity at the BOL;
- Breeding ratios.

To calculate the reactivity effects due to alterations in microscopic cross sections and material densities, material compositions for the base (nominal) and perturbed states are obtained using burnup-dependent data from the performed calculations with REBUS-3. Appendix B contains the source code of the auxiliary program that has been created and used to generate various perturbations in material properties of the ALM-FR system. Using the burnup-dependent data from the REBUS-3 equilibrium cycle modeling, the real and adjoint flux distributions have been calculated with DIF3D for subsequent modeling with VARI3D.

In this dissertation, the following reactivity coefficients and kinetic parameters have been calculated for the different ALM-FR core layouts:

- Radial core expansion reactivity coefficients;
- Axial fuel expansion reactivity coefficients;
- Axial fuel and cladding expansion reactivity coefficients;
- Doppler reactivity coefficients;
- Coolant void reactivity worth;
- Effective delayed neutron fraction;
- Effective neutron generation time.

To calculate effective kinetic parameters, VARI3D uses unperturbed and adjoint fluxes, which have been obtained with DIF3D. The 6-group delayed neutron data are used for all fissionable nuclides. The ALM-FR model parameters for calculations of the reactivity coefficients are summarized in Table IV.

TABLE IV

Parameters of the ALM-FR Reactivity Coefficients Modeling

Problem Type	Equilibrium Cycle
Number of Energy Groups	21
Maximum Number of Down-Scattering Groups	20
Maximum Number of Upscattering Groups	0
Cross Section Library	Pre-Calculated, Burnup-Independent
Geometry Type	Triangular Rhombic Boundary in Plane
Number of Zones (Compositions)	101
Number of Regions	101
Number of zone classifications	1
Number of 1st Dimension Coarse Mesh Intervals	150
Number of 2nd Dimension Coarse Mesh Intervals	75
Number of 3rd Dimension Coarse Mesh Intervals	11
Number of 1st Dimension Fine Mesh Intervals	150
Number of 2nd Dimension Fine Mesh Intervals	75
Number of 3rd Dimension Fine Mesh Intervals	18
Outer Boundary Shape	120 Degree Rhombic Boundary
Hexagon Flat-to-Flat Distance	1.6238e+01
Length of Mesh-Triangle Side	3.1250e+00

Sensitivity analyse have been performed for different geometry type and different numbers of point mesh per hexagon side. It has been observed that one mesh-point per hexagon side is not enough to satisfy expected accuracy with respect to the obtained data. However, 3 mesh-points per hexagon side provide sufficient accuracy. Although further increase of a number of mesh points per hexagon side would allow better accuracy, it requires much longer computational time and does not provide more than 0.1% in obtained results. Thus, all calculations have been performed using 3 mesh-points per hexagon side.

The overall ALM-FR modeling procedure is shown in Fig. 12. Criticality calculations with DIF3D and whole-core burnup calculations with REBUS-3 provide the ALM-FR performance characteristics. The resulting burnup-dependent data are used to calculate reactivity coefficients and kinetics parameters with VARI3D.

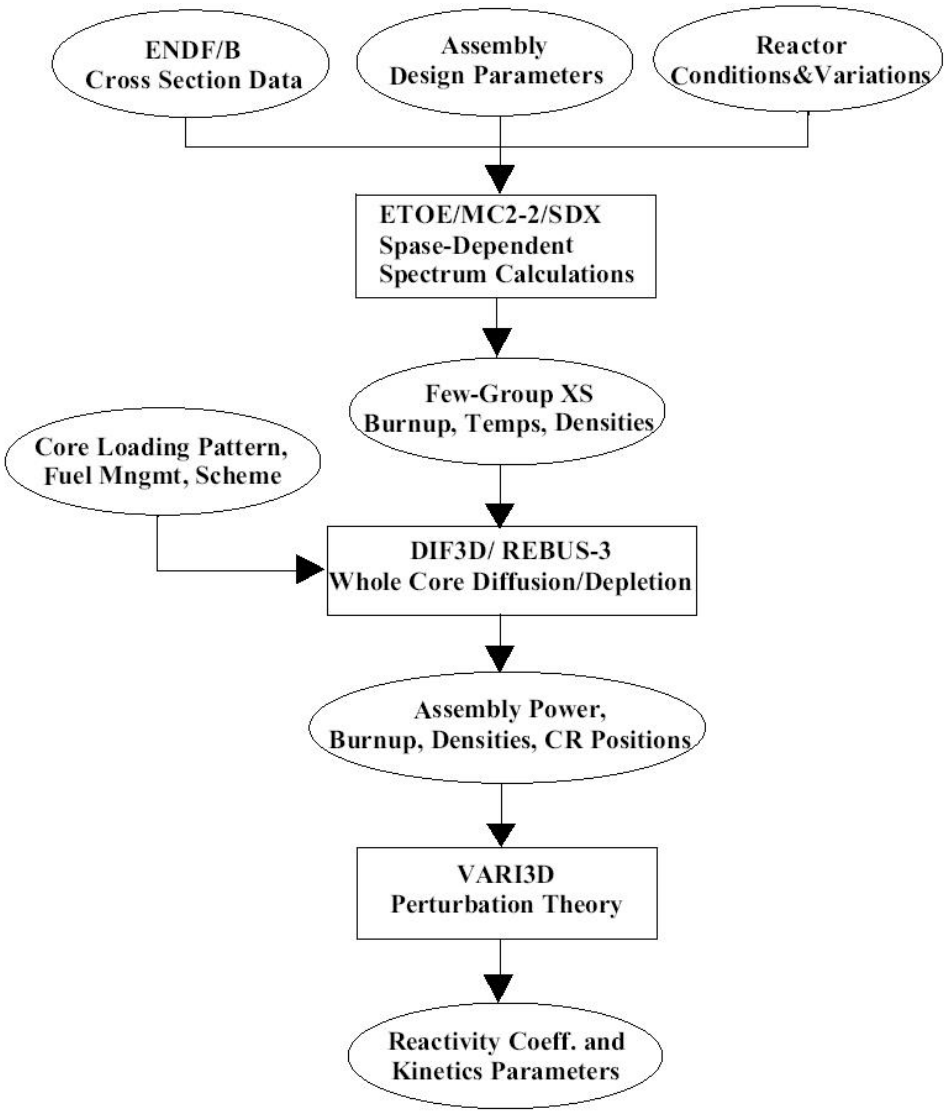

Fig. 12. Overall ALM-FR modeling with DIF3D, REBUS-3 and VARI3D

CHAPTER IV

SELECTION OF REACTOR CORE MATERIALS FOR THE ALM-FR DESIGN

This chapter presents the reactor physics analysis of the ALM-FR configurations with different fuel compositions and structural materials. The results, which were obtained, have been used as a basis for selection of materials for the ALM-FR design.

IV.A. Advanced Uranium-Transuranic-Nitride Fuel

Nitride fuels are considered as a promising alternative to oxide and metal fuels for liquid metal fast reactors. Because of their attractive properties at elevated temperatures, nitride fuels are under consideration for application in the STAR-H2 systems including the ALM-FR design that is considered in this dissertation.

As illustrated in Table V, nitride fuels are characterized by very good thermal conductivities and high metal densities.[25,43,44] In addition, nitride fuels have demonstrated good compatibility with lead. To reduce the formation of radioactive ^{14}C from (n,p)-reactions on ^{14}N in nitride fuels as well as to mitigate the neutron parasitic absorption by ^{14}N, enrichment by ^{15}N up to 90-99% is envisioned as a promising method.

In this dissertation, the specific correlations, which were developed for UN, have been applied to describe thermal properties of the considered nitride fuel compositions:[45]

- Thermal expansion coefficient:

$$\alpha = 7.096 \cdot 10^{-6} + 1.409 \cdot 10^{-9} T\,,\ 298 < T \le 2523\,,\ \Delta\alpha = \pm 2.0\,, \qquad (13)$$

where α is the thermal expansion coefficient (1/K); T is the fuel temperature (K); $\Delta\alpha$ is the corresponding standard deviation of the correlation (%);

- Fuel density:

$$\rho = 1.42 - 2.997 \cdot 10^{-4} T - 4.897 \cdot 10^{-8} T^2\,,\ 298 < T \le 2523\,,\ \Delta\rho = \pm 0.1\,, \qquad (14)$$

where ρ is the fuel density (g/cm^3); T is the fuel temperature (K); $\Delta\rho$ is the corresponding standard deviation of the correlation (%).

TABLE V

Physical Properties of UN and PuN Fuels

Material	UN		PuN
Composition	94% U, 5.56% N		94.56% Pu, 5.43% N
Melting Point (°C) Theoretical Density (g/cm^3) Heavy Atom Density (g/cm^3) Thermal Conductivity at 500 °C (W/(cm·°C))	2600 14.32 13.51 0.12		2500 14.22 13.43 0.12
Thermal Expansion Coefficient at 500 °C (m/(m· °C))	T (°C) 16-1023	 3.02E-8	
Heat Capacity (J/kg· °C)	327 736 1121	7.02 7.56 8.1	

Performance characteristics of (U,Pu)N under irradiation have been experimentally studied at the Battelle-Columbus Laboratories for use as an advanced LMFBR fuel.[46] It has been concluded that the observed physical, thermal, and neutronics properties of mixed U-Pu nitrides make them suitable for applications as base fuels for

LMFBR's. Thermal irradiation tests have been performed with $(U_{0.8}Pu_{0.2})N$. These tests have demonstrated outstanding dimensional and structural stability of the specimens at high linear power densities up to 1.312 kW/cm and at high burnup levels up to 100 MWd/kg. The series of fast irradiation tests have confirmed excellent performance characteristics and extended the burnup levels achieved in thermal irradiation tests to 150 MWd/kg. The experimental results indicate low fuel swelling of ~0.48% per 10^{20} fissions/cm^3 due to fuel growth induced by solid-state fission products and point out to 1350^{o}C as the temperature limit for fuel due to onset of fission gas bubble mobility and agglomeration effects. The experimentally observed fission gas release is reported as ~10% at the achieved burnup level of 150 MWd/kg.

Thus, the available experimental data on the nitride fuel performance characteristics under fast spectrum irradiation allow selecting nitrides as the base components of an advanced actinide fuel for the ALM-FR system. The ALM-FR performance characteristics, which have been obtained in the computational analysis, are compared with the available experimental performance limits to assure the validity of the selected design solutions and the conclusions on the ALM-FR performance characteristics.

IV.B. Liquid Lead Coolant

There are several specific performance characteristics that have to be taken into account in order to select an appropriate coolant for a given nuclear reactor. The factors

to choose one or another liquid metal coolant are similar to those considered for proper selection of other types of coolants, namely:

- Low melting point and high boiling point;
- Low neutron absorption cross section;
- High heat transport and thermal conductivity;
- Radiation stability;
- Thermal stability;
- Low induced radioactivity;
- No reaction with turbine working fluid;
- Non-corrosive properties;
- Low pumping power.

The extraordinary heat transfer properties of liquid metals make them attractive nuclear reactor coolants. They are excellent heat-transfer media mainly because of the high thermal conductivity. Liquid metals provide the possibility to attain high temperature levels, which are desirable to generate steam for modern turbine generators. In addition, application of liquid metals allows operation at low pressure and minimized pumping power.

The performance characteristics of sodium, lead and lead-bismuth are summarized in Table VI.[47-50] Sodium is the material that has been traditionally considered for use as a primary coolant in LMFBR's.[51,52] Compared to the characteristics of lead as a coolant, sodium has a lower melting point and a considerably higher thermal conductivity. However, several serious problems exist with the application of sodium in LMFBR's. These include:

- Reactions with water, steam and air are very rapid and explosive:

$$2Na + H_2O \rightarrow Na_2O + H_2O,\ Na_2O + H_2O \rightarrow 2NaOH; \quad (15)$$

- Neutron absorption by ^{23}N results in highly radioactive ^{24}N:

$$^{23}N + n \rightarrow {}^{24}N. \quad (16)$$

TABLE VI

Physical Properties of Sodium, Lead and Lead-Bismuth

Material	Na		Bi		Pb		44.5% Pb, 55.5% Bi	
At. Weight	22.997		209		207.21		208	
$T_{melt.}$ (^oC) $T_{boil.}$ (^oC)	97.8 883		271 1477		327.4 1737		125 1670	
	T (^oC)		T (^oC)		T (^oC)		T (^oC)	
Density (g/cm^3)	400 550 700	0.854 0.817 0.780	300 400 600 802 962	10.03 9.91 9.66 9.4 9.2	400 500 600 800 1000	10.51 10.39 10.27 10.04 9.81	200 400 600 800 100	10.46 10.19 9.91 9.64 9.36
Thermal Conductivity ($W/(cm\cdot{}^oC)$)	300 400 500	0.757 0.712 0.668	300 400 500 600 700	0.172 0.155 0.155 0.155 0.155	330 400 500 600 700	0.163 0.159 0.155 0.151 0.151	160 200 240 320	0.0092 0.0096 0.1 0.113
Heat Capacity ($J/(kg\cdot K)$)	400 600 800	1239.0 1255.0 1269.0	271 400 600 800 1000	142.4 148.213 157.424 166.216 175.427	327 400 500	163.285 154.912 154.912	144 - 358	146.538
Fast Neutron Activation Cross Section (b)	0.67E-3		4.697E-3		3.6E-3		-	
Scattering Cross Section (b)	4.0		5.798		7.5		-	
Average log Energy Decrement	0.0852		-		0.0097		-	
Cost/t ($)	0.17		-		0.25		0.55	

Lead and lead-bismuth are considerably safer than sodium because they do not intensively react with air and water. Consequently, it assures inherent system safety in accident situations when the primary coolant does not interact with atmosphere or with secondary coolant. Thus, integral reactor layouts become feasible.

It has to be emphasized that the previous LMFBR designs were intended for operation at about 600^{o}C that is substantially lower than the boiling temperature of sodium. The STAR-H2 systems including the ALM-FR design require operating temperatures of about 800^{o}C. As a result, in these systems, operating temperatures will be higher than the boiling temperature of sodium and sodium boiling will most probably occur.

In nuclear reactors with a fast neutron spectrum, coolant boiling must be avoided, because the introduced void due to boiling is likely to result in a positive reactivity effect. According to Table VI, the boiling temperatures of lead and lead-bismuth are much higher than the required operating temperatures. Therefore, to avoid primary coolant boiling, lead or lead-bismuth should be considered for use in the STAR-H2 systems including the ALM-FR design.

Lead and lead-bismuth perform as good neutron reflectors due to the large scattering cross sections and high densities. Their presence in the core and in the surrounding pool region provides possibility to reduce the neutron leakage and improve neutronics performance of the reactor core.

Both lead and lead-bismuth are taken into consideration as the most promising candidates for application as a primary coolant of the STAR-H2 systems including the ALM-FR design. In comparison with sodium, these materials allow harder neutron

spectrum, lower neutron leakage, lower specific activation, and considerably reduced probability for coolant boiling in the reactor core. Application of lead and lead-bismuth as coolants provides the possibility to design systems that use natural circulation as a primary heat removal mechanism. Since lead and lead-bismuth are capable of maintaining 100% of primary heat removal by natural circulation, the nuclear reactor designs can be substantially simplified to allow inherent safety features resulting from natural circulation cooling.

As illustrated in Fig. 13, the local void formation effects in liquid lead are anticipated to be smaller than in cases with sodium because of the higher density of lead at high temperatures. Thus, the positive void reactivity coefficient should be smaller in the systems that use lead or lead bismuth as a coolant. However, because of the very high boiling temperatures, there are virtually no mechanisms that can produce voiding in the core.

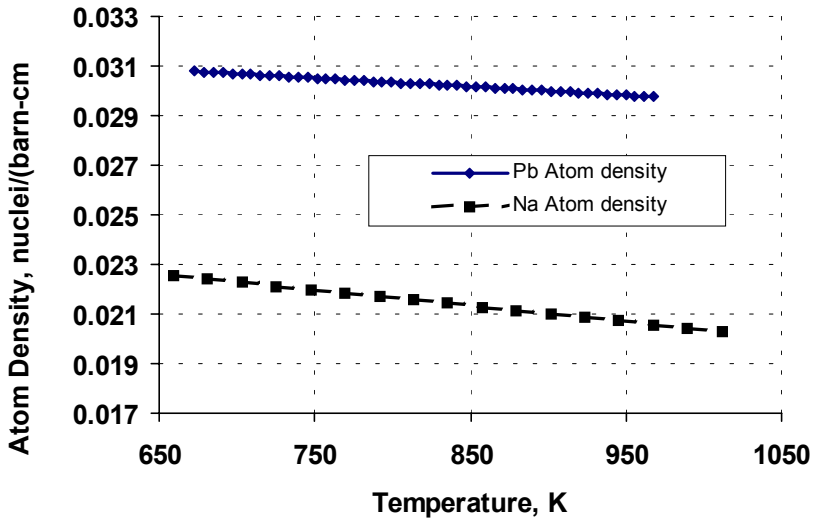

Fig. 13. Temperature-dependent atom densities of sodium and lead.

One of the disadvantages of lead as a coolant is its high solidification point. Pure lead solidifies with 3% reduction of volume. In the case of solidification or freezing, pure lead may break the fuel elements because of the asymmetricity of potential volumetric changes. However, since lead reduces in volume when it freezes, open fuel pin lattice and specially designed core inlet and outlet plenums should allow mitigation of this problem.

According to Table VI, the melting point of lead-bismuth is substantially lower than the melting point of pure lead, if lead-bismuth is used in its eutectic form. Lead-bismuth becomes an eutectic structure when its component ratio is Pb:Bi/44.5:55.5. Consequently, solidification of lead-bismuth should not occur during reactor operation and should be preventable during maintenance reactor shutdowns. Furthermore, the volume of lead-bismuth eutectic does not change when the material solidifies. As a result, solidification of lead-bismuth does not result in breakage of fuel elements as in case of solidification of lead.

Another main problem associated with use of lead-bismuth is the coolant activation.[53] Highly radioactive ^{210}Po is formed in large quantities as a result of neutron absorption in ^{209}Bi. ^{210}Po is the α-emitter with a half-life of 138 days. The average energy of α-particles emitted from ^{210}Po is about 5.3 MeV. Its presence in reactor coolant creates severe problems due to Po-volatility and migration characteristics. Another problem is the corrosion of the structural materials by lead-bismuth. Structural material corrosion is caused primary by presence of Bi whose effect is about 40 times higher than that of Pb according to the performed experimental studies.[53,54] The corrosive effect increases with increasing concentration of Bi in lead-bismuth.

On the basis of the analysis performed in this work of the available experimental data and taking into account the design requirement of operation at temperatures of about 800^{o}C and higher, pure lead has been chosen for further reactor physics analysis as the ALM-FR coolant. The selection of lead is based on its excellent neutronics characteristics, low activation, low corrosion and high boiling point. Although addressed and discussed in this dissertation, the design and performance problems associated with the high solidification point of lead are left beyond the scope of the detailed reactor physics analysis as they are envisioned as the appropriate focus areas for future research efforts. Although not yet proven experimentally, the performed analysis of the STAR-H2 layout, shown in Fig. 1, indicates the possibility to provide 100% of the primary heat removal via natural circulation of the pure lead coolant.[20,22] To further mitigate the structural material corrosion effects, in this dissertation, analysis of different structural materials and the structural material selection for the ALM-FR design have been performed taking into account material compatibility with lead as a coolant.

IV.C. S316 Stainless Steel as Material for Neutron Reflector

Analogous to the STAR-H2 design, in the ALM-FR system the central active fuel pin array is surrounded by the radial reflector assemblies and structures, which form the radial reflector region. The principal functions of the radial reflector are to limit neutron leakage from the fuel element array, to provide neutron and gamma shielding for the major support components within the reactor vessel, and to prevent any access to the active fuel pins.

The radial reflector elements fit into the regular hexagonal lattice with the central fuel pin array. In addition to the above-mentioned functions, they also serve to transmit a stress load between the central region and the core restraint system.

In the STAR-H2 design and in the ALM-FR design as an applied option of the STAR-H2 system, the material choice for the radial reflector elements is narrowed to 316 stainless steel (SS316). It has high melting point and is resistant to void swelling. This material can experience relatively high fluence since it is not a load-bearing component. The SS316 nuclide composition and some of its thermal characteristics are summarized in Table VII.[25,51,52]

TABLE VII

Physical Properties of 316 Stainless Steel

SS316 Composition	Fe-base, 0.08% C, 16-18% Cr, 10-14% Ni, 2% Mn, 2-3% Mo, 1% Si, 0.045% P, 0.03%S
Melting Point (K)	1700
Heat of Fusion (J/kg)	2.70E+5
Boiling Point (K)	3090
Heat of Vaporization (J/kg)	7.45E+6
Specific Heat at 800 K (J/(kg·K))	569.2
Thermal Conductivity at 800 K (W/(m·K))	21.816
Thermal Expansion Coefficient at 800 K (m/(m·K))	2.0E-5

IV.D. Silicon Carbide as Material for Fuel Element Cladding

IV.D.1. Cladding Material Candidates

The material strength under reactor operation conditions and its ability to retain its performance characteristics during the entire reactor lifetime are the main factors that

determine selection of in-core materials for the ALM-FR design. Several different materials, such as HT9, Nb-1%Zr, SiC, ZrC, ZrN, V-alloys, and Mo-alloys, have been considered as potential candidates for use as a cladding for fuel pins in the ALM-FR design. This group of materials has been chosen for this study as potential cladding candidates because of their high strength and resistance to oxidation at elevated temperatures in such an aggressive medium as liquid lead. All of these materials have high thermal conductivities and good thermal shock resistance.

Similar to the 400 series steels, HT9 ferritic alloy has been considered and extensively studied for applications as a cladding material in LMFBR's.[55] Experimental data describing thermal properties of HT9 steel are available for high temperatures up to about 1200 K. In particular, the HT9 thermal conductivity can be estimated using the following experimental relations:[55]

$$\lambda = 17.622 + 2.428 \cdot 10^{-2} T - 1.696 \cdot 10^{-5} T^2, \quad 500\text{K} < T < 1030\text{K} \tag{17}$$

$$\lambda = 12.027 + 1.218 \cdot 10^{-2} T, \quad 1030\text{K} < T < 1200\text{K}, \tag{18}$$

where λ is the HT9 thermal conductivity (W/(m·K)), and T is the HT9 temperature (K). The HT9 thermal characteristics used in the present study are given in Table VIII.

TABLE VIII

Physical Properties of HT9 Stainless Steel

HT9 Composition	0.5% Ni, 12% Cr, 0.2% Mn, 1.0% Mo, 0.25% Si, 0.5% V, 0.2% C	
Melting point (^{o}C)	1420	
Theoretical Density (g/cm^3)	7.8	
	T (^{o}C)	
Thermal Conductivity (W/(m·K))	400 600	22.5 27.7
Thermal Expansion Coefficient (m/(m·K))	600	12.6E-6
Specific Heat (J/(kg·K))	600	800

It was experimentally proven that the HT9 steel has a phase transition at temperatures around 1030K, which is usually considered above the recommended service temperature of HT9 but is within the operation temperature range of the ALM-FR design. However, due to extensive accumulated experience of HT9 applications in LMFBR's, this material has been taken into consideration in this study as a reference material that can be used for the fuel element cladding.

Niobium is another material that offers promising performance characteristics as a component of fuel element cladding in the ALM-FR design. In general, pure niobium has good ductility and weldability in a clean, dry, inert gas atmosphere or in a vacuum. It is very similar to tantalum with respect to its performance characteristics. Thermal characteristics of pure niobium are summarized in Table IX.[47]

TABLE IX

Physical Properties of Pure Niobium

Atomic Number	41
Atomic weight	92.9064
Valences	2, 3, 4, 5, 6
Density at 300 K (g/cm^3)	8.57
Melting Point (K)	2750
Boiling Point (K)	5017
Thermal Expansion Coefficient at 300 K (m/(m·K))	7.1E-6
Specific Heat (J/(kg·K))	527.537
Thermal conductivity (W/(cm·K))	2.19

Niobium is resistant to corrosion due to interactions with wet or dry chlorine, bromine, ferric chloride, hydrogen sulfide, sulfur dioxide, nitric and chromic acids.[56] However, this material cannot be used in air at temperatures exceeding 200^{o}C. Niobium

is also resistant to many liquid metals within the corresponding temperature limits as illustrated in Table X.[57]

TABLE X

Temperature Limits of Corrosion Resistance for Niobium

Corrosive Substance or Reagent	Temperature Limit (^{o}C)
Li	< 1000
Na, K+NaK	< 1000
ThMg	< 850
U	< 1400
Zn	< 450
Pb	< 850
Bi	< 550
Hg	< 600

Considering interactions and compatibility with reactor materials, niobium has remarkable strength at elevated temperatures but experiences some corrosion effects due to interactions with liquid metals like lead, sodium and lithium. According to Table X, niobium is resistant to interaction with bismuth at temperatures up to 550^{o}C, but it is not resistant above the temperature limit as it exhibits dissolving effects interacting with bismuth at temperatures above 600^{o}C.

In liquid bismuth, pure niobium has performance characteristics similar to iron and tantalum but is a bit less corrosion resistant than molybdenum. It is more resistant to corrosion at temperatures below 750^{o}C.[47] In comparison with molybdenum, tungsten, tantalum, and titanium, pure niobium is characterized by the lowest melting point, the lowest thermal conductivity, the lowest strength and density, and the highest thermal expansion.

In comparison with pure niobium, niobium alloys have significantly improved physical properties, in particular higher resistance to neutron radiation damage. Because of better performance characteristics under nuclear reactor operation conditions, niobium alloys are extensively used as materials for fuel element cladding, reactor vessel components, shells and tubes of heat exchangers. They have also been identified as the preferred construction material for space power systems.[47] Niobium alloy C-103 is the typical material for rocket nozzles and jet exhaust nozzles because of its high strength and oxidation resistance at high temperatures. Among the considered niobium alloys, Nb-1%Zr alloy is a promising candidate for application as a cladding material in the ALM-FR design because it does not interact with lead as elevated temperatures. Physical properties of Nb-1%Zr alloy and Zr-2.5%Nb alloy are given in Table XI.[47,57]

TABLE XI

Physical Properties of Nb-1%Zr Alloy and Zr–2.5% Nb Alloy

Material	Zr-2.5%Nb	Nb-1%Zr
Alloy Composition	Nb - 0.025938 O - 0.001397 Zr - 0.972665	C – 0.000100 Fe – 0.000100 H – 0.000020 Hf – 0.000100 Mo – 0.000050 N – 0.000300 Nb – 0.984931 Ni – 0.000050 O – 0.000300 Si – 0.000050 Ta – 0.002000 W – 0.000500 Zr – 0.011499
Density (g/cm^3)	6.44	8.59
Modulus of Elasticity (GPa)	97.9	68.9
Heat Capacity (J/(kg·K))	285	270
Thermal Conductivity (W/(m·K))	17.1	41.9
Melting Point (^oC)	1840	2407

Silicon carbide (70.03% Si, 29.97% C) is a typical high temperature material. At high temperatures of about 900–1100^{o}C, it is characterized by such excellent performance characteristics as hardness and stiffness, strength and oxidation resistance, high thermal conductivity and low thermal expansion coefficient. Physical properties of SiC are presented in Table XII.[45,47]

TABLE XII

Physical Properties of SiC, Si-SiC and ZrC

Material	SiC		Si-SiC		ZrC	
Composition	70.03% Si, 29.97% C		84% SiC, 15% Si, 1% C		88.36% Zr, 11.63% C	
Density, g/cm^3	~3.2		3.1		6.4	
Melting Point (^{o}C)	2200		1400		2400-3530	
	T (^{o}C)		T (^{o}C)		T (^{o}C)	
Thermal Expansion (m/(m·^{o}C))	0-1700	4.4E-6	27–1480	9.18E-6	21-590	6.73E-6
Thermal Conductivity (W/(cm·^{o}C))	600 1000 1300	0.167-0.205 0.138-0.18 0.113-0.167	150 538 400-1000	0.54 0.389 0.84-0.251	0.205	

Because of its excellent characteristics at high temperatures, SiC has been taken into consideration as a potential candidate for application as a fuel element cladding in the ALM-FR design. Similar to SiC, siliconized silicon carbide Si-SiC (84% SiC, 15% Si, 1% C) may also be considered for application as a cladding material in the ALM-FR design. Its physical properties are given in Table XII.

Zirconium carbide (88.36%Zr, 11.63%C) is typically considered for applications as one of coatings in HTGR micro-particles. This material is highly resistant to chemical

attacks by corrosive liquids and gasses up to very high temperatures of thousands Kelvin. It is also used as a corrosion-resistant barrier protecting from hot ammonia, hydrogen, hydrochloric and molten metals.

As a result of long interaction with sodium, ZrC exhibits signs of slow oxidation due to interactions of sodium with zirconium. Physical properties of ZrC are summarized in Table XII.[45,47]

TABLE XIII

Corrosion Resistance of ZrC in Interactions with Liquid Metals

Liquid Metals	Corrosion Resistance		
	300°C	600°C	800°C
Bi	-	Poor	Poor
57%Bi, 25.2%In, 17.3%Sn	-	Poor	-
55%Bi, 44.5%Pb	Good	Limited	-
55.5%Bi, 25.8%Pb, 21.9%In	-	Poor	-
52%Bi, 32%Pb, 16%Sn	Good	Limited	-
Na, K, NaK	Good	Good	-
Pb	Good	Limited	Limited

Bismuth is more corrosive than lead and, in general, materials are more soluble in bismuth. The corrosion resistance of ZrC in interactions with various liquid metals is illustrated in Table XIII.[47]

Energy dependence of microscopic neutron absorption cross sections of ^{56}Fe, Si, Zr, V, and ^{93}Nb is illustrated in Fig. 14.[58-61] Among the considered materials, niobium has the highest neutron absorption cross section.

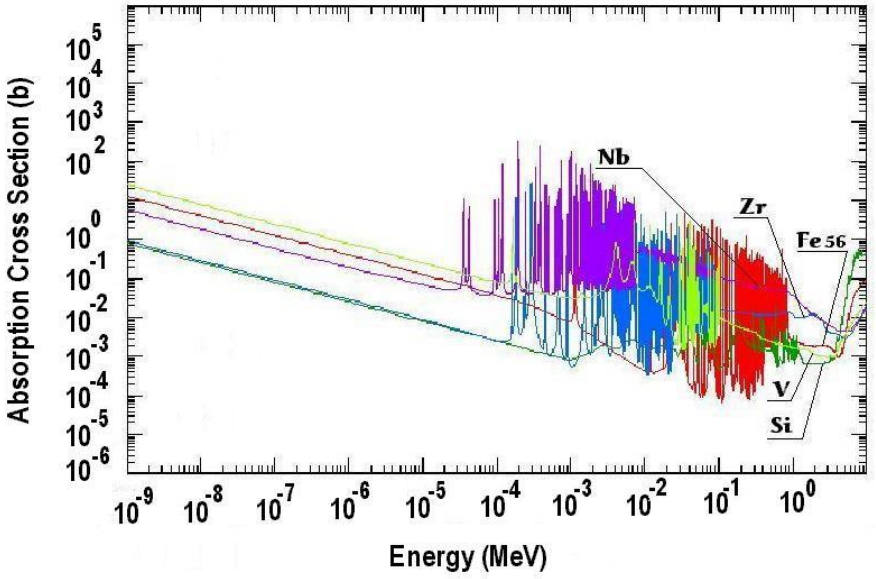

Fig. 14. Microscopic neutron absorption cross sections of ^{56}Fe, Si, Zr, ^{93}Nb, V.

Since nitride fuels are considered for use in the ALM-FR systems, nitride compounds of Zr have also been taken into consideration in the present study. Physical properties of ZrN are summarized in Table XIV.[57]

TABLE XIV

Physical Properties of ZrN

Composition	13.31% N, 86.69% Zr
Molecular Weight (g/mol)	105.231
Melting Point (^{o}C)	2960
Density (g/cm^{3})	7.09
Thermal Conductivity (W/(m·K))	25
Thermal Expansion Coefficient (m/m·^{o}C))	3.0E-3
Maximum Service Temperature (in Air) (^{o}C)	1650

Figure 15 illustrates the energy dependence of microscopic capture cross section for ^{14}N and ^{15}N in comparison with microscopic cross section of ^{12}C.[58-61] Since parasitic neutron capture must be minimized, carbon-based cladding seems to be more advantageous than nitrogen-based cladding. However, as it is shown in Fig 15, carbon-based cladding can be replaced with nitrogen-based cladding if the nitrogen is enriched with ^{15}N. The nitrogen-based cladding with increased content of ^{15}N offers significant reduction in parasitic neutron absorption within a reactor core. Furthermore, use of nitrogen-based cladding simplifies fabrication process for fuel elements with TRU-nitride fuels.

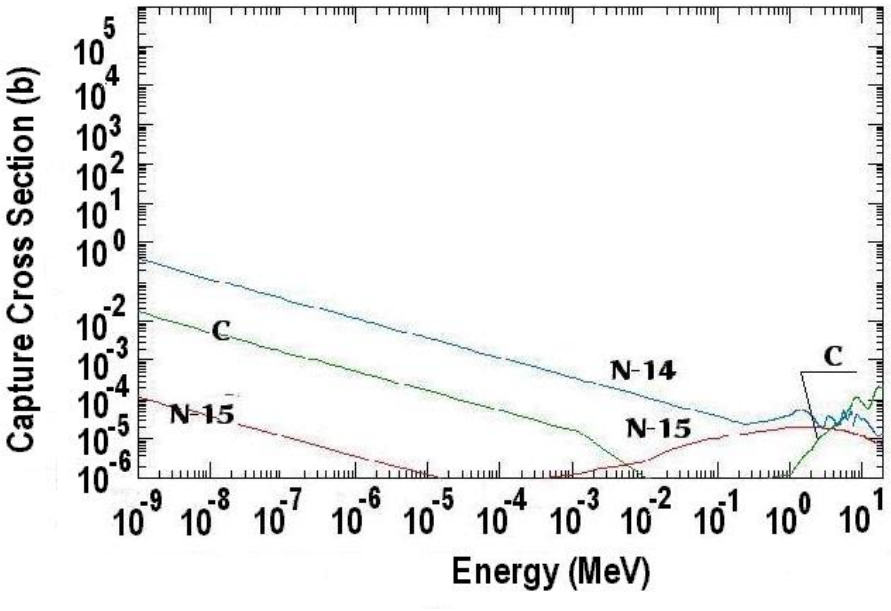

Fig. 15. Microscopic neutron capture cross sections of ^{14}N, ^{15}N, and ^{12}C.

Good physical and nuclear properties make vanadium very attractive as a structural material for use in LMFBR's. As illustrated in Fig. 14, vanadium has a low microscopic neutron absorption cross section. Similar to niobium, it has a good resistance to lead and lead-bismuth coolants at elevated temperatures up to 1200°C. In addition, it has a high melting point. Table XV summarizes the physical properties of VN.[57]

TABLE XV

Physical Properties of VN

Composition	21.57% N, 78.43% V	
Molecular Weight (g/mol)	69.949	
Melting Point (°C)	2050	
Density (g/cm^3)	6.13	
Boiling Point (°C)	3800	
Specific Heat (J/(kg·°C))	T (°C)	
	0	502.416
	300	531.724
	900	636.39
	1300	736.88
	1600	824.8
Thermal Expansion Coefficient (m/(m·K))	23-100	8.3E-6
	100-500	9.6E-6
	500– 900	10.4E-6
	900- 1000	10.9E-6
Thermal Conductivity (W/(cm·K))	100	0.31
	500	0.368

Unfortunately, properties of vanadium are extremely sensitive to small quantities of impurities. Furthermore, vanadium and its components are toxic and must be handled with care to avoid inhalation or ingestion.

Different alloys of molybdenum such as TZM and Mo/30W can also be considered for use as a fuel element cladding in the ALM-FR design. The interest in use

of molybdenum alloys is caused by the excellent thermal properties of these materials such as good thermal conductivity, low thermal expansion, low emissivity, corrosion resistance, high strength, ductility and manufacturability. Molybdenum provides corrosion resistance similar to tungsten.[56,57] It has good resistance to liquid metals such as bismuth, lithium, and sodium.

TZM (0.5% Ti, 0.08% Zr, 0.02% C, 99.0% Mo) is a strengthened molybdenum-based alloy. This material has excellent strength properties because of fine dispersed Ti-carbides in Mo-matrix. Comparing to pure molybdenum, TZM has several advantageous characteristics such as better high-temperature strength, better welding properties and creep resistance.[56,57] TZM offers twice the strength of pure molybdenum at temperatures over 1300^{o}C.

Another molybdenum alloy with advantageous properties is Mo-Tungsten (70% Mo, 30% W). It has a very high melting point, high strength at elevated temperatures, good thermal conductivity, and low thermal expansion.[57] It can be used at operational temperatures up to 2000^{o}C. The main disadvantage is that molybdenum alloys are very difficult to machine and manufacture. Forming must be done at very high temperatures and with special stress relieve procedures.

Microscopic neutron absorption cross sections of Mo, W, Nb and Zr are compared in Fig. 16.[58-61] It can be concluded that W has the highest absorption cross section that can cause significant reactivity losses by the end of reactor lifetime if this material is used as a cladding in ALM-FR system. However, it can be used as a structural material for radiation shield.

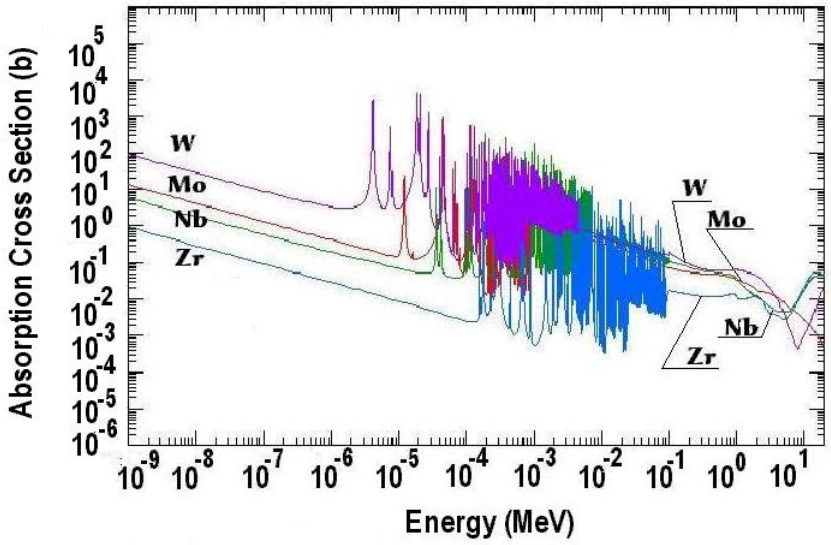

Fig. 16. Microscopic neutron absorption cross sections of Mo, ^{93}Nb, Zr and W.

Figure 17 compares vanadium with other candidates. This material has the lowest neutron absorption cross section in both thermal and fast neutron energy ranges.

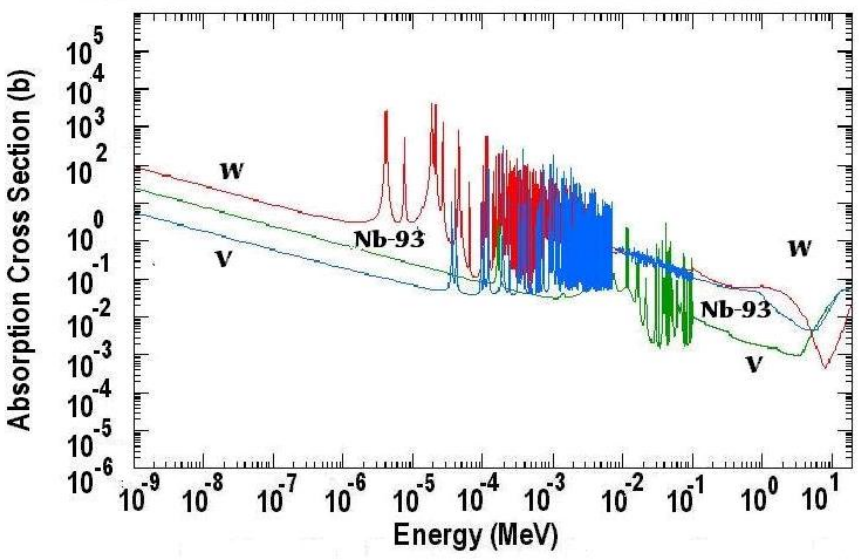

Fig. 17. Microscopic neutron absorption cross sections of V, W, and ^{93}N.

To facilitate proper selection of a cladding material for the ALM-FR design, operational temperature ranges have been analyzed for the considered cladding material candidates using performance data computed for the STAR-H2 configurations.[28,62] The permissible operational temperature ranges for the cladding material candidates are shown in Table XVI.

TABLE XVI

Permissible Operational Temperature Ranges for the Cladding Material Candidates

Operational Temperature	Low Temperature Limit (^{o}C)		Nominal Temperature (^{o}C)		Upper Temperature Limit (^{o}C)	
Radiation Damage (dpa)	0.1-10	10-50	0.1-10	10-50	0.1-10	10-50
Mo-W	800- 1000	800-1000	1000-1200	1000-1210	1200-1280	1210-1280
TZM	700-900	700-900	900-1110	900-1110	1110-1190	1110-1190
Ta-8W-2Hf	620-780	620-780	780-980	780-980	980-11050	980-1050
Nb-1Zr-0.1C	500-600	500-600	600-810	600-810	810-890	810-890
V-4Cr-4Ti	390-410	390-410	410-650	410-650	650-750	650-750
Ferritic Steel (ODS)	250-320	250-320	320-700	320-700	700-800	700-800
Ferritic/ Martensitic Steel (HT9)	180-250	220-270	250-500	270-500	500-580	500-580
SS316	-	-	50-580	350-570	580-650	570-600
Inconel 718	-		50-780	50-500	780-820	500-600
SiC	550-650	550-650	650-950	650-950	950-1020	950-1020

In the present study, final selection of a cladding material for the ALM-FR design has been made using the results of the performed reactor physics analysis and taking into account data presented in Table XVI. The reactor physics analysis of the ALM-FR design configurations with different cladding materials is discussed in the next section of this dissertation.

IV.D.2. Performance Characteristics of the ALM-FR with Different Cladding Materials

In this dissertation, detailed reactor physics analysis of the ALM-FR design configurations with different cladding materials have been performed under equilibrium cycle approximation using capabilities of the REBUS-3 computer code system as described in Chapter III. The baseline parameters of the ALM-FR design as an evolutionary modification of the STAR-H2 system are summarized in Table XVII.

TABLE XVII

Baseline Parameters of the ALM-FR Design

Core Thermal Power (MW_{th})	400
Fuel Residence Time (years)	15
Coolant	Pb
Core Diameter/Active Core (Heated Zone) Height (m)	2.5/1.99
Fission Gas Plenum Height (m)	0.50
Fuel Pellet Diameter (cm)	1.51
Fuel Density, (g/cm^3)	13.10
Cladding-Fuel Pellet Gap Thickness (cm)	0.0996
Gap Bond Material	Pb-Be
Cladding Thickness, (cm)	0.10
Fuel Pin Outer Diameter (cm)	1.905
Fuel Pin Triangular Lattice Pitch-to-Diameter Ratio	1.50
Number of Fuel Pins per Fuel Assembly	32
Fuel Assembly Hexagonal Lattice Pitch (cm)	16.147
Total Number of Fuel Pins in the ALM-FR Core	6940
Core-Wide Fuel Volume Fraction	0.252
Core-Wide Cladding Volume Fraction	0.0802
Core-Wide Bond Volume Fraction	0.0710
Core-Wide Coolant Volume Fraction	0.597
Core Fuel Mass (kg)	35300
Core Flow Area (m^2)	2.93
Number of Spacer Grids	3
Number of Support and Flow Distributor Plates Below Core	2
Plate Open Area Fraction	0.6
Core Coolant-to-Fuel Pin Volume Ratio	1.48
Reflector Region Thickness (cm)	14.86
Core Barrel Region Thickness (cm)	14.82
Effective Core Barrel Thickness (cm)	7.595
Axial Thermal Expansion Factor	1.00489
Radial Thermal Expansion Factor	1.00596

In the present reactor physics analysis targeting selection of a cladding material for the ALM-FR design, the performance characteristics of principal interest are the following:

- The burnup reactivity swing during reactor operation (difference between the core effective multiplication factors at the BOL and at the EOL);
- The average and peak discharge burnup levels;
- The peak discharge fast fluence;
- The power peaking factor variation during reactor operation (core lifetime).

The estimated performance characteristics of the ALM-FR design configurations, which have fuel pin claddings made of HT9 steel, Nb-1%Zr alloy and SiC, are summarized in Table XVIII.

According to the computational analysis, significant reactivity loss was observed by the end of fuel residence time in the ALM-FR design configuration with Nb-1%Zr alloy as a cladding material. To use this material as a cladding, other design modifications would be required in order to attain a positive reactivity gain within a single fuel loading.

Based on the thermal properties, compatibility with lead as a coolant, energy dependence of neutron absorption cross-sections and computational results presented for HT9 steel, Nb-1%Zr alloy and SiC in Table XVIII, SiC is the most promising candidate material among these compounds for use as a cladding in the ALM-FR design. Since it has the lowest neutron capture cross section in comparison with Nb and Zr, application of SiC as a cladding make it possible to achieve the most significant reactivity gain at the end of the fuel residence time in the ALM-FR core.

TABLE XVIII

Reactor Physics of the ALM-FR Designs with HT9, Nb-1%Zr, and SiC Claddings

Cladding Material	HT9	Nb-1%Zr		SiC	
Search for %Pu/HM	BOL	BOL	EOL	BOL	EOL
Capacity Factor (%)	80				
Heavy Metal Loading (kg)					
^{235}U	53.1	51.4	50.3	52.2	52.8
^{238}U	26536.5	25974.5	25433.6	26389.2	26701.0
^{239}Pu	-	3378.4	3886.1	2989.1	2696.5
^{240}Pu	-	206.4	237.4	182.6	164.7
^{241}Pu	-	10.9	12.5	9.7	8.7
^{241}Am	-	10.9	12.5	9.7	8.7
Total Fissile	-	3440.7	3948.9	3051.0	2758.0
Total HM	29632.0	29632.5	29632.5	29632.5	29632.5
Net Gain (kg/year) (Equilibrium Discharge - Equilibrium Loading)					
^{235}U	-	-1.4	-1.2	-1.6	-1.7
^{236}U	-	+0.3	+0.3	+0.4	+0.4
^{238}U	-	-120.2	-106.9	-148.0	-159.2
^{238}Pu	-	+0.2	+0.2	+0.3	+0.3
^{239}Pu	-	-14.3	-28.3	+5.9	+16.5
^{240}Pu	-	+14.4	+14.3	+21.1	+21.2
^{241}Pu	-	+0.9	+0.8	+1.6	+1.6
^{242}Pu	-	+0.1	+0.1	+0.2	+0.2
^{241}Am	-	+0.3	+0.3	+0.3	+0.3
Total Fissile	-	-14.8	-28.0	+5.9	+16.5
Total HM	-	-119.3	-120.0	-120.1	-119.8
Performance Characteristics					
Total Power (MWt)	400.00	400.00	400.00	400.00	400.00
Driver Power at BOL (MWt)	395.80	395.80	395.80	395.80	395.80
Driver Power Fraction at BOL (%)	98.95	98.77	98.91	99.12	99.05
Total Power Density, kW/liter	32.887				
Driver Power Density at BOL (kW/liter)	43.335	43.256	43.31	43.409	43.38
Driver Specific Power at BOL (kW/kgHM)	13.357	13.499	13.49	13.499	13.499
BOL Peaking Factor	1.71504	1.80310	1.80182	1.7313	1.72583
EOL Peaking Factor	1.70750	1.60363	1.55503	1.74761	1.8711
Peak Driver Power Density, kW/l	74.32	77.99	78.04	74.60	74.867
Discharge Burnup (MWd/kg)	57.48	57.08	57.37	57.53	57.41
Peak Fast Fluence (10^{23}n/cm^2)	3.00	2.9	2.69	2.54	2.69
Breeding Ratio	1.003	0.883	0.788	1.009	1.0642
BOL k-effective	1.000	1.000	1.093	1.000	0.941
EOL k-effective	1.020	0.950	1.000	1.0208	1.000
Reactivity Swing (%)	-2.030	+5.037	+8.976	-2.079	-5.918

Performance characteristics of the ALM-FR designs with SiC, ZrC, ZrN, VN and Nb-1%Zr claddings are summarized in Table XIX. The modeling has been performed assuming that ALM-FR system operates with the capacity factor of 90%. As emphasized above, use of SiC as a cladding material provides significantly higher reactivity gains at the end of fuel residence time that is achievable with other cladding material candidates.

TABLE XIX

Reactor Physics of the ALM-FR Designs with SiC, ZrC, ZrN, VN, Nb-1%Zr Claddings

Cladding Material	SiC	ZrC	ZrN	VN	Nb-1%Zr
Capacity Factor (%)	90				
Enrichment (%Pu/HM)	8.36	8.38	8.65	8.67	9.53
Heavy Metal Loading (kg)					
^{235}U	52.3	52.3	52.1	52.3	51.4
^{239}Pu	2962.8	2970.3	3067.7	2966.1	3390.3
Pu & Am	3164.4	3155.3	3274.8	3282.6	3608.4
Net Gain (kg/year) (Equilibrium Discharge – Equilibrium Loading)					
^{241}Am	+0.4	+0.4	+1.0	+0.5	+0.3
^{239}Pu	+7.2	+5.9	+1.1	+2.7	-15.4
Total HM	-134.8	-134.8	-134.7	-134.7	-134
Performance Characteristics					
BOL Peaking Factor	1.89	1.74	1.77	1.88	1.81
EOL Peaking Factor	1.83	1.76	1.69	1.9	1.6
Peak Driver Power Density, kW/l	587.6	545.5	550.31	594.65	559.21
Discharge Burnup (MWd/kg)	64.62	64.56	64.52	64.55	64.1
Peak Discharge Burnup (MWd/kg)	111.7	112.0	112.46	121.11	107.74
Peak Fast Fluence, (10^{23} n/cm^2)	2.8	3.07	3.05	3.03	3.31
Breeding Ratio	1.0073	1.0009	0.98	0.99	0.88
BOL k-effective	1.000	1.000	1.000	1.000	1.000
EOL k- effective	1.0246	1.020	1.0011	1.0053	0.946
Reactivity Swing (%)	-2.45	-1.99	-0.1	-0.53	+5.44

As illustrated in Table XIX, the highest values of power peaking factors occur for SiC and VN providing some design challenges to overcome or minimize this effect. Average discharge burnup is almost the same for all materials considered.

The peak fast fluence for cladding does not exceed its limiting value of 4.5 10^{23} n/cm^2 for any of the considered materials. According to the data presented in Table XVIII and Table XIX, the values of peak fast fluence fluctuate around 3.0 10^{23} n/cm^2 leaving substantial performance margins with respect to radiation damage effects.

Advantageous reactor physics characteristics of the ALM-FR system with SiC cladding after 15 years of operation on one fuel loading indicate possibility to prolong fuel residence time approaching reactor lifetime limit. High excess reactivity remaining in the system with SiC cladding offers possibility to extend reactor operation up to complete fuel consumption characterized by nearly zero excess reactivity. Since it allows complete utilization of the loaded fuel, this approach improves fuel utilization economics for the ALM-FR unit. In this case, the ALM-FR operation is limited by the performance characteristics of structural material under prolonged operation in radiation environment.

Furthermore, the estimated peak fast fluence in the ALM-FR system with SiC cladding, which is operated for 15 years, does not exceed limiting values set by the material performance characteristics with respect to radiation damage. Therefore, 15 years of operation is below the structural material performance limits and the ALM-FR system can be considered for longer fuel residence time.

As a result, because the ALM-FR system is intended for ultra long operation on one fuel loading, the reactor physics analysis of the ALM-FR performance has been

performed considering ultra long operation extending far beyond above-postulated 15 years of fuel residence time. Performance characteristics of the ALM-FR system with SiC cladding during ultra-long operation are summarized in Table XX.

TABLE XX

Fuel Residence Time and Performance Characteristics of the ALM-FR with SiC

Fuel Residence Time (years)	15		20		24		27	
Enrichment (%Pu/HM)	8.356		8.356		8.356		8.336	
Heavy Metal Loading (kg)								
^{235}U	52.3		52.3		52.3		52.3	
Pu & Am	3163.0		3163.0		3163.0		3163.0	
Net Gain (kg/year) (Equilibrium Discharge – Equilibrium Loading)								
Capacity Factor (%)	80	90	80	90	80	90	80	90
^{235}U	-1.6	-1.8	-1.5	-1.6	-1.4	-1.4	-1.3	-1.4
^{241}Am	+0.4	+1.9	+0.5	+0.6	+0.6	+0.7	+0.6	+0.8
^{239}Pu	+7.4	+7.2	+4.9	+4.3	+3.2	+2.3	+2.1	+1.0
Total HM	-119.8	-134.9	-120.0	-135.1	-120.1	-135.2	-120.2	-135.3
Performance Characteristics								
BOL Peaking Factor	1.89	1.89	1.89	1.89	1.89	1.89	1.89	1.89
EOL Peaking Factor	1.83	1.83	1.85	1.88	1.9	1.93	1.94	1.97
Peak Discharge Burnup (MWd/kg)	99.4	111.70	141.70	148.10	170.00	176.40	191.20	197.30
Peak Fast Fluence (10^{23} n/cm^2)	2.49	2.80	3.34	3.73	4.02	4.55	4.60	5.10
Breeding Ratio	1.017	1.0073	0.992	0.9817	0.976	0.971	0.965	0.955
BOL k-effective	1.000	1.000	1.000	1.000	1.000	1.000	1.000	1.000
EOL k-effective	1.025	1.025	1.022	1.018	1.016	1.009	1.009	1.001
Reactivity Swing (%)	-2.53	-2.45	-2.17	-1.82	-1.56	-0.94	-0.94	-0.12
Discharge Burnup (MWd/kg)								
Inner Core Region	60.11	69.23	84.89	97.67	105.43	121.08	121.08	138.80
Medium Core Region	60.64	69.89	83.70	95.44	102.56	116.86	116.86	133.10
Outer Core Region	56.04	62.59	73.4	81.99	87.12	97.34	97.35	108.80
Average over the Core Region	57.42	64.62	76.65	86.26	92.04	103.00	103.60	116.60

According to Table XX, use of SiC as a cladding material in the ALM-FR system allows to prolong reactor operation on one fuel loading up to 27 years. At the end of 27

years of fuel residence time, the ALM-FR performance characteristics reach their limiting values, which are set when the average burnup approaches 116 MWd/kg whereas the maximum burnup increases up to 197 MWd/kg. Due to power redistribution effects, the EOL peaking factor increases and attains 1.97 by the end of fuel residence time. The peak fast fluence reaches its maximum value of $5.1 \cdot 10^{23}$ n/cm^2. The breeding ratio becomes less than 1.0 after 20 years of irradiation and it drops below 0.95 after 27 years.

TABLE XXI

Fuel Residence Time and Performance Characteristics of the ALM-FR with ZrC

Fuel Residence Time (years)	15	20	24	27
Enrichment (%Pu/HM)	8.34	8.34	8.34	8.34
Capacity Factor (%)	90	90	90	90
Heavy Metal Loading (kg)				
^{235}U	52.3	52.3	52.3	52.3
Pu & Am	3155.3	3155.3	3155.3	3155.3
Total HM	29632.5	29632.5	29632.5	29632.5
Net Gain (kg/year) (Equilibrium Discharge – Equilibrium Loading)				
^{235}U	-1.7	-1.5	-1.4	-1.3
^{241}Am	+0.4	+0.5	+0.6	+0.7
^{239}Pu	+5.9	+3.2	+1.4	+0.2
Total HM	-134.8	-134.9	-135.0	-135.1
Performance Characteristics				
BOL Peaking Factor	1.74	1.74	1.74	1.74
EOL Peaking Factor	1.76	1.81	1.80	1.78
Peak Discharge Burnup (MWd/kg)	111.2	147.1	175.0	195.4
Peak Fast Fluence (10^{23} n/cm^2)	3.07	4.11	4.97	5.51
Breeding Ratio	1.0009	0.98	0.96	0.95
BOL k-effective	1.000	1.000	1.000	1.000
EOL k-effective	1.02	1.013	1.004	0.996
Reactivity Swing (%)	-1.99	-1.013	-0.40	+0.44
Discharge Burnup (MWd/kg)				
Inner Core Region	68.26	93.91	116.80	134.18
Medium Core Region	68.29	94.33	115.62	131.18
Outer Core Region	63.097	82.59	97.99	109.5
Average over the Core Region	64.56	86.17	103.48	116.47

Although offering lower reactivity gain during reactor operation compared to SiC, the use of ZrC as a cladding material in the ALM-FR system provides a more uniform power distribution in the core that results in a lower power peaking factor, as shown in Table XIX. Performance characteristics of the ALM-FR system with ZrC cladding during ultra-long operation are summarized in Table XXI. If ZrC is used as a cladding material, the available excess reactivity is consumed during 24 years of operation instead of 27 years as in the case of SiC.

IV.D.3. Selection of the Cladding Material for the ALM-FR Design

As was discussed in the preceding sections, based on the baseline ALM-FR design characteristics, extensive reactor physics studies have been performed for different cladding material candidates. Because of good compatibility with lead, high strength, resistance to oxidation at elevated temperatures, high thermal conductivity, and good thermal shock resistance, the following materials are taken into consideration: HT9, NB-1%Zr, SiC, ZrC, ZrN, V-alloys (VN, V-4Cr-4Ti), Mo-alloys (TZM, Mo-W). In this section, final selection of the cladding material for the ALM-FR system is made on the basis of the analysis.

The existing thermal limitations for the candidate cladding materials are summarized in Table XXII.[57,62] Using these data and the reactor physics characteristics obtained with REBUS-3, temperature distributions in the ALM-FR fuel pins with different cladding materials have been evaluated. The results of the performed fuel pin thermal performance analysis are given in Table XXIII.

TABLE XXII

Thermal Limitations for HT9, NB-1%Zr, SiC, ZrC, ZrN, VN, TZM and V-4Cr-4Ti

Material	Melting Point (^{o}C)	Allowed Temperature in Lead (^{o}C)	Thermal Conductivity (W/(m·K))
HT9	1420	-	24.6
Nb-1Zr	1840	1000	41.9
SiC	2200	650-950 (not to exceed 1000)	17.3
ZrC	3530	815	20.5
ZrN	2960	1200	25
VN	2050	-	36.8
TZM	-	900-1100	-
V-4Cr-4Ti	1890	400-600	30

To select the cladding material, thermal properties, reactor physics performance characteristics and compatibility with lead at elevated temperatures must be taken into account and analyzed for the cladding material candidates.

TABLE XXIII

Thermal Performance Characteristics of the ALM-FR Fuel Pin

Maximum Temperature Drop across Fuel (^{o}C)		221.8		
Maximum Temperature Drop across Gap (^{o}C)		75.2		
(U-Pu)N Fuel Melting Point (^{o}C)		2500		
ALM-FR Operation (years)		3	15	27
Maximum Temperature Drop across Cladding (^{o}C)	HT9	42.00	43.00	43.70
	Nb-1Zr	64.52	64.52	64.52
	SiC	66.81	66.81	69.66
	ZrC	51.81	52.42	52.97
	ZrN	43.20	43.20	43.20
	VN	31.41	31.86	31.19
Maximum Centerline Temperature (^{o}C)	HT9	1144.48	1154.30	1161.70
	Nb-1Zr	1193.06	1193.06	1193.06
	SiC	1214.55	1214.55	1235.50
	ZrC	1165.30	1170.46	1175.14
	ZrN	1163.50	1163.50	1163.50
	VN	1179.15	1185.63	1176.03
Maximum Cladding Temperature (^{o}C)	HT9	862.50	865.70	868.10
	Nb-1Zr	1164.77	1164.77	1164.77
	SiC	898.77	898.77	906.21
	ZrC	875.11	876.87	878.43
	ZrN	868.24	868.24	868.24
	VN	863.37	865.34	862.42

For a particular ALM-FR design configuration, the attained fuel discharge burnup should not exceed the maximum burnup value allowed for the applied fuel type. As was mentioned above, the maximum allowed burnup level for the TRU fuel is 150MWd/kg.[46] Figure 18 illustrates the difference between the fuel discharge (average) burnup level and the maximum burnup level. Whereas an average burnup may still be below the burnup limit, the corresponding maximum burnup level will exceed the allowed burnup level.

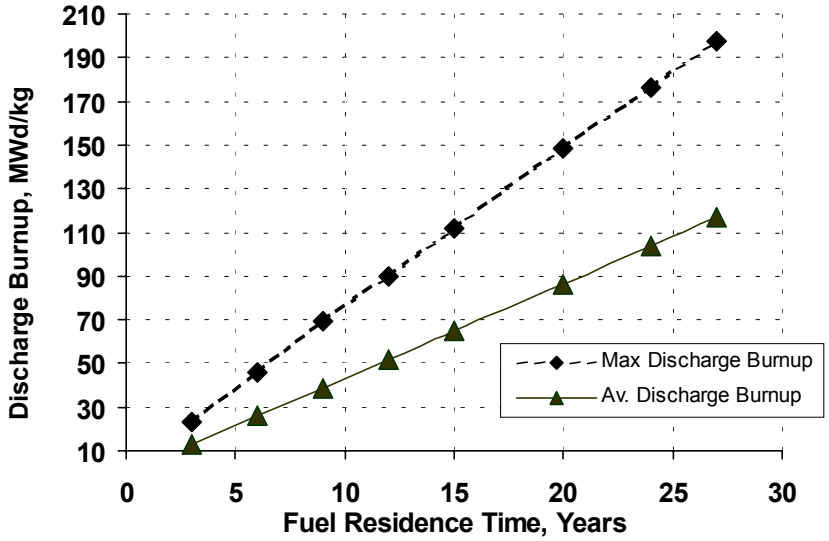

Fig. 18. Discharge (average) burnup and maximum discharge burnup in the ALM-FR system (SiC cladding, capacity factor 90%).

As emphasized above, the results of the reactor physics performance analysis with REBUS-3 indicate that HT9, SiC, ZrC, ZrN and VN are potential cladding materials for the ALM-FR long-lived core. From the effective multiplication factor

behavior shown in Fig. 19, it can be seen that a long-term operation during 15 – 27 years can be achieved with all cladding materials except Nb-1%Zr. The required fuel enrichment (defined by Pu weight fraction) varies from ~8 to ~9% depending on the cladding material that is much lower than in conventional fast reactors.

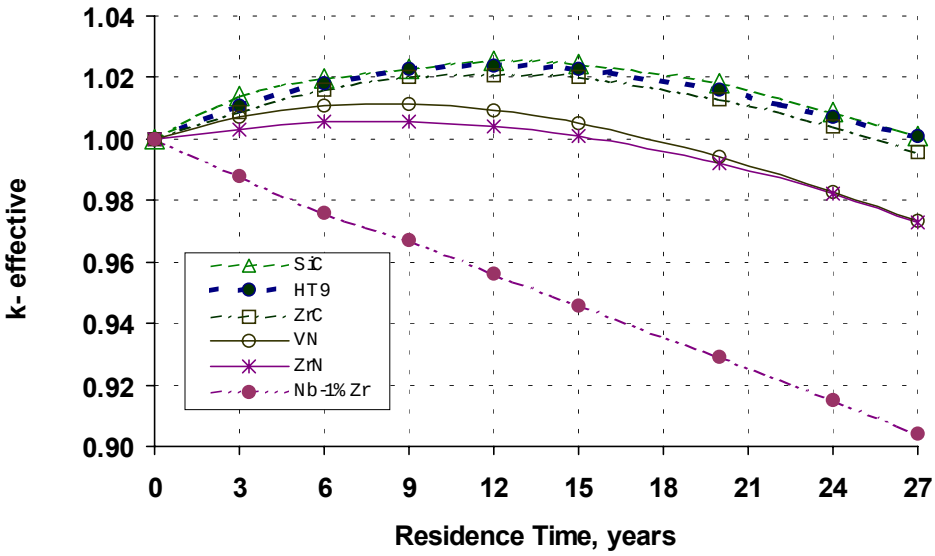

Fig. 19. Effective multiplication factor of the ALM-FR systems with different cladding materials as a function of fuel residence time.

HT9 steel has good compatibility with lead, low neutron absorption cross section, and high thermal conductivity. However, it has the lowest melting point (1420^{o}C) among the considered cladding material candidates. Thus, this material cannot be used as a cladding in the ALM-FR system, which is intended for high temperature hydrogen production.

Although unalloyed niobium has good resistance to attack by lead up to only 850^{o}C, Nb-1%Zr alloy exhibits resistance to attack by lead at temperatures above 2000^{o}C. However, despite of the attractive thermal properties, Nb-1%Zr is eliminated from the list of the cladding material candidates, because its presence in the ALM-FR core causes dramatic reactivity loss during reactor operation as shown in Fig. 19.

As the most promising candidate material for use as a cladding in the ALM-FR system, SiC (70.03% Si, 29.97% C) has the required hardness, stiffness, strength and oxidation resistance at elevated temperatures, high thermal conductivity and low coefficient of thermal expansion. In comparison with Nb and Zr, it has the lowest neutron capture cross section, and as a result, its use as a cladding in the ALM-FR system make it possible to achieve the largest reactivity gain during reactor operation that leads to the ultra-long operation up to 27 years on one fuel loading.

In case of SiC, the major concern is its limited compatibility with lead at elevated temperatures. However, it is experimentally confirmed that 815^{o}C can be considered as a reference nominal temperature at which SiC, ZrC as well as Si_3N_4 perform reliably as corrosion resistant ceramics that are compatible with high temperature lead. The temperature of 1000^{o}C is the reference temperature at which SiC has limited resistance to lead. Recent experimental studies provide evidence that the estimated allowed operational temperature for SiC in lead is up to 950^{o}C. It is anticipated that use of SiC as a cladding material would require additional experimental studies.

Alternatively, ZrC (88.36% Zr, 11.63% C) can be considered as a cladding material for the ALM-FR system but it cannot provide sufficient reactivity gain for more than 24 years of operation on one fuel loading. It has high resistance to chemical attacks

by corrosive liquids and gasses at very high temperatures, and has good resistance to lead at temperatures up to 816^{o}C. Zirconium is oxidized slowly in sodium, but has no reaction with molten salts. Compared with other materials from the list of cladding candidates, ZrC has the highest melting point and one of the highest thermal conductivities. These properties provide possibility to attain lower operational cladding temperatures and higher temperature margins under accident conditions.

Comparing physical properties of ZrN with properties of SiC and ZrC, it is noted that ZrN has a lower melting point than ZrC, but higher than SiC. The allowed operational temperature for ZrN in lead is 1200^{o}C, which is higher than for SiC (950 ^{o}C). Furthermore, ZrN has a higher thermal conductivity than SiC that allows lower cladding temperatures.

In the case of ZrN, the breeding ratio is less than 1.0 during the entire period of reactor operation up to 27 years. Consequently, the available excess reactivity is completely consumed during 15 years of operation. It is possible to mitigate reactivity loss if ZrN is enriched with ^{15}N. However, this will increase the cost of fuel fabrication.

On the basis of this analysis, it can be concluded that ZrN can compete with SiC as a cladding material for the ALM-FR system designed for 15 years of operation on one fuel loading, especially if an economic technology is established for enriching ZrN with ^{15}N. This possibility is very attractive because it might simplify fabrication of fuel pins with TRU-nitride fuel.

Vanadium is not used in thermal reactors because of its relatively large thermal cross sections. However, in a fast neutron spectrum it has a relatively low neutron-absorption cross-section and inelastic scattering cross section. In comparison with other

materials, the vanadium absorption cross section in a fast neutron spectrum is slightly higher than Si but is lower than HT9 and Zr.

Vanadium has a high melting point (2050^{o}C). Like niobium, vanadium has a good resistance to lead at elevated temperatures up to 1200^{o}C. Good thermal and reactor physics properties make this material very attractive as a cladding candidate for the ALM-FR system. Properties of vanadium alloys are sensitive to small quantities of impurities, and depend on fabrication methods. Among the considered materials, VN alloy has the highest thermal conductivity in comparison. Use of VN as a cladding material in the ALM-FR system results in decreasing cladding temperature. In the case of the ALM-FR design configuration with VN, the available excess reactivity is consumed during 15 years of operation.

Several alloys of molybdenum such as TZM (0.5% Ti, 0.08% Zr, 0.02% C, 99t% Mo) and Mo/30W (70% Mo, 30% W) can also be considered for use as a cladding in the ALM-FR system. The main advantage of these materials is that they have good resistance to liquid metals at elevated temperatures. However, comparing absorption cross sections of W and Mo with absorption cross sections of Nb and Zr, it can be concluded that W and Mo have the highest absorption cross sections which result in significant reactivity losses during reactor operation. Because of the high parasitic neutron absorption, Mo-alloys are not suitable for use as a cladding materials in the ALM-FR systems. However, they can efficiently be used in the ALM-FR shielding components and structures.

Figure 20 shows behavior of peak fast fluence as a function of average discharge burnup attained in the ALM-FR system. It can bee seen that the highest value of peak

fast fluence occurs for HT9 steel whereas the lowest peak fast fluence occurs for SiC. As can be seen from Fig. 18, the average discharge burnup of 60-65 MWd/kg corresponds to 15 years of fuel residence time, and 100-110 MWd/kg corresponds to 27 years of fuel residence time.

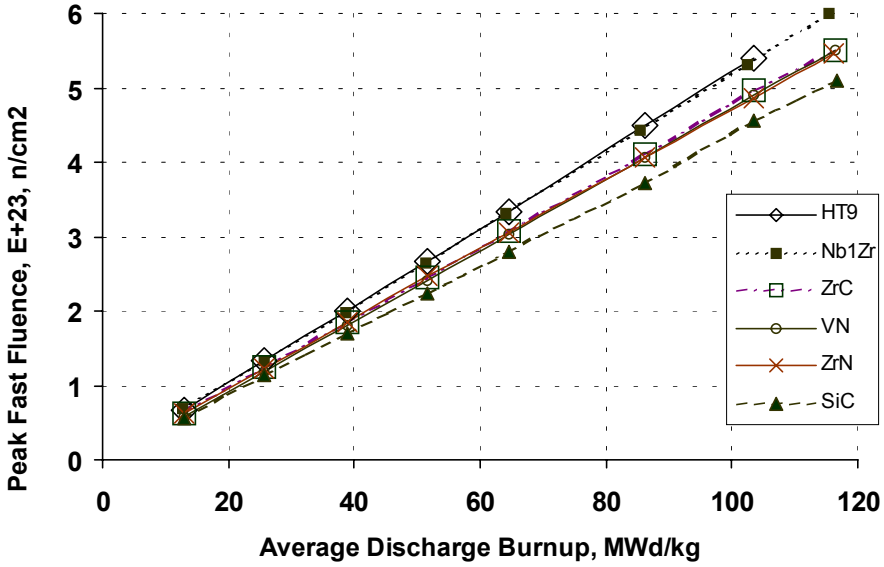

Fig. 20. Peak fast fluence in the ALM-FR as a function of average discharge burnup.

As a result of the detail analysis of thermal properties of cladding material candidates and the reactor physics analysis of the ALM-FR system with different cladding materials, it can be concluded that SiC, ZrC, ZrN, and VN can be used as cladding materials for the ALM-FR system. Among the selected material candidates, SiC has the most promising characteristics with respect to thermal performance and reactor physics of the ALM-FR system. For the remainder of this dissertation, the ALM-FR systems will be assumed to have fuel pins with SiC cladding.

CHAPTER V

CONFIGURATION OPTIMIZATION OF THE ALM-FR CORE

This chapter deals with the design and performance of the ALM-FR core. It presents the results of the configuration optimization analysis. The set of optimization studies have been performed in order to identify the reactor core configurations allowing autonomous long-term operation on one fuel loading.

V.A Internal Heterogeneous Blanket Configurations for the ALM-FR Core

In this dissertation, a detailed optimization of the ALM-FR core has been performed to further improve reactor performance characteristics and to identify core configurations allowing autonomous long-term operation on one fuel loading. Application of internal heterogeneous blanket is assumed as a design solution that makes it possible to flatten power density distribution in the ALM-FR core.

The optimized number of blanket assemblies and the corresponding blanket core configurations with improved performance characteristics are obtained as the result of the analysis. As will be discussed and illustrated later, the core layout optimization makes it possible to increase the achievable discharge burnup level and to improve the fluence-to-burnup ratio for the ALM-FR system.

Core layouts with various internal blanket locations were taken into account in the optimization studies. Figure 21 shows the two most promising configurations of the ALM-FR core layouts with internal heterogeneous blanket.

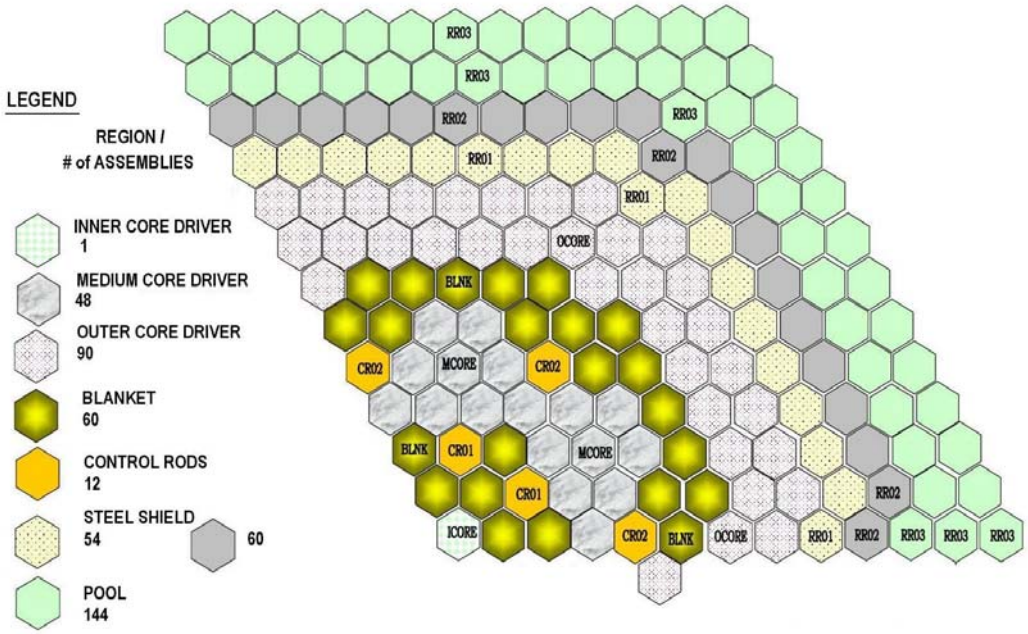

Configuration A.

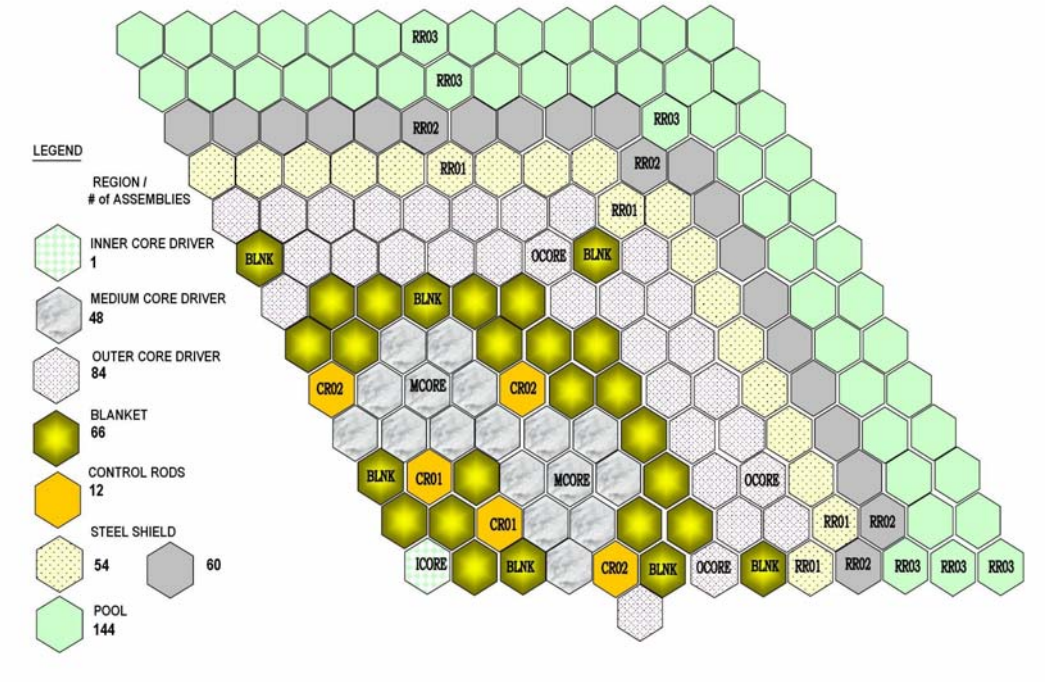

Configuration B.

Fig. 21. Optimized ALM-FR core configurations with internal heterogeneous blanket.

In the configuration A of the ALM-FR core, blanket assemblies are located in the second, third, sixth and seventh rings. The total number of blanket assemblies in this core layout is 60. The inner core and medium core driver pins have the same plutonium enrichment whereas plutonium enrichment of the outer core region is about 50% higher.

In configuration B of the ALM-FR core, the blanket assemblies are loaded in the second, third, sixth, seventh, and eighth rings. The total number of blanket assemblies in the core is 66 instead of 60 of the configuration A. However, as in the configuration A, the inner core and medium core driver pins have the same plutonium enrichment whereas the outer core region consists of the driver pins with about 50% higher plutonium enrichment.

In addition to the variation of the internal blanket configuration in the ALM-FR core, two different blanket pin designs have been considered. The outer diameter of blanket pins is 1.905 cm for the optimized configurations A and B. For the configurations denoted AA and BB, the outer diameter of blanket pins is 2.049 cm. The arrangements of blanket assemblies in the configurations AA and BB are the same as in the configurations A and B, respectively. Due to differences in blanket pin diameters, the region-wise distributions of optimized plutonium enrichment are different for pairs of the ALM-FR core configurations A and AA, and B and BB.

For the purposes of comparison, the design and performance characteristics of the optimized configurations A and AA, and B and BB are summarized in Table XXIV together with the corresponding characteristics of the configuration without blanket. According to the results of the analysis, the number of blanket assemblies in the ALM-FR core is limited by the maximum temperatures attained in the driver pins.

TABLE XXIV

ALM-FR System (SiC, 15 years, 90% Capacity) with Internal Heterogeneous Blanket

ALM-FR Core Layout	No Blanket	Internal Heterogeneous Blanket			
Optimized Configuration	-	A	AA	B	BB
Driver Pin Enrichment (%Pu/HM)					
Inner Core Region	8.36	12.50	11.91	13.14	12.60
Medium Core Region	8.36	12.50	11.91	13.14	12.60
Outer Core Region	11.70	17.50	17.87	18.40	18.90
Driver Fuel Pin Dimensions					
Outer Diameter (cm)	1.905				
Fuel Volume Fraction	0.247657				
Cladding Volume Fraction	0.078858				
Coolant Volume Fraction	0.666785				
Blanket Fuel Pin Dimensions					
Outer Diameter (cm)	N/A	1.905	2.049	1.905	2.049
Fuel Volume Fraction	N/A	0.247657	0.302152	0.247657	0.302152
Cladding Volume Fraction	N/A	0.078858	0.097848	0.078858	0.097848
Coolant Volume Fraction	N/A	0.666785	0.600000	0.666785	0.600000
Performance Characteristics					
BOL k-effective	1.000	1.000	1.000	1.000	1.000
EOL k-effective	1.0246	1.008	1.012	1.013	1.0185
BOL Peaking Factor	1.89	1.71	1.73	1.77	1.79
EOL Peaking Factor	1.83	1.81	1.75	1.84	1.78
BOL Power Splitting (%)					
Driver Pins	99.4	94.89	94.44	94.21	93.64
Blanket Pins	N/A	3.85	4.32	4.59	5.19
EOL Power Splitting (%)					
Driver Pins	99.4	76.68	74.25	75.14	72.66
Blanket Pins	N/A	22.4	24.88	23.96	26.49
Average Discharge Burnup (MWd/kg)					
Driver Pins	64.62	79.82	78.5	82.17	80.73
Blanket Pins	N/A	27.98	25.25	28	25.3
Peak Discharge Burnup (MWd/kg)	111.7	117.0	115.0	126.0	123.0
Peak Fast Fluence (n/cm^2)	2.8 E+23	2.62 E+23	2.56 E+23	2.70 E+23	2.60 E+23
Core Breeding Ratio	1.0073	1.0132	1.039	1.0078	1.034
Reactivity Swing (%)	-2.45	-0.76	-1.198	-1.27	-1.84
Number of Driver Pins in the Core	6940	4848	4848	4638	4638
Number of Blanket Pins in the Core	N/A	2092	2092	2301	2301
Number of Inner Core Driver Assemblies	13	1	1	1	1
Number of Medium Core Driver Assemblies	48	48	48	48	48
Number of Outer Core Driver Assemblies	138	90	90	84	84
Number of Blanket Assemblies	N/A	60	60	66	66
Number of Control Rod Locations	12	12	12	12	12
Number of Reflector Locations	54	54	54	54	54
Number of Core Barrel Locations	60	60	60	60	60
Max. BOL Fuel Temperature (Driver) (^{o}C)	1213.8	1325.4	1329.8	1362.9	1226.6
Max. EOL Fuel Temperature (Driver) (^{o}C)	1195.4	1240.7	1206	1259.0	954.6
Max. BOL Clad Temperature (Driver) (^{o}C)	898.5	938.10	939.7	951.4	954.6
Max. EOL Clad Temperature (Driver) (^{o}C)	892	908.04	895.7	914.6	903.1

V.B. Selection of the Internal Heterogeneous Blanket for the ALM-FR Design

As emphasized above, the development of the ALM-FR concept is aimed towards achievability of a fully autonomous, sustainable operation during the entire reactor lifetime. The targeted reactor lifetime-long operation without refueling allows the system to attain self-consistency in a single power unit.

To maintain ultra-long term, fully autonomous, sustainable operation on one fuel loading, the ALM-FR system should have near-zero burnup reactivity swing with minimized reactivity and power density fluctuations. Application of the internal heterogeneous blanket enables enhanced self-regulation capability by providing efficient internal breeding at rates that are sufficient for self-feeding but limited with respect to new fissile material buildup at the end of reactor lifetime. The detailed optimization studies discussed above are performed under the requirements to reduce power peaking factors for the ALM-FR core configurations, to maximize the achievable fuel burnup levels, and to maintain minimized reactivity swing due to fuel depletion.

According to the analysis, during reactor operation the maximum of the power density distribution shifts from the peripheral regions of the ALM-FR core to its center. The effect is manly due to the specific distribution of plutonium content in the fresh ALM-FR core that is chosen so that it yields flatten power density distribution. As shown in Table XXIV, to flatten power density distribution in the ALM-FR core, the outer core regions have about 50% higher plutonium enrichment than medium and central regions. The spatial shifting of power density maximum in the optimized ALM-FR core configurations A and B is illustrated in Fig. 22 and Fig. 23, respectively.

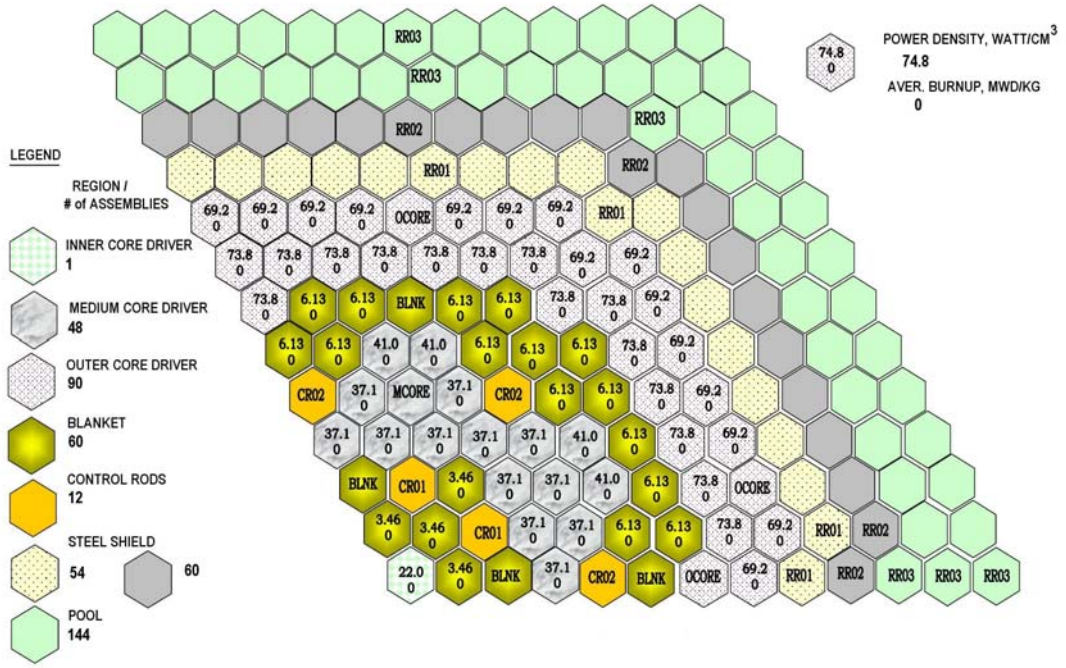

Beginning of the ALM-FR core life.

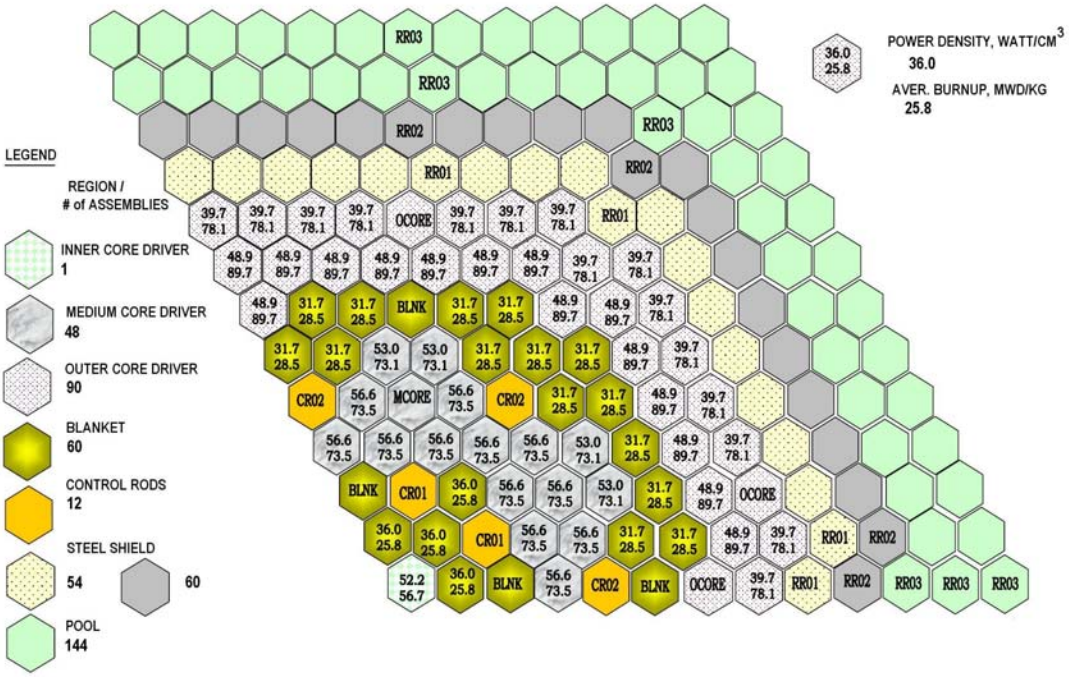

End of the ALM-FR core life.

Fig. 22. Power density distribution in the optimized ALM-FR core configuration A.

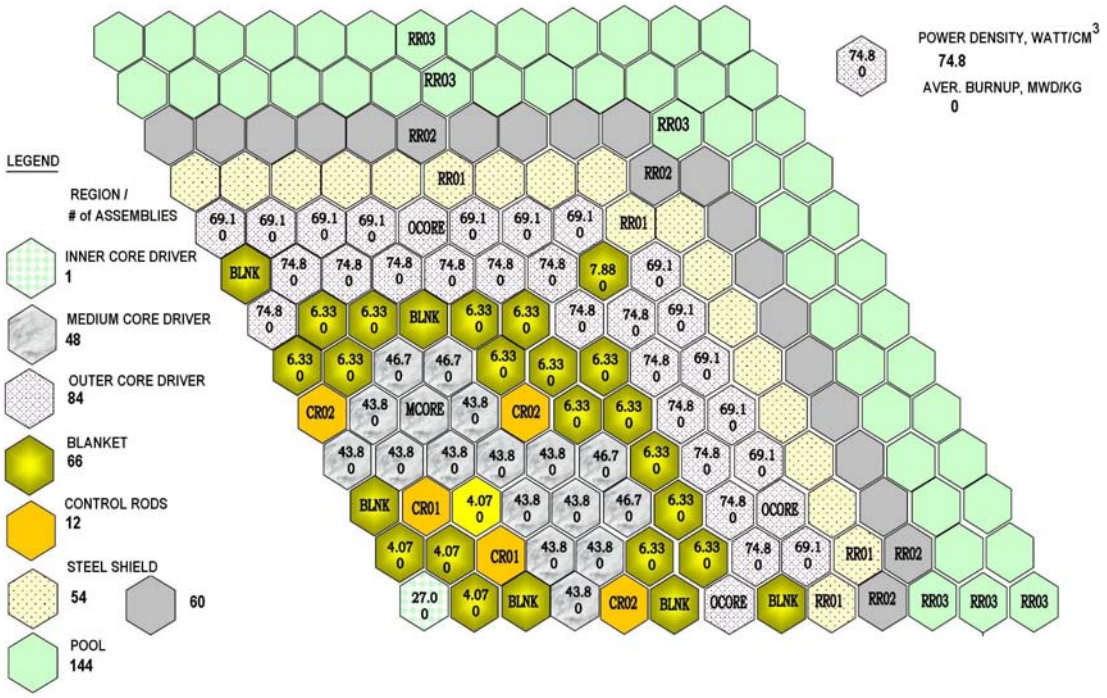

Beginning of the ALM-FR core life.

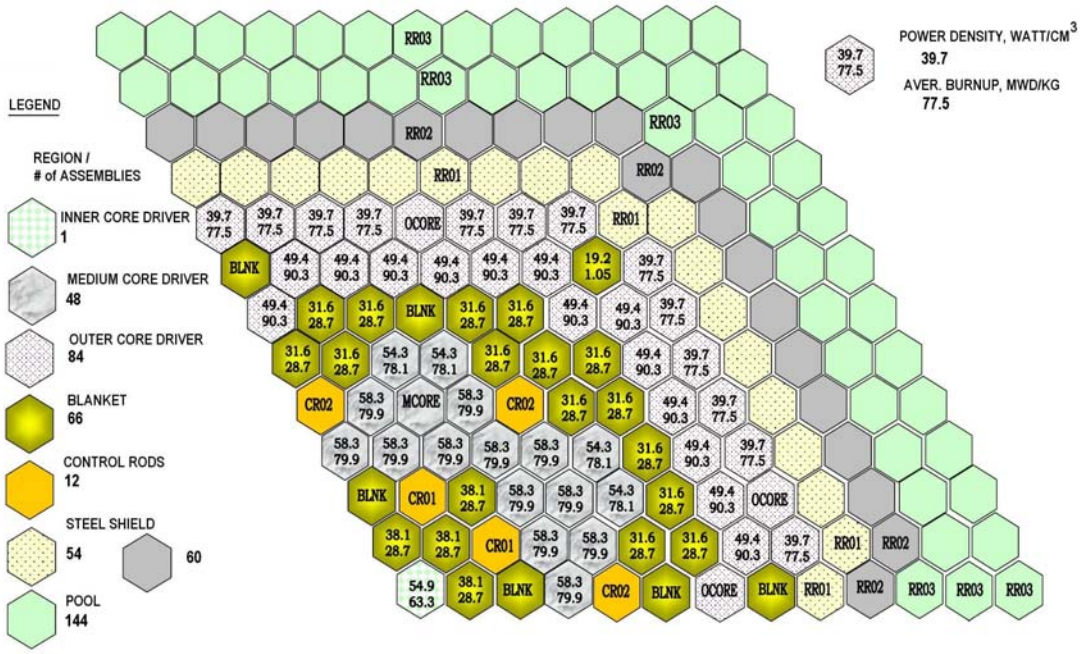

End of the ALM-FR core life.

Fig. 23. Power density distribution in the optimized ALM-FR core configuration B.

According to Fig. 22 and Fig. 23, both optimized configurations A and B demonstrate similar behavior of power density distribution as a function of fuel residence time. Power shift from the outer core regions to the inner core regions and from driver pins to blanket pins.

The spatial shifting of power density maximum results in the pendulum effect for the ALM-FR core peaking factors. The ALM-FR core configurations optimized to have significantly decreased BOL power peaking factors may have much higher EOL peaking factors. Conversely, the requirement to minimize EOL peaking factors results in the maximized BOL values.

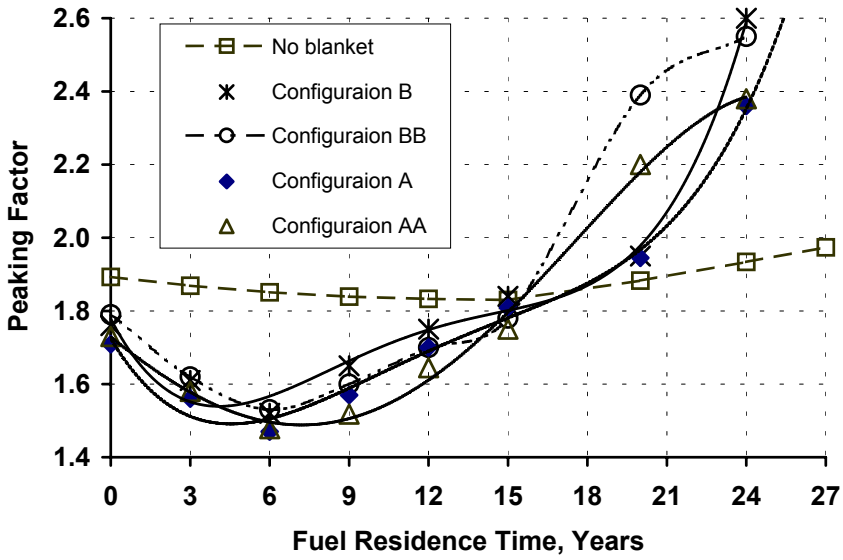

Fig. 24. Power peaking pendulum effect in the optimized ALM-FR cores.

The pendulum effect observed for the optimized ALM-FR core configurations is illustrated in Fig. 24. The effect is not pronounced for the configuration without blanket

but is very important for the optimized core configurations with internal heterogeneous blanket.

The addition of the internal heterogeneous blanket and the specific selection of the BOL fissile material distribution to flatten power density in the ALM-FR core decreases the power peaking factors from average values of about 1.85 for the ALM-FR cores without blanket to average values of about 1.77 for the cores with internal heterogeneous blanket. The average values of peaking factors for the ALM-FR core configurations are higher than those usually considered for fast reactors with 3 years refueling, but they are relatively reasonable for fast spectrum systems designed for long-term operation on one fuel loading.

High values of power peaking factors lead to increased cladding and fuel temperatures. Furthermore, due to spatial power shifting with fuel irradiation, the maximum cladding temperature varies with burnup and shifts within the ALM-FR core. The maximum cladding temperature at the EOL for both cases is lower than for BOL. For the optimized configuration A the cladding temperature drops from 938^{o}C to 908^{o}C. Analogously, for the optimized configuration B the cladding temperature drops from 950^{o}C to 914^{o}C.

The effect becomes significant only after the addition of internal heterogeneous blanket. Because of power shifting from driver pins to blanket pins during reactor operation, in the ALM-FR core the maximum cladding temperatures remain within the allowed operational limits even with elevated power peaking factors.

Figure 25 shows the average discharge burnup levels in the ALM-FR cores as a function of the attained peak fast fluence. The average discharge burnup is significantly

increased for the configurations with internal heterogeneous blanket in comparison with the cores without blanket. The increase of the average discharge burnup does not result in the values of peak fast fluence that exceed material performance limits.

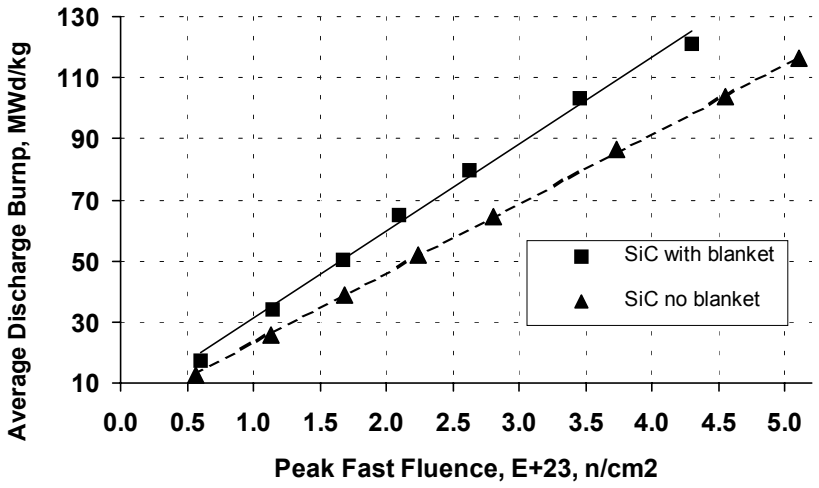

Fig. 25. Burnup levels in the ALM-FR cores with and without internal blanket.

The attainable burnup levels in the optimized ALM-FR core configurations are shown in Fig. 26. The optimized configuration B provides the possibility to attain larger average burnup levels of about 82MWd/kg in comparison with the burnup of about 80MWd/kg attained in the configuration A. Configurations BB and A give almost the same values of discharge burnup. Configuration AA has the lowest average discharge burnup among the configurations with the internal heterogeneous blanket.

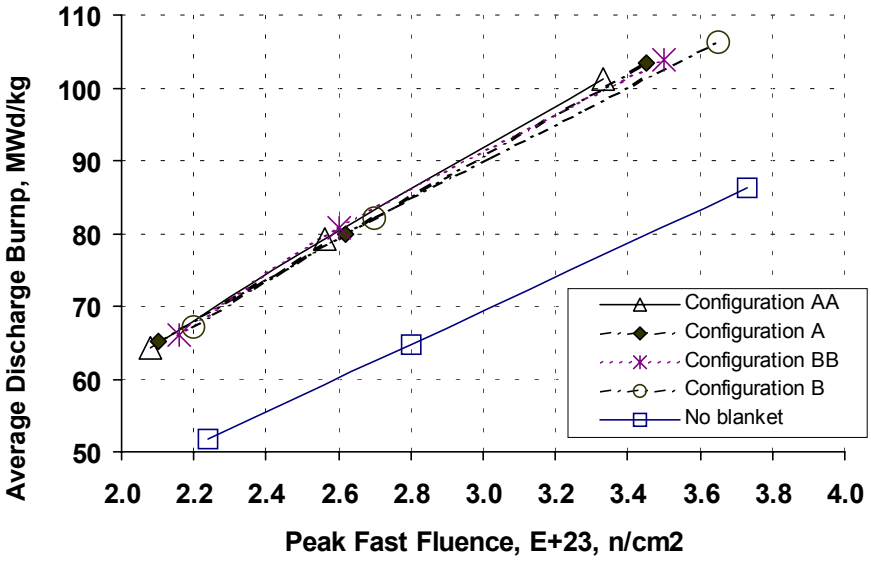

(a) Peak fast fluence scale

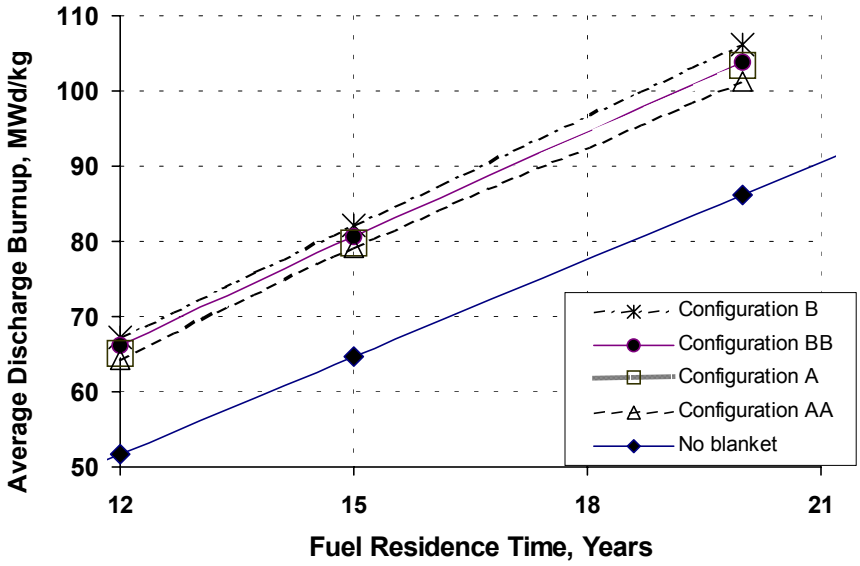

(b) Fuel residence time scale

Fig. 26. Burnup levels in the optimized ALM-FR cores with internal blanket.

Thermal analysis shows that the configuration B yields high cladding temperatures in the driver pins that may exceed the allowed operational temperature of 950^{o}C for SiC cladding in lead. Use of this configuration in the ALM-FR design requires additional studies addressing safety issues due to elevated temperatures. On the contrary, the ALM-FR core configuration A is characterized by a larger safety margin with respect to the allowed operational temperature.

Figure 27 shows the relationship between the average and maximum discharge burnup levels in the ALM-FR core. Due to the initial distribution of the fissile material and the power shifting with burnup, addition of the internal heterogeneous blanket increases the average discharge burnup without substantial increase of the corresponding maximum discharge burnup.

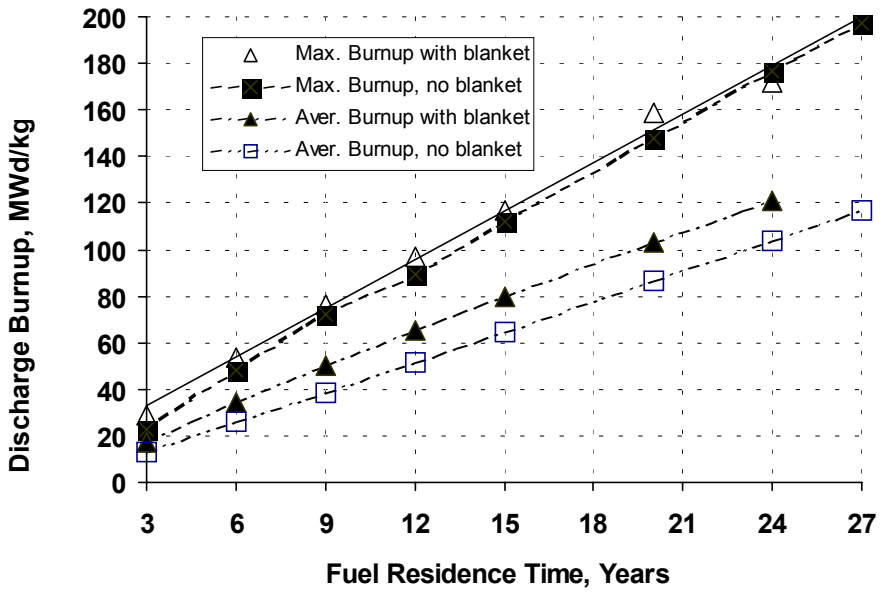

Fig. 27. Average and maximum burnup levels in the ALM-FR with internal blanket.

The largest values of the peak fast fluences in the ALM-FR cores are observed for configurations without internal heterogeneous blanket. As shown in Fig. 28, for 15 years of operation, for example, the peak fast fluence in the ALM-FR core without internal heterogeneous blanket reaches the largest value of 2.8E+23n/cm^2, whereas the corresponding lowest peak fast fluence of 2.5E+23n/cm^2 is observed for the optimized configuration AA with internal heterogeneous blanket.

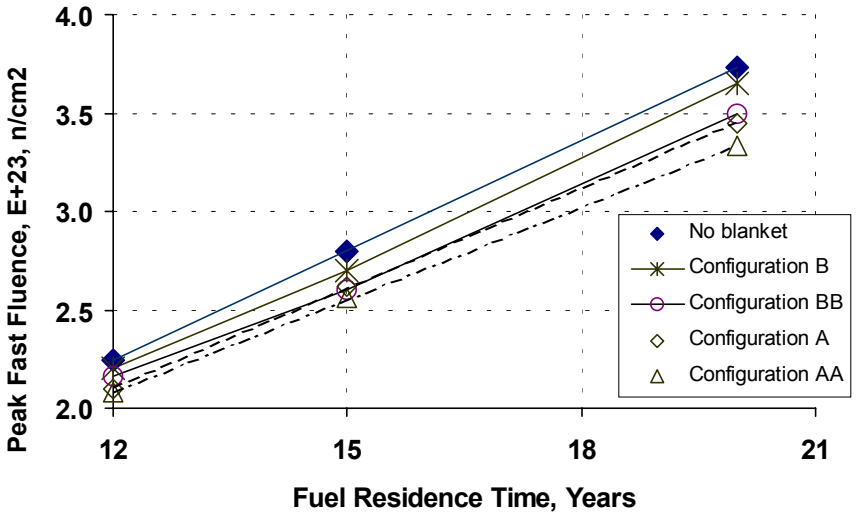

Fig. 28. Peak fast fluences in the ALM-FR cores.

The number of internal blanket pins in the ALM-FR core is optimized to increase average discharge burnup up to 80MWd/kg. Further increase of number of blanket pins is limited by the corresponding values of power peaking factors that yield cladding temperatures that are too high and exceed the thermal limits for the materials.

The behavior of the effective multiplication factor for the considered ALM-FR core configurations with and without blanket is shown in Fig. 29. Although all configurations allow long-term operation on one fuel loading, the optimized configurations with internal heterogeneous blanket offer the possibility to maintain minimized reactivity swing in the ALM-FR core during operation. The optimized ALM-FR core configuration A has the lowest reactivity swing during operation among the considered configurations. This configuration may allow autonomous operation on one fuel loading up to 24 years.

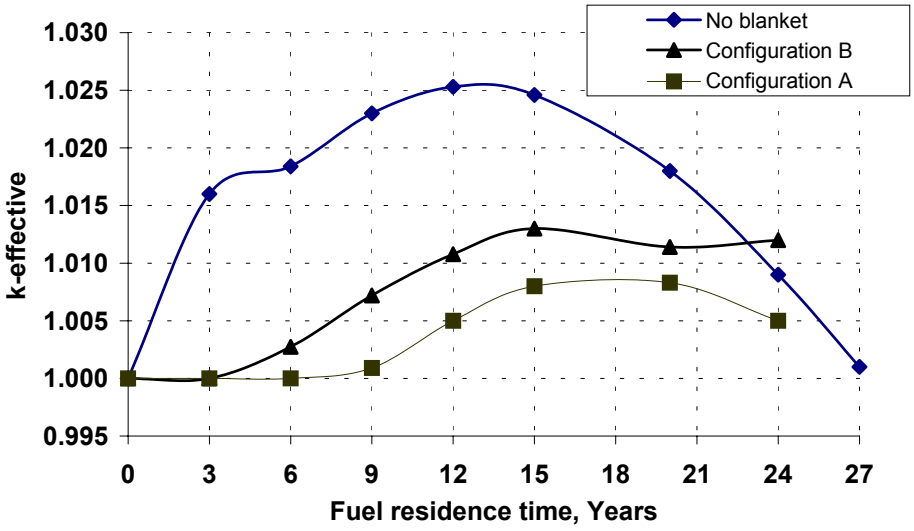

Fig. 29. Multiplication in the ALM-FR cores with and without internal blanket.

As a result of the analysis performed here, it can be concluded that both optimized configurations A and B of the ALM-FR core have promising characteristics and are chosen for the further analysis and development in this study.

CHAPTER VI

DYNAMICS AND SAFETY OF THE ALM-FR DESIGN

Together with the characteristics discussed and analyzed in the preceding chapters, the calculated reactivity feedback coefficients define the physics of the ALM-FR system. In this dissertation, different kinetic parameters and responses to a variety of perturbations have been taken into account. Considering the optimized ALM-FR core configurations A and B, the reactivity feedback coefficients are computed for the entire reactor lifetime including the BOL and EOL points.

The following reactivity coefficients and kinetic parameters have been estimated for the optimized ALM-FR configurations:

- Reactivity feedback coefficients with respect to radial core expansion;
- Reactivity feedback coefficients with respect to axial fuel expansion;
- Reactivity feedback coefficients with respect to axial fuel and structure expansion;
- Doppler reactivity coefficients;
- Coolant void worth;
- Effective delayed neutron fraction;
- Neutron generation time.

During normal operation and off-normal transients changes in reactor core dimensions may occur as a result of temperature variations. For example, when the coolant inlet temperature increases, fuel elements expand in the axial direction whereas the structure expands radially causing overall radial core expansion.

In the analysis, the reactivity coefficients due to radial core expansion are estimated assuming motion of the active core radial boundary associated with a 1% uniform pitch expansion. To calculate the effect, the number densities of solid materials were consistently decreased by a factor of $1/(1.01)^2$ but the coolant density was kept unchanged.

Consequently, the radial core expansion reactivity coefficient is determined by the following expression:

$$\alpha_R = \frac{1}{\overline{\beta}_{eff}} \cdot \left(\frac{1}{\Delta R} \cdot \frac{k_2 - k_1}{k_1 \cdot k_2} \right), \tag{19}$$

where α_R is the radial core expansion reactivity coefficient (\$/cm); ΔR is the effective core radius variation (cm); $\overline{\beta}_{eff}$ is the effective delayed neutron fraction; k_1 and k_2 are the effective multiplication factors of the ALM-FR core configurations calculated for the nominal case with unchanged dimensions and for the case with radially expanded dimensions respectively.

For configurations A and B, the calculated reactivity coefficients with respect to radial core expansion are shown in Fig. 30. Radial expansion of the ALM-FR core leads to a negative reactivity effect. This effect is more pronounced for the optimized configuration B that has fewer driver pins in comparison with the configuration A. However, for both configurations the radial core expansion coefficient remains negative during the entire reactor operation.

The observed differences in the radial core expansion coefficients between two configurations are due to geometrical and reactor physics effects. As is shown in Fig. 30,

after the first seven years of reactor operation the core composition becomes more uniform and the geometrical effects begin dominating reactor physics effects.

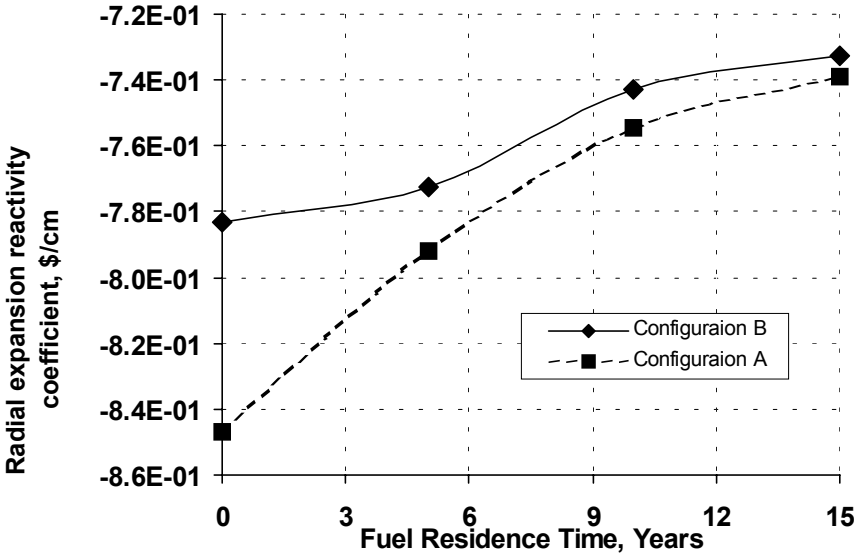

Fig. 30. Radial core expansion reactivity coefficients of the ALM-FR configurations.

With increasing coolant temperature in the core, fuel and structure temperatures also increase. This may occur during the rise to a full power operation or in a power transient. Increasing fuel temperatures cause radial and axial fuel expansion.

Radial fuel expansion does not have an influence on the reactivity effect describe above due to radial core expansion. The radial core expansion is governed primarily by structure and support material expansion but not fuel radial expansion.

The axial fuel expansion due to increasing temperature has significant impact on the overall core reactivity variation. In this dissertation, the axial fuel expansion reactivity coefficient is estimated using the following expression:

$$\alpha_H = \frac{1}{\overline{\beta}_{eff}} \cdot \left(\frac{1}{\Delta H} \cdot \frac{k_2 - k_1}{k_1 \cdot k_2} \right), \tag{20}$$

where α_H is the axial fuel expansion reactivity coefficient (\$/cm); ΔH is the effective core height variation (cm); $\overline{\beta}_{eff}$ is the effective delayed neutron fraction; k_1 and k_2 are the effective multiplication factors of the ALM-FR core configurations calculated for the nominal case with unchanged dimensions and for the case with axially expanded dimensions respectively.

Although axial neutron leakage is not affected by axial fuel expansion, the radial neutron leakage may increase significantly due to increasing migration areas and fuel height. These effects result in a negative reactivity feedback at the beginning of power transients causing temperature increases in the core. The axial fuel expansion reactivity coefficients of the ALM-FR core configurations are shown in Fig. 31.

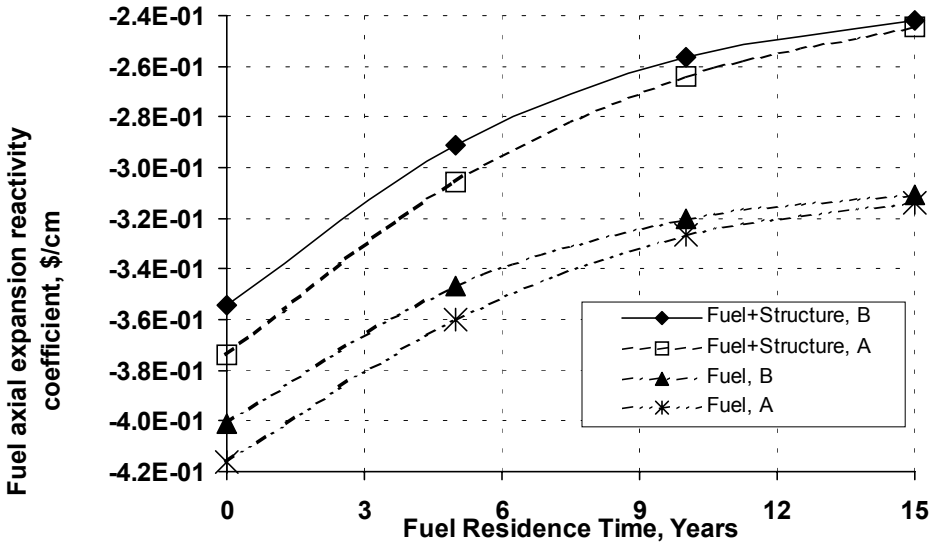

Fig. 31. Axial fuel expansion reactivity coefficients of the ALM-FR configurations.

It is unclear whether the fuel expands alone or together with the cladding and other structural components in the core. To account for both variations, the axial fuel expansion reactivity coefficients have been estimated assuming axial expansion of fuel only and with the corresponding expansion of the cladding and structure. As shown in Fig. 31, the structure has a small positive contribution to the axial fuel expansion reactivity effect if it expands together with fuel.

The negative axial fuel expansion coefficient is smaller for the core configuration A that has more driver pins. Analogous to the radial core expansion reactivity coefficient, the difference is caused by differences in geometrical characteristics and reactor physics of the optimized configurations. After the first seven years of operation, the core composition becomes more uniform and the difference between the core configurations becomes smaller, almost disappearing by the end of fuel residence time.

In the case of power transients, it is important to have a prompt negative reactivity feedback that mitigates positive reactivity effects due to transients. The Doppler effect is the phenomenon that provides the required prompt negative reactivity feedback. As power increases, the fuel temperatures also increase because of excess fission energy. The increased fuel temperature results in increase of parasitic neutron absorption by fertile nuclides, such as ^{238}U. The negative reactivity feedback is more prompt if the fissile and fertile nuclides are mixed together. In that case stopping fission products from fissile nuclides can cause prompt temperature increases in fertile nuclides. The Doppler reactivity effect is caused mostly by the capture of low-energy neutrons because self-shielding effects are substantially reduced at high neutron energies.

Consequently, for carbide and nitride fuels the Doppler effect is smaller than for oxide fuel.

In this dissertation, the Doppler reactivity coefficient is estimated using the following expression:

$$\alpha_D = \frac{1}{\overline{\beta}_{eff}} \cdot \left(\frac{1}{\Delta T_F} \cdot \frac{k_2 - k_1}{k_1 \cdot k_2} \right), \tag{21}$$

where α_D is the Doppler reactivity coefficient (\$/K); ΔT_F is the fuel temperature variation due to transient process (K); $\overline{\beta}_{eff}$ is the effective delayed neutron fraction; k_1 and k_2 are the effective multiplication factors of the ALM-FR core configurations calculated for the nominal case with unchanged temperatures and for the case with elevated fuel temperatures respectively. To account for temperature dependence of microscopic cross sections, a special set of the fuel microscopic cross sections has been prepared at elevated fuel temperatures and used in the calculations of the Doppler reactivity coefficient. The cross sections for this set are calculated assuming doubled nominal fuel region temperature.

As emphasized above, the ALM-FR core consists of three regions that differ by the plutonium enrichment in each region and by the number of blanket assemblies per region. In the present study, the Doppler reactivity coefficients are calculated considering the ALM-FR core regions as following:

- Fuel temperature increase in driver pins in each region independently;
- Uniform fuel temperature increase in driver pins throughout the core;
- Uniform fuel temperature increase in blanket pins throughout the core;

- Uniform fuel temperature increase throughout the core.

The Doppler reactivity coefficients due to driver pins are shown in Fig. 32.

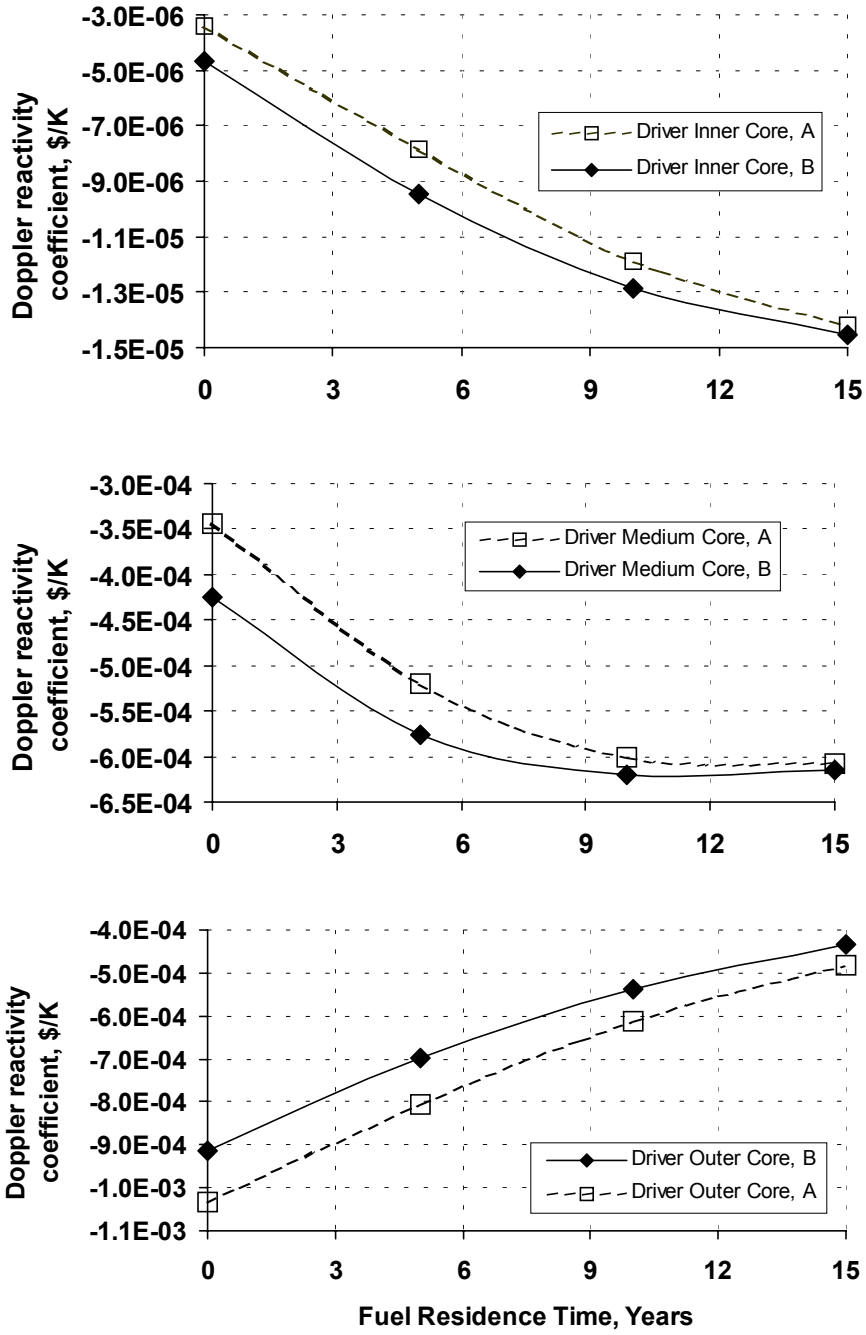

Fig. 32. Doppler reactivity coefficients of the ALM-FR core due to driver pins.

The number of driver and blanket pins in the inner core regions is the same for both optimized configurations. However, as shown in Fig. 32, the magnitude of the Doppler effect is larger for the configuration B. This difference illustrates the fact that the entire core configuration contributes to the Doppler effect due to temperature increase in the specific region. Similar effects are observed for the medium core where no blanket pins are present. The magnitude of the Doppler effect increases as a function of fuel residence time due to accumulation of new fuel nuclides, which have more pronounced resonance structure of neutron capture cross sections.

The Doppler effect in the outer core region exhibits opposite behavior as a function of fuel residence time. The magnitude of the Doppler effect in this region decreases with fuel irradiation because more blanket pins are present.

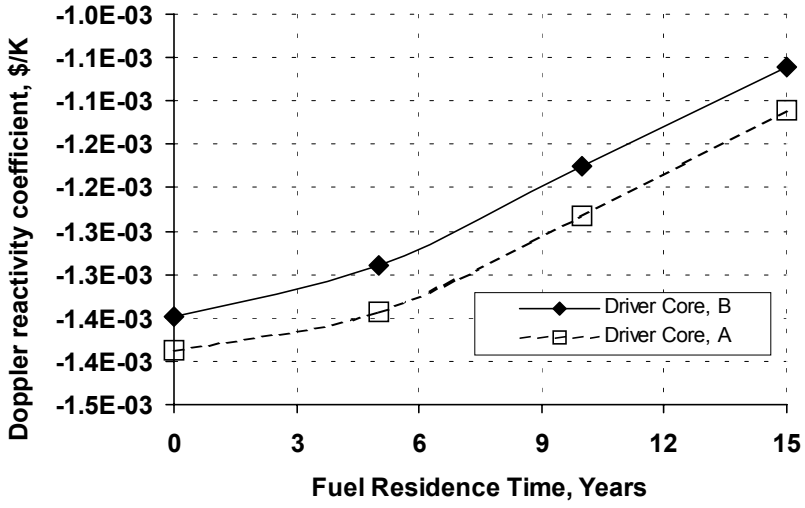

Fig. 33. Cumulative Doppler effect in the ALM-FR core due to driver pins.

The cumulative Doppler effect in the ALM-FR core due to driver pins is shown in Fig. 33. Although exhibiting a tendency to decrease in absolute values with fuel irradiation, for both core configurations the Doppler reactivity coefficients remain negative during the entire core lifetime. Comparison of Fig. 33 with Fig. 32 leads to the conclusion that the reactor physics characteristics of the outer core region determine the behavior of the Doppler effect as a function of fuel residence time.

The Doppler reactivity coefficients due to blanket pins are shown in Fig. 34. As in the cases considered above involving driver pins, for both core configurations the Doppler reactivity coefficients remain negative during the entire core lifetime. The Doppler feedback is less pronounced for configuration A that has smaller numbers of blanket pins in the core. The time-dependent behavior of the Doppler effect due to blanket pins is analogous to the behavior of the effect due to driver pins observed for the inner and medium core regions as shown in Fig. 32.

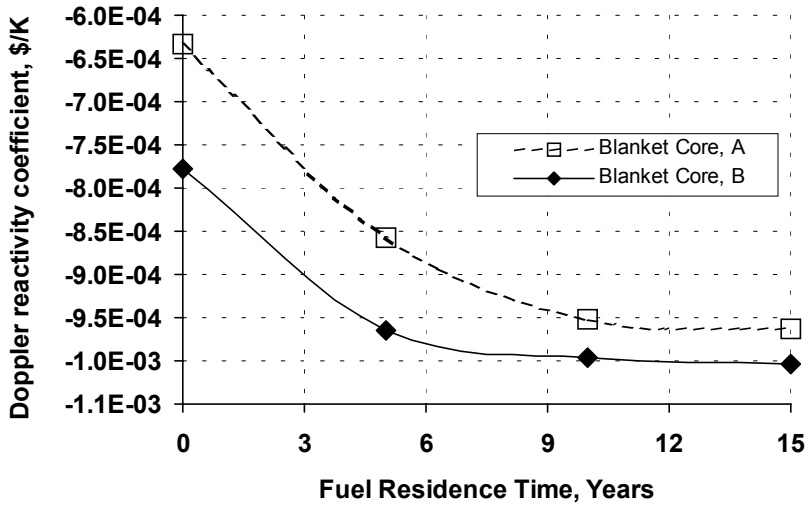

Fig. 34. Doppler reactivity coefficients of the ALM-FR core due to blanket pins.

Figure 35 shows the Doppler reactivity coefficients due to temperature increases in the entire ALM-FR core. The overall Doppler effect remains negative during the entire core lifetime. Furthermore, it increases in magnitude as a function of fuel residence time. The later is a very important feature of the ALM-FR core that assures inherent safety of this system. Similar to the Doppler reactivity coefficients considered above, the difference in the overall Doppler reactivity coefficients for the optimized configurations tends to decrease as a function of fuel residence time due to increasing uniformity of the core fuel composition.

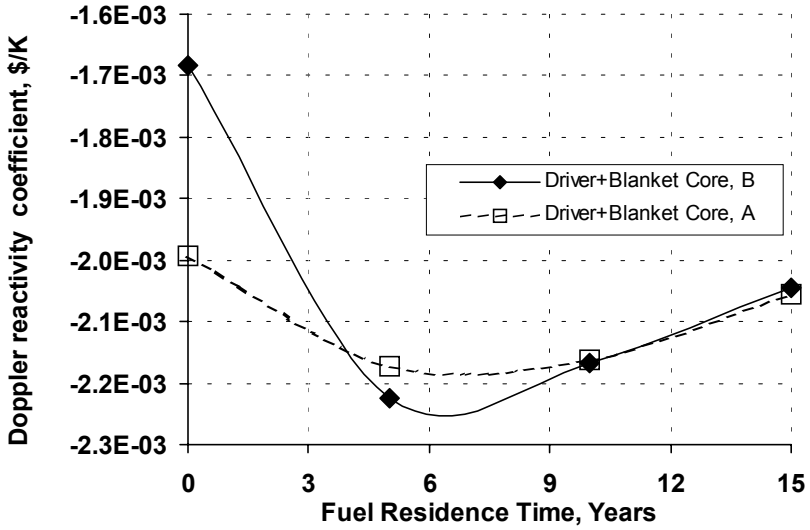

Fig. 35. Doppler reactivity coefficients of the ALM-FR core.

The actual behavior of the Doppler reactivity coefficient is difficult to predict theoretically because many different factors, which change simultaneously, influence its

value. Fissile and fertile compositions change significantly during reactor operation. At the same time, various fission products are produced in the core.

The loss of coolant in a fast reactor can potentially cause a large positive reactivity effect. The coolant void reactivity coefficient is highly space dependent. Spectral hardening, increasing neutron leakage, neutron capture reduction, and changes in self-shielding effects influence the coolant void reactivity coefficients in the ALM-FR core. Increasing the neutron leakage leads to a negative reactivity feedback. However, spectral-hardening effects provide large positive reactivity due to decrease in neutron moderation. Reduction of neutron capture and changes in self-shielding effects are less significant. All these effects are highly spatially dependent due to spatial the flux distribution in the core.

In this dissertation, the coolant void reactivity coefficient is estimated as:

$$\alpha_V = \frac{1}{\overline{\beta}_{eff}} \cdot \left(\frac{1}{\Delta\rho} \cdot \frac{k_2 - k_1}{k_1 \cdot k_2} \right), \tag{22}$$

where α_V is the coolant void reactivity coefficient (\$); $\Delta\rho$ is the coolant void fraction; $\overline{\beta}_{eff}$ is the effective delayed neutron fraction; k_1 and k_2 are the effective multiplication factors of the ALM-FR core configurations calculated for the nominal case with $\Delta\rho = 0$ and for the voided-core case. It is assumed that the coolant void fraction of 20% is introduced to the core regions under consideration.

Taking into account the anticipated spatial dependence, the overall core voiding is considered together with analysis of the region-wise effects. The region-wise coolant void reactivity coefficients due to voiding in driver assemblies are shown in Fig. 36.

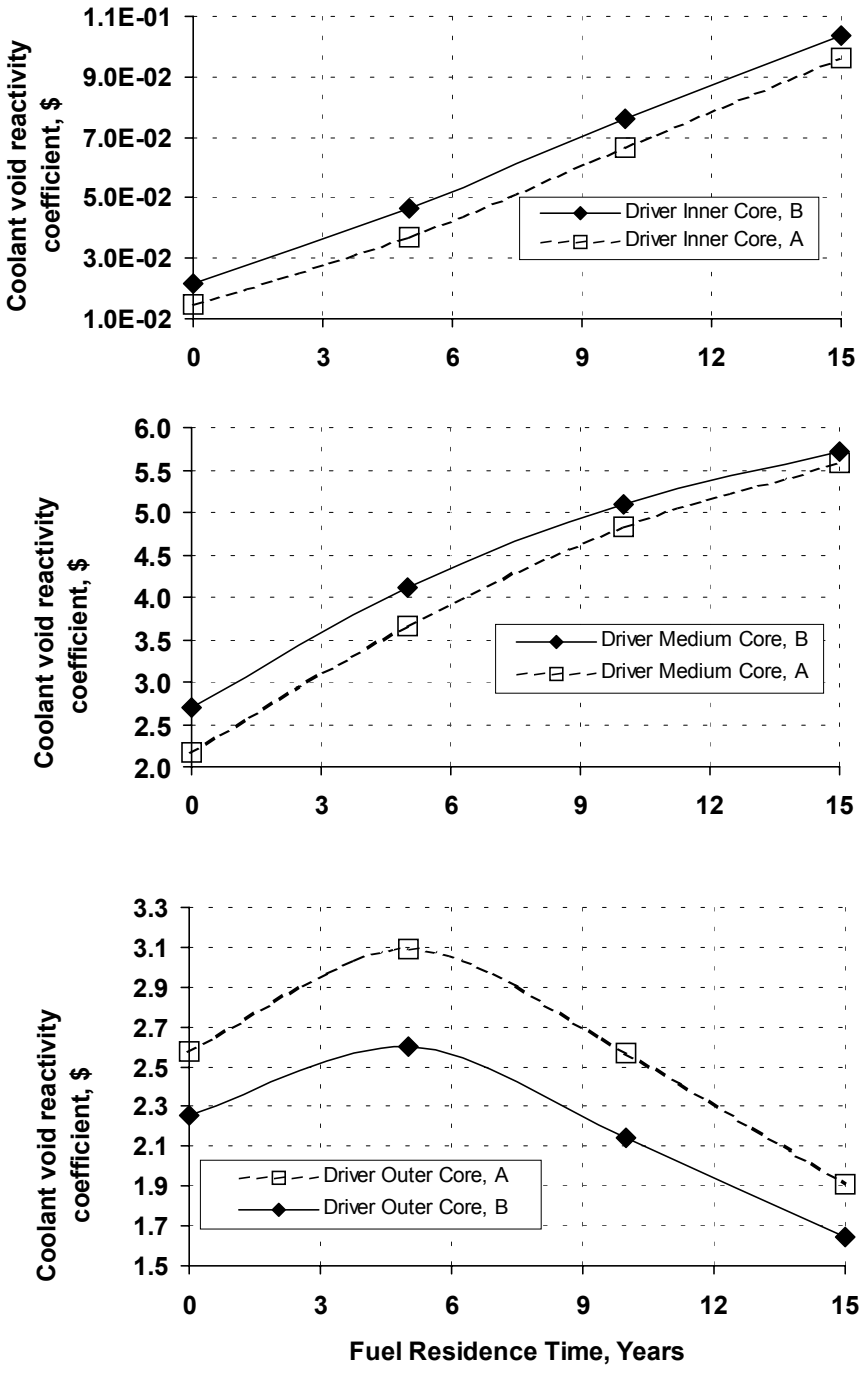

Fig. 36. Coolant void reactivity coefficients due to voiding in driver assemblies.

According to Fig. 36, for the optimized core configurations A and B the coolant void reactivity coefficients for inner and medium core regions with voided driver assemblies are positive and increase with burnup up to +$0.1 and +$5.7, respectively. The medium core region with voided driver assemblies has the highest values of the coolant void reactivity coefficients because this region has no blanket assemblies. The specific behavior of the void reactivity coefficient in the outer core region can be explained by the dynamics of reactor physics changes with burnup including power density shift and composition changes. The cumulative void reactivity effect in the ALM-FR core due to voiding in driver assemblies in all core regions is shown in Fig. 37. Both core configurations have positive coolant void reactivity coefficients due to voiding in driver assemblies that increase with burnup. Time-dependence of the overall coefficients is consistent with region-wise effects.

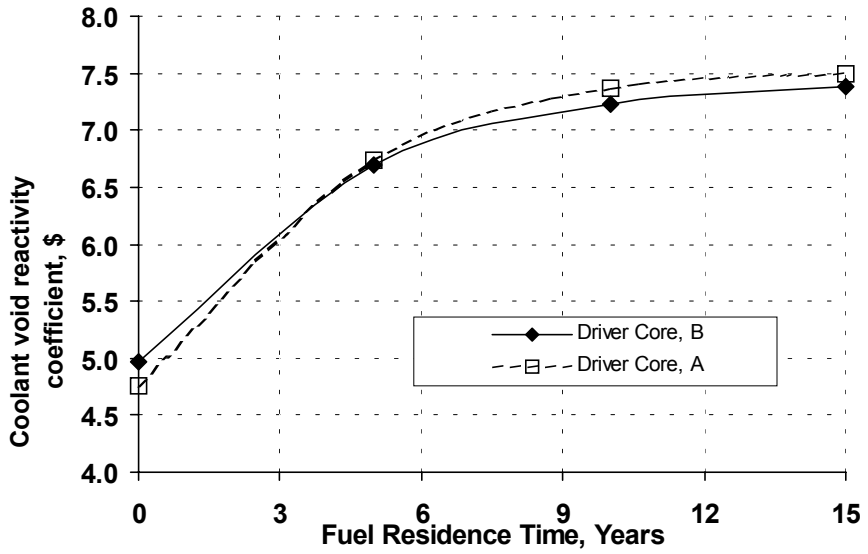

Fig. 37. Cumulative void reactivity effect due to voiding in driver assemblies.

The coolant void reactivity coefficients due to voiding in blanket assemblies are shown in Fig. 38. Similar to the considered above cases involving voiding in driver assemblies, for both core configurations the coolant void reactivity coefficients are positive. The increase with burnup is up to +$5.5.

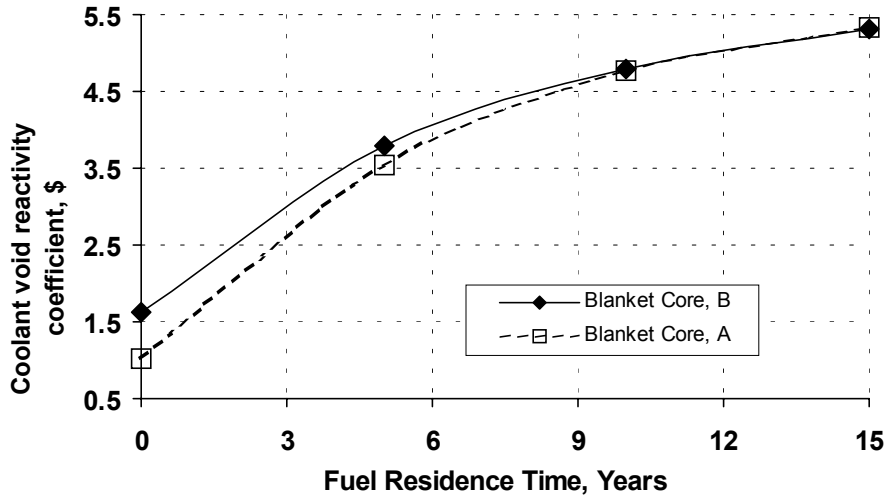

Fig. 38. Coolant void reactivity coefficients due to voiding in blanket assemblies.

Figure 39 shows the coolant void reactivity coefficients due to voiding in the entire ALM-FR core. The overall coolant void reactivity coefficients are positive and increase with burnup up to +$12. Although the values of the coolant void reactivity coefficients are positive and large even for 20% overall core voiding, it must be emphasized that this potential feature of the ALM-FR core does not create a threat to the reactor safety. Due to the very high boiling point of lead, void formation in the ALM-FR is highly improbable event.

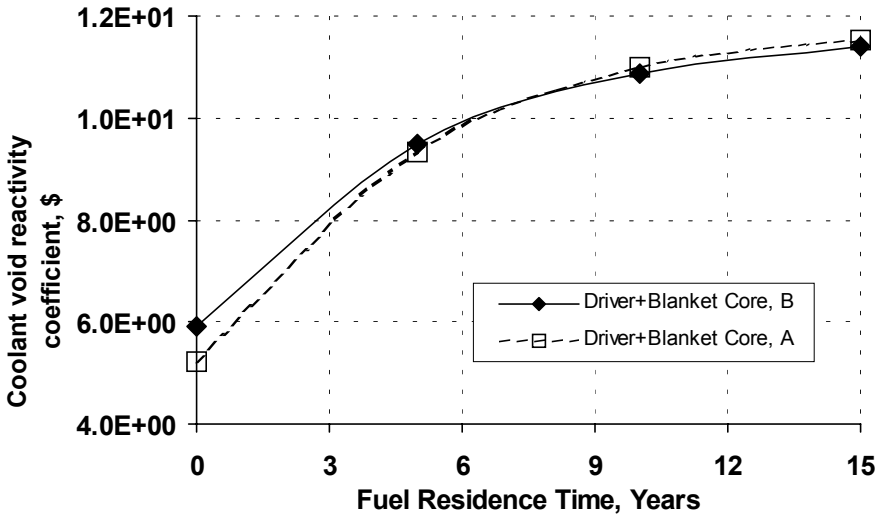

Fig. 39. Coolant void reactivity coefficients of the ALM-FR core.

Summarizing the results discussed above, for the considered optimized configurations A and B, the Doppler reactivity coefficients and the dimensional expansion reactivity coefficients are negative during the entire core lifetime. The coolant void reactivity coefficient is large and positive. The estimated values of the effective delayed neutron fractions are typical for fast reactors and do not experience significant variations with burnup.

Table XXV provides values of the estimated reactivity coefficients and effective delayed neutron fractions for the optimized ALM-FR configurations A and B at the beginning and at the end of the core lifetime. Increasing in magnitude, negative Doppler reactivity coefficients assure inherent safety of the ALM-FR systems with respect to the potential prompt transient processes.

TABLE XXV

Dynamics and Safety Characteristics of the ALM-FR System

ALM-FR Core			Configuration A			
Fuel			BOL		EOL (15 years)	
k-effective			1.000		1.009372441	
			Reactivity Coeff.	$\overline{\beta}_{eff}$	Reactivity Coeff.	$\overline{\beta}_{eff}$
α_R (Core) ($/cm)			-8.470E-1	3.3964945E-3	-7.392E-1	3.30991264E-3
α_H (Fuel) ($/cm)			-4.163E-1	3.39186601E-3	-3.136E-1	3.31059676E-3
α_H (Fuel and Structure) ($/cm)			-3.739E-1	3.39234333E-3	-2.446E-1	3.31089539E-3
α_D ($/°C)	Driver Pins	Inner Core	-3.390E-6	3.39240045E-3	-1.417E-5	3.31198550E-3
		Medium Core	-3.448E-4	3.39157430E-3	-6.079E-4	3.31107836E-3
		Outer Core	-1.034E-3	3.39202310E-3	-4.829E-4	3.33124074E-3
		Overall	-1.387E-3	3.39113234E-3	-1.111E-3	3.31116921E-3
	Blanket Pins		-6.335E-4	3.39119156E-3	-9.629E-4	3.33107922E-3
	Overall		-1.992E-3	3.33899706E-3	-2.055E-3	3.30997099E-3
α_V ($)	Driver Pins	Inner Core	+1.501E-2	3.39243219E-3	+9.647E-2	3.31223218E-3
		Medium Core	+2.163	3.39943177E-3	+5.585	3.32640991E-3
		Outer Core	+2.573	3.42280361E-3	+1.908	3.32459545E-3
		Overall	+4.757	3.34295647E-3	+7.491	3.33863567E-3
	Blanket Pins		+1.013	3.34007137E-3	+5.330	3.32397454E-3
	Overall		+5.225	3.43614540E-3	+1.154E+1	3.34717613E-3
ALM-FR Core			Configuration B			
Fuel			BOL		EOL (15 years)	
k-effective			1.000		1.01440574869	
			Reactivity Coeff.	$\overline{\beta}_{eff}$	Reactivity Coeff.	$\overline{\beta}_{eff}$
α_R (Core) ($/cm)			-7.833 E-1	3.39491716E-3	-7.326E-1	3.30151136E-3
α_H (Fuel) ($/cm)			-4.008E-1	3.39621952E-3	-3.110E-1	3.30219116E-3
α_H (Fuel and Structure) ($/cm)			-3.542E-1	3.39621952E-3	-2.416E-1	3.30254457E-3
α_D ($/°C)	Driver Pins	Inner Core	-4.675E-6	3.39677980E-3	-1.452E-5	3.30360771E-3
		Medium Core	-4.256E-4	3.39572679E-3	-6.140E-4	3.30278625E-3
		Outer Core	-9.141E-4	3.39664818E-3	-4.347E-4	3.30366630E-3
		Overall	-1.349E-3	3.39551614E-3	-1.061E-3	3.30280104E-3
	Blanket Pins		-7.780E-4	3.39545596E-3	-1.004E-3	3.30250030E-3
	Overall		-1.684E-3	3.39528443E-3	-2.045E-3	3.30168935E-3
α_V ($)	Driver Pins	Inner Core	+2.145E-2	3.39679154E-3	+1.037E-1	3.30386202E-3
		Medium Core	+2.694	3.40609432E-3	+5.722	3.31816735E-3
		Outer Core	+2.252	3.42407474E-3	+1.643	3.31531542E-3
		Overall	+4.967	3.43305782E-3	+7.378	3.32956507E-3
	Blanket Pins		+1.758	3.40538403E-3	+5.303	3.31568973E-3
	Overall		+5.929	3.43942318E-3	+1.139E+1	3.33815136E-3

CHAPTER VII

PLUTONIUM AND MINOR ACTINIDES IN THE ALM-FR AS POSSIBILITY TO MAINTAIN ULTRA-LONG OPERATION

Considering nuclear technology worldwide, the largest fraction of the generated nuclear energy is provided by conventional light water reactors. Most of the existing LWR units are fueled with LEU fuel. Consequently, if LEU compositions are continued to be the most widely used components of nuclear fuels, further nuclear technology development will retain its association with limited resources of natural uranium and continuous accumulation of minor actinides, which constitute the most undesirable long-term radiotoxicity.

If the expanded nuclear technology development is presumed for many centuries ahead, new nuclear fuel components, plutonium and higher actinides, should be considered. The efficient utilization of plutonium and higher actinides in reactor systems may have positive impact on the global nuclear fuel cycle since it provides the long-term utilization of MA's.

The feasibility of very high burnup fuels in thermal and fast reactors fueled with plutonium and MA's has already been demonstrated theoretically. Recognizing advantageous characteristics of MA's as advanced fuel components, it has to be acknowledged that extraction of Pu and MA's, especially from MOX fuel, is technologically difficult and has some limitations from the reprocessing point of view.

As emphasized in the preceding chapters of this dissertation, the ALM-FR system is intended to provide fully autonomous, sustainable operation during the entire

reactor lifetime. As a result, it should allow the achievement of self-consistency in a single power unit. The ALM-FR design will be able to demonstrate economic performance only if its operation lifetime is maximized matching the fuel lifetime with the entire reactor lifetime.

The basic mechanism to create a long-lived ALM-FR core depends on creating large initial reactivity excesses. It can be done using conventional ^{235}U-enriched fuel with an upper enrichment limit of 20% that is chosen in order to assure proliferation resistance of the design.

Alternatively, plutonium and MA's can be used as components of an advanced actinide fuel. In this case, additional measures are required to assure proliferation resistance of the design.

One of the approaches to improve non-proliferation characteristics consists of making access to the fresh and spent fuel extremely difficult. In the ALM-FR design, this approach is achieved by requiring reactor lifetime-long operation on one fuel loading.

Since the ALM-FR systems do not require refueling, there is no need for any on-site fuel handling facilities. In addition, the ALM-FR core cartridge is specifically designed to prevent unauthorized access to the fuel array. It is assembled at the factory and transported to the power unit site where it is inserted into the coolant module.

To make fuel materials with sufficiently high levels of inherent physical protection from any kinds of diversion attempts, the heat-spiked fuel compositions can be manufactured. In the case of mixed U-Pu-fuels, the heat-spike barrier, which can be

created by excessive decay heat of ^{238}Pu, is one of the methods that can be used to reduce the risk of proliferation.[63,64]

The spiked fuel composition presumes ^{238}Pu-enrichment. The presence of ^{238}Pu causes a very high heat generation (~567W/kg) in comparison with heat generation of ^{239}Pu (~1.9W/kg). The effect leads to elevated fuel temperature that would severely complicate disassembly process.

Unlike gamma emitters such as ^{60}Co, ^{238}Pu cannot be removed chemically from fuel composition. The isotope separation would be required, which is extremely difficult because of the small mass differences between ^{238}Pu and ^{239}Pu and other plutonium isotopes in the fuel composition.

The requirement of 5% of ^{238}Pu is sufficient to produce conditions desirable from a safeguards viewpoint.[63,64] Plutonium composition with 5% of ^{238}Pu is considered as proliferation-resistant for all practical purposes for both reactor-grade plutonium (RGPu) and weapons-grade plutonium (WGPu) compositions.

The reactor physics characteristics of the ALM-FR system, configuration A, fueled with (U,Pu)N-fuel containing pure and spiked compositions of RGPu and WGPu are summarized in Table XXVI. Only WGPu-compositions with 90% of ^{239}Pu provide the possibility to maintain 15 years of reactor operation on one fuel loading. The high relative content of ^{239}Pu in the Pu-composition allows low fuel enrichment of about 12-13% of plutonium. The presence of ^{238}Pu in the initial fuel compositions results in minor variations of the achievable burnup levels, attained peak fast fluences and peaking factors. According to Table XXVI, the EOL Pu-compositions still have substantial content of fissile isotopes of plutonium and do not deteriorate below the grade of the

initial plutonium composition. Consequently, the ALM-FR system does not have ability to provide de-weaponized EOL Pu compositions if it is loaded with WGPu. Both BOL and EOL fuel compositions of the ALM-FR system must be protected. Furthermore, the EOL fuel composition does not have the required 5% ^{238}Pu heat-spike protection because of ^{238}Pu depletion during reactor operation.

TABLE XXVI

Reactor Physics of the ALM-FR Systems (Configuration A) with RGPu and WGPu

Plutonium Composition	RGPu	Spiked RGPu	WGPu	Spiked WGPu
Fuel Residence Time (Years)	15	15	15	15
Capacity Factor (%)	90	90	90	90
BOL k-effective	1.000	1.000	1.000	1.000
EOL k-effective	0.9947	0.99645	1.00765	1.00968
Pu Enrichment (%/HM)	14.93	15.04	12.49	12.72
BOL Peaking Factor	1.708	1.712	1.709	1.715
EOL Peaking Factor	1.879	1.869	1.809	1.800
Breeding Ratio	1.062	1.076	1.013	1.013
Average Discharge Burnup (MWd/kg)	79.36	79.43	79.82	79.90
Reactivity Swing (%)	+0.561	+0.381	-0.751	-0.960
Peak Fast Fluence (n/cm^2)	2.65 E+23	2.61 E+23	2.61 E+23	2.57 E+23
Peak Discharge Burnup (MWd/kg)	116.2	115.7	115.8	116.3
BOL Pu Composition (%/Pu)				
^{238}Pu	1.89	4.95	0.01	4.99
^{239}Pu	58.52	56.72	93.80	89.15
^{240}Pu	22.84	22.12	5.82	5.54
^{241}Pu	10.98	10.64	0.35	0.32
^{242}Pu	5.76	5.57	0.02	0.00
EOL Pu Composition (%/Pu)				
^{238}Pu	1.45	2.96	0.12	2.41
^{239}Pu	64.95	64.3	84.14	82.4
^{240}Pu	24.15	23.57	14.6	14.11
^{241}Pu	4.2	4.08	1.01	0.96
^{242}Pu	5.25	5.09	0.12	0.12

To increase the amount of ^{238}Pu in the EOL fuel composition, the BOL fuel composition must contain nuclides that will produce ^{238}Pu during reactor operation. The analysis of neutron cross-sections and decay chains for various heavy nuclides results in

the conclusion that ^{237}Np has the desirable capability to produce ^{238}Pu during reactor operation. For the ALM-FR system (configuration A) with WGPu, the relative content of ^{238}Pu in the EOL Pu composition as a function of the relative content of ^{237}Np in the BOL fuel composition is shown in Figure 40.

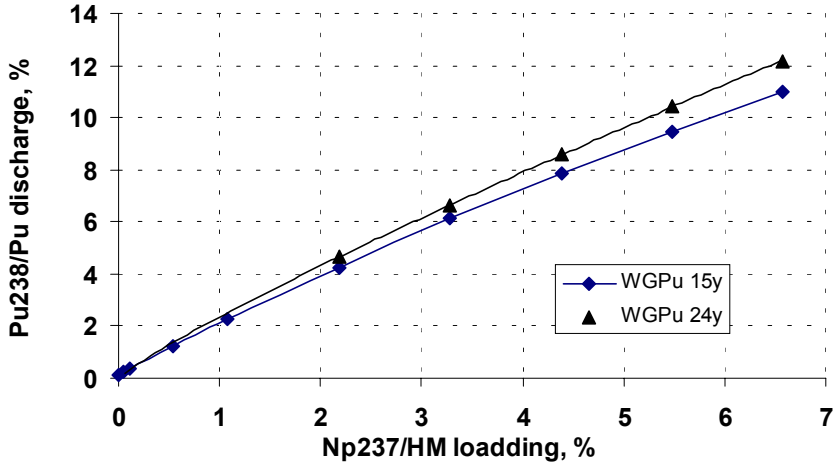

Fig. 40. ^{238}Pu in the EOL Pu as a function of ^{237}Np in the BOL fuel.

According to the results of the analysis, the presence of about 3% of ^{237}Np in the initial fuel composition is sufficient to provide about 6% of ^{238}Pu in the EOL Pu-composition. This amount of accumulated ^{238}Pu in the EOL Pu-composition is sufficient to maintain conditions desirable from a non-proliferation safeguards point of view during the entire core lifetime. The BOL fuel composition may be protected with added 5% of ^{238}Pu whereas protection of the EOL fuel composition is assured by presence of ^{237}Np in the BOL composition.

The presence of ^{237}Np in the BOL fuel composition greatly improves performance characteristics of the ALM-FR system. Only about 7% of ^{237}Np is required in the BOL fuel composition in order to increase core lifetime up to 40 years. Dependence of the core multiplication on the initial ^{237}Np content is shown in Fig 41 for the ALM-FR system (configuration A) with WGPu.

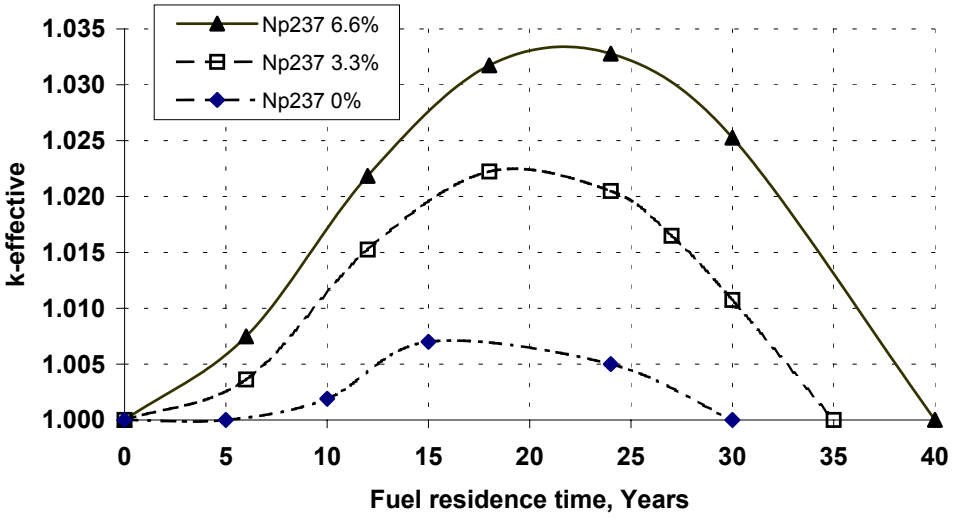

Fig. 41. Multiplication in the ALM-FR core (WGPu, configuration A) with ^{237}Np.

The addition of ^{237}Np to the BOL fuel composition allows the use RGPu-based BOL fuel compositions instead of WGPu-based compositions. Only 8% of ^{237}Np is required in the BOL RGPu-based fuel in order to maintain criticality during 40 years of operation. Dependence of the core multiplication on the initial ^{237}Np content is shown in Fig 42 for the ALM-FR system (configuration A) with RGPu. According to the analysis,

the ALM-FR system operation during 40 years on one RGPu-based fuel loading without ^{237}Np is impossible without an increase of the Pu-enrichment for the BOL fuel.

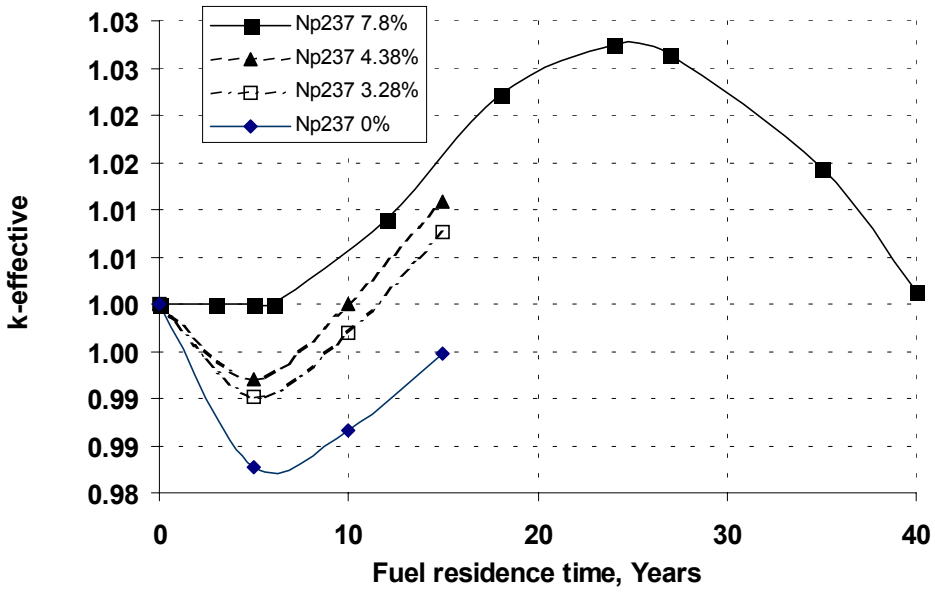

Fig. 42. Multiplication in the ALM-FR core (RGPu, configuration A) with ^{237}Np.

The amount of ^{237}Np can be added to the BOL fuel composition in the form of the MA mixture extracted from the spent LWR fuel. Table XXVII gives a typical Pu-MA composition that can be extracted from the spent LWR fuel.[10] Existing spent fuel reprocessing technologies allow to extract this composition from the spent LWR fuel and produce the BOL mixed fuel composition containing the LWR RGPu-composition and the LWR MA-composition. Consequently, the U-TRU-nitride fuel for the ALM-FR system can be fabricated as (LWR RGPu - MA,U)N.

TABLE XXVII

Typical Pu – MA Composition from the Spent LWR Fuel

Nuclide	Amount (kg)
^{238}Pu	4.52
^{239}Pu	166.0
^{240}Pu	76.7
^{241}Pu	25.4
^{242}Pu	15.5
^{237}Np	14.5
^{241}Am	16.6
^{243}Am	2.99
^{243}Cm	0.01
^{244}Cm	0.58

Assuming the spent LWR fuel composition given in Table XXVII, the dependence of the core multiplication on the initial ^{237}Np content is shown in Fig 43 for the ALM-FR system (configuration A) with LWR Pu - MA. Concentrations of 0% - 7.7% ^{237}Np are considered.

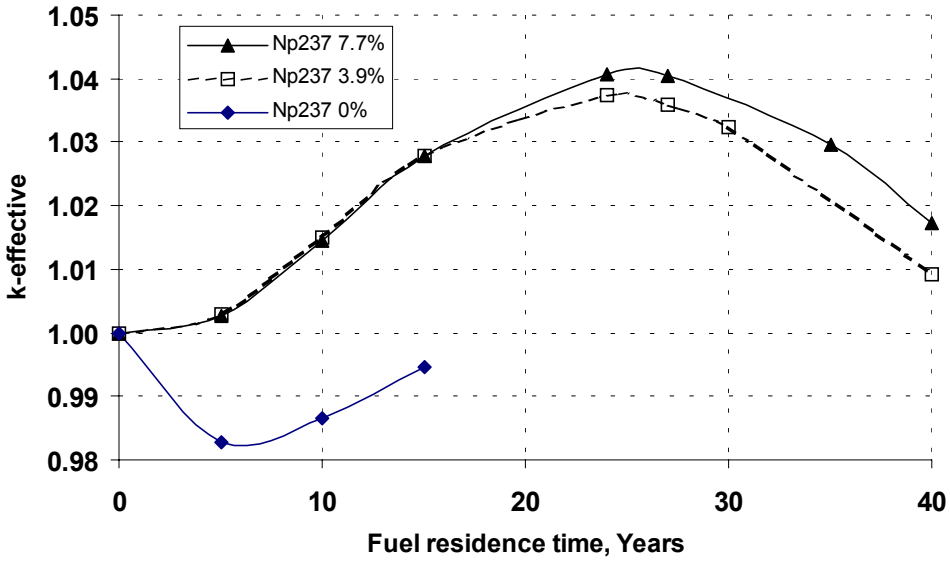

Fig. 43. Multiplication in the ALM-FR core (configuration A) with LWR Pu - MA.

Figure 44 illustrates the ability of ^{237}Np to maintain 40 years of operation under conditions of minimized Pu-content in the BOL fuel for the ALM-FR system. The actual unchanged MA composition from the spent LWR fuel is compared with the artificially-enriched ^{237}Np compositions based on RGPu and WGPu. Similarity between the characteristics of the ALM-FR systems with artificially-enriched ^{237}Np-RGPu and with the actual LWR Pu – MA compositions confirms the possibility to use compositions from the spent LWR fuel to achieve 40 years of operation on one fuel loading.

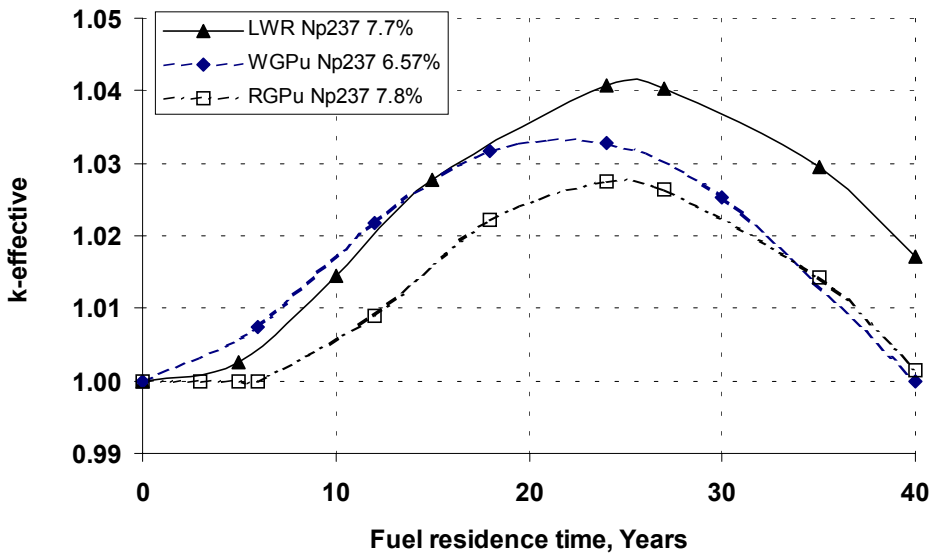

Fig. 44. Multiplication in the ALM-FR (configuration A) with ^{237}Np-Pu Compositions.

The reactor physics characteristics of the ALM-FR systems with the considered BOL fuel compositions are summarized in Table XXVIII. According to the analysis, the

use of ^{237}Np or LWR Pu – MA composition in the BOL fuel improves the ALM-FR performance characteristics and assures proliferation resistance of the fuel.

TABLE XXVIII

Reactor Physics of the ALM-FR (Configuration A) with RGPu, WGPu, LWR Pu-MA

Pu-Np Composition	RGPu	LWR	LWR	WGPu	WGPu	WGPu
^{237}Np Content (%/HM)	7.8	3.9	7.7	0	3.28	6.57
Fuel Residence Time (years)	15	15	15	15	15	15
Capacity factor (%)	90	90	90	90	90	90
BOL k-effective	1.000	1.000	1.000	1.0000	1.000	1.000
EOL k-effective	1.01643	1.02776	1.02783	1.00765	1.0198	1.0279
Pu Enrichment (%)	24.12	25.8	27.9	12.49	16.48	20.3
BOL Peaking Factor	1.83	1.84	1.88	1.709	1.77	1.82
EOL Peaking Factor	1.66	1.71	1.61	1.809	1.745	1.67
Breeding Ratio	1.038	1.025	1.025	1.013	1.001	0.993
Average Burnup (MWd/kg)	81.93	82.14	82.64	79.82	81.03	81.9
Reactivity Swing (%)	-1.643	-2.78	-2.79	-0.751	-1.947	-2.84
Peak Fast Fluence (n/cm^2)	2.66 E+23	2.68 E+23	2.68 E+23	2.61 E+23	2.61 E+23	2.61 E+23
Peak Burnup (MWd/kg)	131.0	133.4	137.1	115.8	122	128
BOL Pu Composition (%/Pu)						
^{238}Pu	1.89	1.89	1.89	0.01	0.01	0.01
^{239}Pu	58.55	58.55	58.55	93.80	93.80	93.80
^{240}Pu	22.84	22.84	22.84	5.82	5.82	5.82
^{241}Pu	10.96	10.96	10.96	0.35	0.35	0.35
^{242}Pu	5.76	5.76	5.76	0.02	0.02	0.02
BOL LWR MA (%/MA)						
^{241}Am	-	48.16	26.35	-	-	-
^{243}Am	-	8.75	4.79	-	-	-
^{243}Cm	-	0.03	0.01	-	-	-
^{244}Cm	-	1.7	0.93	-	-	-
^{247}Np	-	41.37	67.91	-	-	-
Total (%MA/HM)	-	9.4	11.35	-	-	-
EOL Pu Composition (%/Pu)						
^{238}Pu	12.65	11.31	14.54	0.12	6.12	11.01
^{239}Pu	57.24	56.8	55.14	84.14	80.05	76.6
^{240}Pu	21.31	21.84	20.93	14.6	12.9	11.61
^{241}Pu	3.91	3.95	3.86	1.01	0.85	0.71
^{242}Pu	4.88	6.11	5.52	0.12	0.08	0.08

In general, the presence of MA's, such as americium and curium, in the initial fuel composition does not automatically improve the proliferation-resistance of the fuel. During reactor operation, several isotopes of curium are produced. Two of them, ^{242}Cm and ^{244}Cm, decay with half-lives of 165 days and 18.1 years to ^{238}Pu and ^{240}Pu, respectively.

Due to the excellent neutronics characteristics, the use of plutonium and MA's results in ultra-long operation on one fuel loading and in maintaining near-zero burnup reactivity swing with minimized spatial reactivity fluctuations during the entire core lifetime. The later features assure fully autonomous, sustainable operation.

CHAPTER VIII

CONCLUSIONS AND RECOMMENDATIONS

This dissertation presents a conceptual design of an autonomous long-term multi-purpose fast reactor (ALM-FR) that is based on the STAR-H2 concept. The ALM-FR design represents further refinement of this concept with the goal of achieving an economical, proliferation-resistant, sustainable, multi-purpose nuclear energy system. The main difference of the ALM-FR design from the original STAR-H2 system consists in the design requirement to provide fully autonomous, sustainable operation during the entire reactor lifetime while the STAR-H2 system is designed assuming 15-years refueling cycle.

Life long reactor operation without refueling makes it possible to achieve self-consistency in a single ALM-FR unit. The ALM-FR design can be considered as the "once-through-then-out" version or performance mode of the STAR-H2 system. It must be emphasized that the ALM-FR design will be able to demonstrate economic performance only if its operational lifetime is maximized matching the fuel lifetime with the entire reactor lifetime.

The ALM-FR system layout with evaluated reactor physics characteristics is systematically described in the preceding chapters. The dissertation presents a detailed analysis of the possibility of a long-term operation on one fuel loading through utilization of plutonium and minor actinides in the ALM-FR core. The analysis takes into consideration a wide range of reactor design aspects including selection of technologically feasible fuels and structural materials, core configuration optimization,

dynamics and safety of long-term operation on one fuel loading, and nuclear material non-proliferation. Flexibility of the ALM-FR with respect to fuel compositions is demonstrated acknowledging the principal limitations of the long-term burning of plutonium and minor actinides.

As a result of the computational analysis, the ALM-FR design provides the possibility of continuous operation during about 40 years on one fuel loading containing mixture of depleted uranium with plutonium and minor actinides from the spent LWR fuel. All reactor physics characteristics of the ALM-FR are kept within the identified technological limits ensuring safety of ultra-long autonomous operation. The results allow identification of physical features of the ALM-FR that significantly influence flexibility of the design and its applications. Special emphasis is given to existing limitations on utilization of minor actinides as a fuel component. Results of the performed analysis establish the possibility of the reactor lifetime-long operation on one fuel loading.

VIII.A. Conclusions

The comprehensive analysis, which was performed within the framework of this dissertation, leads to the following specific conclusions regarding the ALM-FR system and its reactor physics performance characteristics:

- Selection of lead as a coolant for the ALM-FR system makes it possible to achieve elevated operational temperatures required for high temperature hydrogen production process.

- Selected high density U-TRU-nitride fuel is compatible with lead, allows operation at elevated temperatures, and provides physical capability to attain high burnup levels. Application of U-TRU-nitride fuel requires ^{15}N enrichment to improve neutronics characteristics and to reduce yield of radioactive ^{14}C from (n,p) reactions on ^{14}N.
- Selection of SiC as a fuel element cladding material provides compatibility of the ALM-FR cladding with lead and U-TRU-nitride fuel. At the same time, it can withstand high burnup levels and fast fluences resulting from ultra-long operation on one fuel loading.
- Specific optimized configurations of the ALM-FR core are suggested to provide near-zero burnup reactivity swing with minimized spatial fluctuations of reactivity and power density distributions during the entire reactor lifetime.
- Analyses of power density and flux distributions in the ALM-FR core have confirmed feasibility of ultra-long operation without exceeding thermal limitations.
- The ALM-FR core provides strong reactivity feedback without deterioration during the entire reactor operation. The system dynamics and safety characteristics improve with reactor operation assuring autonomous inherently safe performance during ultra-long operation.
- A combination of ^{238}Pu and ^{237}Np has been suggested and analyzed as an inherent physical protection barrier assuring proliferation resistance of the ALM-FR system. Presence of ^{237}Np in the ALM-FR core maximizes the

ALM-FR core lifetime up to 40 years approaching operation limitations due to exceeding allowable values of burnup and fast fluences in the system.

- Stability of the ALM-FR system performance characteristics during ultra-long operation and near-zero burnup reactivity swing allows maintaining autonomous operation with minimized human intervention.

VIII.B. Recommendations for Follow-Up Research

The following computational and experimental studies are required for further development of the ALM-FR system:

- Systematic experimental research with the ALM-FR system prototype to verify results of the computational modeling and prove technological feasibility of this system;
- Demonstration that SiC retains its characteristics during the entire period of operation;
- Development and experimental verification of the ALM-FR system startup and shutdown procedures;
- Demonstration and experimental verification of economical manufacturing processes for production of the proliferation resistant U-Pu- LWR MA nitride fuel;
- Demonstration that lead solidification and meltdown do not result in severe damage effects of the ALM-FR system internals.

REFERENCES

1. F. J. Rahn, A. G. Adamantiades, J. E. Kenton, C. Braun, *A Guide to Nuclear Power Technology*, John Wiley & Sons, Inc., New York (1984).

2. G. H. Marcus, "Considering the Next Generation of Nuclear Power Plants", *Progr. Nucl. Energy*, **37**, 5 (2000).

3. "Nuclear Energy Research Initiative, 2002 Annual Report", DOE-NE-0122, Office of Nuclear Energy, Science and Technology, United States Department of Energy, Washington, D.C. (2001).

4. "A Roadmap to Deploy New Nuclear Power Plants in the United States by 2010", Volume 1 – 2, DOE-NERAC Report, October 31, 2001, Nuclear Energy Research Advisory Committee, Office of Nuclear Energy, Science and Technology, United States Department of Energy, Washington, D.C. (2001).

5. "Fiscal Year 2004 Congressional Budget, Energy Supply – Nuclear Energy", Executive Summary, DOE-NE Report, Office of Nuclear Energy, Science and Technology, United States Department of Energy, Washington, D.C. (2003).

6. "Nuclear Power Generation and Fuel Cycle", DOE-EIA-0436(96)/UC-950, Office of Coal, Nuclear and Alternate Fuels, Energy Information Administration, United States Department of Energy, Washington, D.C. (1996).

7. "Actinide and Fission Product Partitioning and Transmutation", *Proc. 6th Information Exchange Meeting on Nuclear Development*, Madrid, Spain, December 11 – 13, 2000, NEA-OECD-EC, EUR 19783EN, Nuclear Energy Agency, Issy-les-Moulineaux, France (2000).

8. L. H. Baetsle, C. De Raedt, "Limitations of Actinide Recycle and Fuel Cycle Consequences: a Global Analysis; Part 1: Global Fuel Cycle Analysis", *Nucl. Eng. Design*, **168**, 191 (1997).

9. L. H. Baetsle, C. De Raedt, "Limitations of Actinide Recycle and Fuel Cycle Consequences. A Global Analysis; Part 2: Recycle of Actinides in Thermal Reactors: Impact of High Burnup LWR-UO, Fuel Irradiation and Multiple Recycle of LWR-MOX Fuel on the Radiotoxic Inventory", *Nucl. Eng. Design*, **168**, 203 (1997).

10. C. H. M. Broeders, E. Kiefhaber, H. W. Wiese, "Burning of Transuranium Isotopes in Thermal and Fast Reactors", *Nucl. Eng. Design*, **202**, 157 (2000).

11. A. Chmelev, V. Artisyuk, M. Suzuki, M. Saito, Y. Fujii-E, "Multi-Component Nuclear Energy System: How to Meet Requirements of Self-Consistency", *Progr. Nucl. Energy*, **32**, 659 (1998).

12. G. V. Tsvetkova, K. L. Peddicord, "Utilization of Plutonium and Higher Actinides in the HTGR as Possibility to Maintain Long-Term Operation on One Fuel Loading", *Proc. 10th International Conference on Nuclear Engineering (ICONE10)*, Arlington, Virginia, April 14 – 18, 2002, Track 6, ICONE10-22213, p. 354, American Society of Mechanical Engineers, Fairfield, New Jersey (2002).

13. D. C. Wade, E. Feldman, J. Sienicki, T. Sofu, A. Barak, E. Greenspan, D. Saphier, N. W. Brown, Q. Hossain, M. D. Carelli, L. Conway, M. Dzodzo, "ENHS: The Encapsulated Nuclear Heat Source – A Nuclear Energy Concept for Emerging Worldwide Energy Markets", *Proc. 10th International Conference on Nuclear Engineering (ICONE10)*, Arlington, Virginia, April 14 – 18, 2002, Track 6, ICONE10-22202, p. 310, American Society of Mechanical Engineers, Fairfield, New Jersey (2002).

14. D. C. Wade, R. Doctor, K. L. Peddicord, "STAR-H2: The Secure Transportable Autonomous Reactor for Hydrogen Production and Desalinization", *Proc. 10th International Conference on Nuclear Engineering (ICONE10)*, Arlington, Virginia, April 14 – 18, 2002, Track 8, ICONE10-22663, p. 834, American Society of Mechanical Engineers, Fairfield, New Jersey (2002).

15. V. M. Mourogov, "Nuclear Energy Development: Global Problems and Strategies", *IAEA Bulletin*, **39**, 2, International Atomic Energy Agency, Vienna, Austria (1997).

16. B. Y. Csik, Y. Kupitz, "Nuclear Power Application: Heat Supply to Population and Industry", *IAEA Bulletin*, **39**, 21, International Atomic Energy Agency, Vienna, Austria (1997).

17. W. Haefele, J. Anderer, A. McDonald, N. Nakicenovic, *Energy in a Finite World, Volume 1: Paths to a Sustainable Future. Report by the Energy Systems Program Group of the International Institute for Applied Systems Analysis,* Ballinger Publishing Co., Cambridge, Massachusetts (1981).

18. W. Haefele, *Energy in a Finite World, Volume 2: A Global Systems Analysis. Report by the Energy Systems Program Group of the International Institute for*

Applied Systems Analysis, Ballinger Publishing Co., Cambridge, Massachusetts (1981).

19. N. Nakicenovic, A. Grubler, A. McDonald, editors, *Global Energy Perspectives,* Cambridge University Press, Inc., New York (1998).

20. D. C. Wade, R. Doctor, K. L. Peddicord, "STAR-H2: A Battery-Type Lead-Cooled Fast Reactor for Hydrogen Manufacture in a Sustainable Hierarchical Hub-Spoke Energy Infrastructure", *Proc. International Conference on Global Environment and Advanced Nuclear Power Plants (GENES4/ANP2003)*, Kyoto Research Park, Kyoto, Japan, September 15 – 19, 2003, GENES/ANP2003-1189, p. 234, Atomic Energy Society of Japan, Kyoto, Japan (2003).

21. "Americas Nuclear Energy Symposium – 2002 (ANES-2002)", *Nucl. News*, February 2003, 40, American Nuclear Society, Inc., La Grange Park, Illinois (2003).

22. J. J. Sienicki, P. V. Petkov, "Passive Safety of the STAR-LM HLMC Natural Convection Reactor", *Proc. 10th International Conference on Nuclear Engineering (ICONE10)*, Arlington, Virginia, April 14 – 18, 2002, Track 6, ICONE10-22290, p. 453, American Society of Mechanical Engineers, Fairfield, New Jersey (2002).

23. J. J. Sienicki, P. V. Petkov, "Autonomous Load Following and Operational Aspects of the STAR-LM HLMC Natural Convection Reactor", *Proc. 10th International Conference on Nuclear Engineering (ICONE10)*, Arlington, Virginia, April 14 – 18, 2002, Track 6, ICONE10-22291, p. 503, American Society of Mechanical Engineers, Fairfield, New Jersey (2002).

24. J. J. Sienicki, B. W. Spencer, "Power Optimization in the STAR-LM Modular Natural Convection Reactor System", *Proc. 10th International Conference on Nuclear Engineering (ICONE10)*, Arlington, Virginia, April 14 – 18, 2002, Track 6, ICONE10-22294, p. 551, American Society of Mechanical Engineers, Fairfield, New Jersey (2002).

25. S. Glasstone, A. Sesonske, *Nuclear Reactor Engineering*, 3d ed., Van Nostrand Reinhold, New York (1981).

26. A. S. Icenhour, R. R. Brunson, R. M. Wham, "Alpha and Gamma Radiolysis Studies for Neptunium Oxides", *Trans. Amer. Nucl. Soc.*, **88**, 387 (2003).

27. M. K. Meyer, J. R. Kennedy, S. L. Hayes, D. D. Keiser, S. M. Frank, R. G. Ambrosek, G. S. Chang, "Fabrication, Characterization, and Irradiation of Minor Actinide Fuels in the AFC-1 Test", *Trans. Amer. Nucl. Soc.*, **88**, 385 (2003).

28. "Integrated Nuclear and Hydrogen-based Energy Supply/Carrier System- Hydrogen Generation Using a Calcium-Bromide Thermochemical Water-Splitting Cycle", NERI-24427-2002, Argonne National Laboratory, Argonne, Illinois (2002).

29. K. L. Derstine, "DIF3D: A Code to Solve One-, Two-, and Three-Dimensional Finite Difference Diffusion Theory Problems", ANL-82-64, Argonne National Laboratory, Argonne, Illinois (1982).

30. R. D. Lawrence, "The DIF3D Nodal Neutronics Option for Two- and Three-Dimensional Diffusion Theory Calculations in Hexagonal Geometry", ANL-83-1, Argonne National Laboratory, Argonne, Illinois (1983).

31. G. Palmiotti, C. B. Carrico, E. E. Lewis, "Variational Nodal Methods with Anisotropic Scattering", *Nucl. Sci. Eng.*, **115**, 223 (1993).

32. J. Y. Doriath, F. Malvagi, G. Palmiotti, J. M. Ruggieri, C. B. Carrico, E. E. Lewis, G. Gastaldo, "Variational Nodal Method (VNM) to Solve 3D Transport Equation: Applications to EFR Design", *Proc. Math. Methods and Supercomputing in Nucl. App.*, Karlsruhe, Germany, April, 1993, I-571, p. 571, American Nuclear Society, Inc., La Grange Park, Illinois (1993).

33. C. B. Carrico, E. E. Lewis, G. Palmiotti, "Three-Dimensional Variational Nodal Transport Methods for Cartesian, Triangular and Hexagonal Criticality Calculations", *Nucl. Sci. Eng.*, **111**, 168 (1992).

34. C. B. Carrico, E. E. Lewis, "Variational Nodal Solution Algorithms for Multigroup Criticality Problems", *Proc. International Topical Meeting on Advances in Math., Computations and Reactor Physics*, Pittsburgh, Pennsylvania, April 28 - May 1, 1991, p. 448, American Nuclear Society, Inc., La Grange Park, Illinois (1991).

35. E. E. Lewis, C. B. Carrico, G. Palmiotti, "Variational Nodal Formulation for the Spherical Harmonics Equations", *Nucl. Sci. Eng.*, **122**, 194 (1996).

36. F. R. Andrade Lima, A. Gandini, A. Blanco, "Recent Advances in Perturbation Methods Applied to Nuclear Engineering Problems", *Progr. Nucl. Energy*, **33**, 23 (1998).

37. B. J. Toppel, "The Fuel Cycle Analysis Capability, REBUS-3", ANL-83-2, Argonne National Laboratory, Argonne, Illinois (1983).

38. R. P. Hosteny, "The ARC System Fuel Cycle Analysis Capability, REBUS-2", ANL-77-21, Argonne National Laboratory, Argonne, Illinois (1977).

39. R. D. O'Dell, "Standard Interface Files and Procedures for Reactor Physics Codes, Version IV", LANL-UC-32, Los Alamos National Laboratory, Los Alamos, New Mexico (1977).

40. H. Henryson, II, B. J. Toppel, C. G. Stenberg, "MC^2-II: A Code to Calculate Fast Neutron Spectra and Multigroup Cross Sections", ANL-81-44, Argonne National Laboratory, Argonne, Illinois (1981).

41. C. G. Stenberg and A. Lindeman, "The ARC System Cross Section Generation Capabilities, ARC-MC^2", ANL-77-22, Argonne National Laboratory, Argonne, Illinois (1977).

42. R. N. Hwang, "A Rigorous Pole Representation of Multilevel Cross Sections and Its Practical Applications", *Nucl. Sci. Eng.*, **96**, 192 (1987).

43. J. Weisman, *Elements of Nuclear Reactor Design*, 2nd ed., Robert E. Kreiger Pub. Comp., Inc., Malabar, Florida (1983).

44. S. M. Reynaud, K. L. Peddicord, "Re-Assessment of Nitride Fuel Potential in the Current Context of the Nuclear Industry", *Proc. 10th International Conference on Nuclear Engineering (ICONE10)*, Arlington, Virginia, April 14 – 18, 2002, Track 11, ICONE10-22771, p. 935, American Society of Mechanical Engineers, Fairfield, New Jersey (2002).

45. S. L. Hayes, D. J. Senor, J. K. Thomas, K. L. Peddicord, "Properties Library for Space Nuclear Reactors", ANFL-10-R, Advanced Nuclear Fuels Laboratory, Department of Nuclear Engineering, Texas A&M University, College Station, Texas (1989).

46. A. A. Bauer, J. B. Brown, E. O. Fromm, V. W. Storhok, "Mixed-Nitride Fuel Irradiation Performance", *Proc. Conference on Fast Reactor Fuel Element Technology*, New Orleans, Louisiana, April 13 – 15, 1971, p. 785, American Nuclear Society, Inc., La Grange Park, Illinois (1971).

47. J. R. Tipton, *Nuclear Reactor Handbook,* 2d ed., Battelle Memorial Institute, Interscience Publishers, Inc., New York (1960).

48. M. W. Chase, "JANAF Thermochemical Tables, 3d Edition", *J. Phys. Chem. Ref. Data*, **14**, 236 (1985).

49. D. Garvin, V. B. Parker, H. J. White, *CODATA Thermodynamic Tables*, Hemisphere Press, New York (1987).

50. "DIPPR Database of Pure Compound Properties", DIPPD-DIPPR-1987, Design Institute for Physical Properties Data, American Institute of Chemical Engineers, New York (1987).

51. M. M. El-Wakil, *Nuclear Power Engineering,* McGraw-Hill Book Comp., Inc., New York (1962).

52. A. E. Waltar, A. B. Reynolds, *Fast Breeder Reactors,* Pergamon Press, New York (1981).

53. N. Sawada, "Fundamental Study on the Lead-Bismuth Cooled FBR System", *Proc. 8th International Conference on Nuclear Engineering (ICONE8)*, Baltimore, Maryland, April 2 – 6, 2000, Track 6, ICONE8-8745, p. 563, American Society of Mechanical Engineers, Fairfield, New Jersey (2000).

54. G. Ilincev, "Research Results on the Corrosion Effects of Liquid Heavy Metals, Pb, Bi and Pb-Bi, on Structural Materials with and without Corrosion Inhibitors", *Nucl. Eng. Design*, **217**, 167 (2002).

55. L. Leibowitz, R. A. Blomquist, "Thermal Conductivity and Thermal Expansion of Stainless Steels D9 and HT9", *Intern. J. Thermophysics*, **9**, 873 (1988).

56. "Advanced Technology in Refractory Metals and Custom Fabrication", *Refractory Material Handbook*, Rembar Company, Inc., Santa Monica, California (2002).

57. W. E. Berry, *Corrosion in Nuclear Applications*, Battelle Memorial Institute, John Wiley & Sons, Inc., New York (1971).

58. "The JEF-2.2 Nuclear Data Library", OECD-AEN/NEA-JEFF-17-4, NEA Data Bank, OECD Nuclear Energy Agency, Issy-les-Moulineaux, France (2000).

59. "ENDF/B-VI.6: The US Evaluated Nuclear Data Library for Neutron Reaction Data", IAEA-NDS-100, International Atomic Energy Agency, Vienna, Austria (1995).

60. K. Shibata, T. Nakagawa, H. Sugano, H. Kawasaki, "Curves and Tables of Neutron Cross Sections in JENDL-3.2", JAERI-DATA/CODE 94-003, Nuclear Data Center, Japan Atomic Energy Research Institute, Ibaraki-ken, Japan (1997).

61. A. Nouri, P. Nagel, "JANIS 1.0 User's Guide", OECD-AEN/NEA-JANIS-1.0, NEA Data Bank, OECD Nuclear Energy Agency, Issy-les-Moulineaux, France (2001).

62. "STAR-H2: Integrated Nuclear and Hydrogen-based Energy Supply/Carrier System", NERI-24427-2002, IWO-MOSF-2000-060, Argonne National Laboratory, Argonne, Illinois (2002).

63. C. D. Heising-Goodman, "An Evaluation of the Plutonium Denaturing Concept as an Effective Safeguard Method", *Nucl. Techn.,* **50**, 242 (1980).

64. Y. Ronen, Y. Kimhi, "A "Non-Proliferating" Nuclear Fuel for Light Water Reactors", *Nucl. Techn.,* **96**, 133 (1991).

APPENDIX A

ALM-FR MODEL FOR REACTOR PHYSICS ANALYSIS

TABLE XXIX

Fuel Regions of the Core Configuration A

Area	Region #, Region Identifier				
1 TCORE	04 OC01D	05 OC01E	06 OC01F	07 OC01G	08 OC01H
	31 OC02D	32 OC02E	33 OC02F	34 OC02G	35 OC02H
	53 OC03D	54 OC03E	55 OC03F	56 OC03G	57 OC03H
	75 OC05D	76 OC05E	77 OC05F	78 OC05G	79 OC05H
	86 OC06D	87 OC06E	88 OC06F	89 OC06G	90 OC06H
	12 OB01D	13 OB01E	14 OB01F	15 OB01G	16 OB01H
	67 OB04D	68 OB04E	69 OB04F	70 OB04G	71 OB04H
2 ICORE	04 OC01D	05 OC01E	06 OC01F	07 OC01G	08 OC01H
3 IBLKT	12 OB01D	13 OB01E	14 OB01F	15 OB01G	16 OB01H
4 MCORE	31 OC02D	32 OC02E	33 OC02F	34 OC02G	35 OC02H
	53 OC03D	54 OC03E	55 OC03F	56 OC03G	57 OC03H
5 OCORE	75 OC05D	76 OC05E	77 OC05F	78 OC05G	79 OC05H
	86 OC06D	87 OC06E	88 OC06F	89 OC06G	90 OC06H
6 OBLKT	67 OB04D	68 OB04E	69 OB04F	70 OB04G	71 OB04H

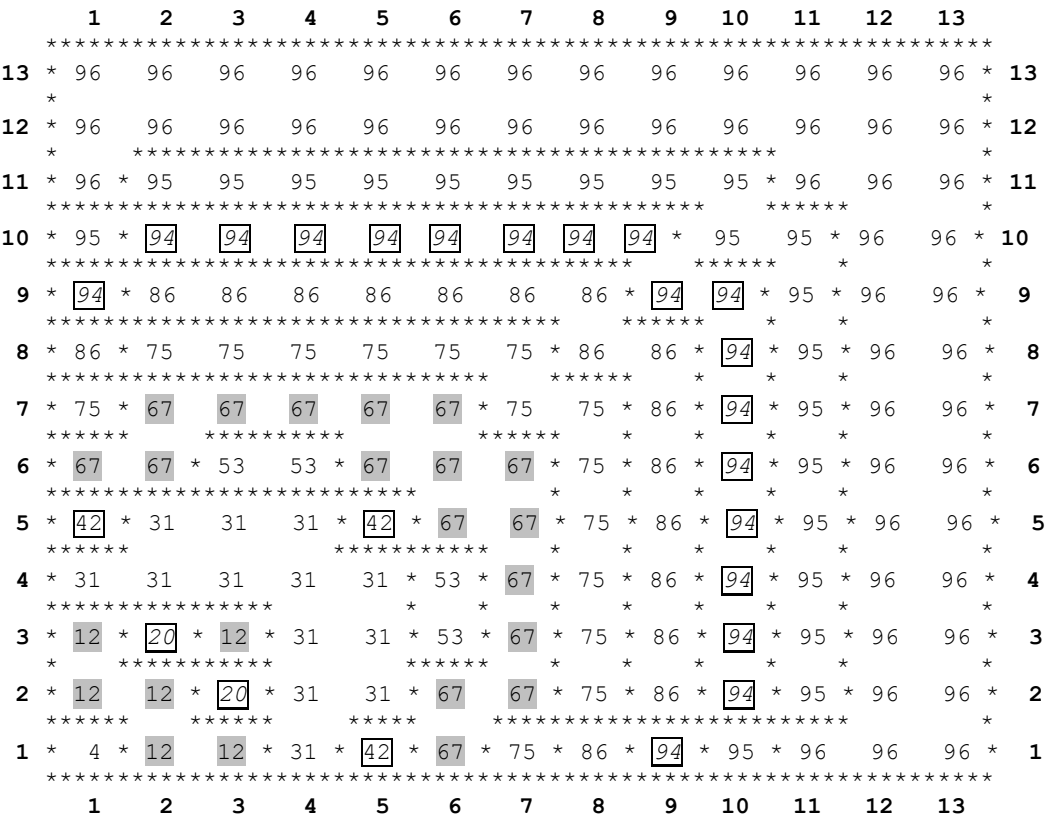

Legend:

Region	Region Identifier
12	OB01 – Inner Core Blanket
67	OB04 – Outer Core Blanket
20	Control Rods
42	Control Rods
94	Steel Shield
9	The Last Fuel Row

Fig. 45. 1/3 Reactor core layout model of the configuration A.

TABLE XXX

List of Region Identifiers and Region Numbers of the Core Configuration A

Reg #	Region Identifier	Zone Volume (cm^3)	Reg #	Region Identifier	Zone Volume (cm^3)
1	OC01A	5.086E+04	49	CR02K	2.283E+04
2	OC01B	2.543E+04	50	OC03A	4.695E+04
3	OC01C	2.474E+04	51	OC03B	2.347E+04
4	OC01D	3.060E+03	52	OC03C	2.283E+04
5	OC01E	3.060E+03	53	OC03D	3.672E+04
6	OC01F	3.060E+03	54	OC03E	3.672E+04
7	OC01G	3.060E+03	55	OC03F	3.672E+04
8	OC01H	3.060E+03	56	OC03G	3.672E+04
9	OC01I	2.474E+04	57	OC03H	3.672E+04
10	OC01J	2.474E+04	58	OC03I	2.283E+04
11	OC01K	4.947E+04	59	OC03J	2.283E+04
12	OB01D	3.672E+04	60	OC03K	4.567E+04
13	OB01E	3.672E+04	61	OC04A	1.878E+05
14	OB01F	3.672E+04	62	OC04B	9.390E+04
15	OB01G	3.672E+04	63	OC04C	9.134E+04
16	OB01H	3.672E+04	64	OC04I	9.134E+04
17	CR01A	2.347E+04	65	OC04J	9.134E+04
18	CR01B	1.174E+04	66	OC04K	1.827E+05
19	CR01C	1.142E+04	67	OB04D	1.469E+05
20	CR01D	1.836E+04	68	OB04E	1.469E+05
21	CR01E	1.836E+04	69	OB04F	1.469E+05
22	CR01F	1.836E+04	70	OB04G	1.469E+05
23	CR01G	1.836E+04	71	OB04H	1.469E+05
24	CR01H	1.836E+04	72	OC05A	1.643E+05
25	CR01I	1.142E+04	73	OC05B	8.216E+04
26	CR01J	1.142E+04	74	OC05C	7.992E+04
27	CR01K	2.283E+04	75	OC05D	1.285E+05
28	OC02A	1.408E+05	76	OC05E	1.285E+05
29	OC02B	7.042E+04	77	OC05F	1.285E+05
30	OC02C	6.850E+04	78	OC05G	1.285E+05
31	OC02D	1.102E+05	79	OC05H	1.285E+05
32	OC02E	1.102E+05	80	OC05I	7.992E+04
33	OC02F	1.102E+05	81	OC05J	7.992E+04
34	OC02G	1.102E+05	82	OC05K	1.598E+05
35	OC02H	1.102E+05	83	OC06A	1.878E+05
36	OC02I	6.850E+04	84	OC06B	9.390E+04
37	OC02J	6.850E+04	85	OC06C	9.134E+04
38	OC02K	1.370E+05	86	OC06D	1.469E+05
39	CR02A	2.347E+04	87	OC06E	1.469E+05
40	CR02B	1.174E+04	88	OC06F	1.469E+05
41	CR02C	1.142E+04	89	OC06G	1.469E+05
42	CR02D	1.836E+04	90	OC06H	1.469E+05
43	CR02E	1.836E+04	91	OC06I	9.134E+04
44	CR02F	1.836E+04	92	OC06J	9.134E+04
45	CR02G	1.836E+04	93	OC06K	1.827E+05
46	CR02H	1.836E+04	94	RR01	1.657E+06
47	CR02I	1.142E+04	95	RR02	1.841E+06
48	CR02J	1.142E+04	96	RR03	4.418E+06

TABLE XXXI

Fuel Regions of the Core Configuration B

Area	Region #, Region Identifier				
1 TCORE	04 OC01D	05 OC01E	06 OC01F	07 OC01G	08 OC01H
	31 OC02D	32 OC02E	33 OC02F	34 OC02G	35 OC02H
	53 OC03D	54 OC03E	55 OC03F	56 OC03G	57 OC03H
	75 OC05D	76 OC05E	77 OC05F	78 OC05G	79 OC05H
	86 OC06D	87 OC06E	88 OC06F	89 OC06G	90 OC06H
	12 OB01D	13 OB01E	14 OB01F	15 OB01G	16 OB01H
	67 OB04D	68 OB04E	69 OB04F	70 OB04G	71 OB04H
	94 OB06D	95 OB06E	96 OB06F	97 OB06G	98 OB06H
2 ICORE	04 OC01D	05 OC01E	06 OC01F	07 OC01G	08 OC01H
3 IBLKT	12 OB01D	13 OB01E	14 OB01F	15 OB01G	16 OB01H
4 MCORE	31 OC02D	32 OC02E	33 OC02F	34 OC02G	35 OC02H
	53 OC03D	54 OC03E	55 OC03F	56 OC03G	57 OC03H
5 OCORE	75 OC05D	76 OC05E	77 OC05F	78 OC05G	79 OC05H
	86 OC06D	87 OC06E	88 OC06F	89 OC06G	90 OC06H
6 OBLKT	67 OB04D	68 OB04E	69 OB04F	70 OB04G	71 OB04H
	94 OB06D	95 OB06E	96 OB06F	97 OB06G	98 OB06H

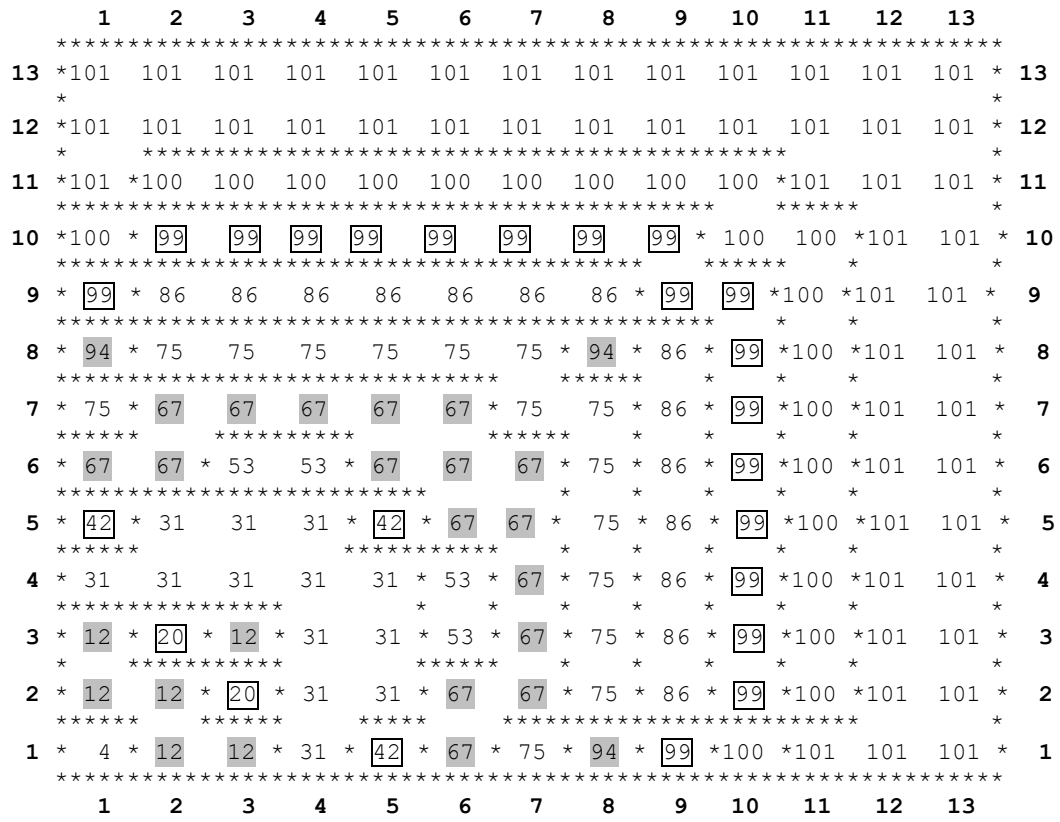

Legend:

Region	Region Identifier
12	OB01 – Inner Core Blanket
67	OB04 – Outer Core Blanket
94	OB06 – Outer Core Blanket
20	Control Rods
42	Control Rods
99	Steel Shield
9	The Last Fuel Row

Fig. 46. 1/3 Reactor core layout model of the configuration B.

TABLE XXXII

List of Region Identifiers and Region Numbers of the Core Configuration B

Reg #	Region Identifier	Zone Volume (cm^3)	Reg #	Region Identifier	Zone Volume (cm^3)
1	OC01A	5.086E+04	52	OC03C	2.283E+04
2	OC01B	2.543E+04	53	OC03D	3.672E+04
3	OC01C	2.474E+04	54	OC03E	3.672E+04
4	OC01D	3.060E+03	55	OC03F	3.672E+04
5	OC01E	3.060E+03	56	OC03G	3.672E+04
6	OC01F	3.060E+03	57	OC03H	3.672E+04
7	OC01G	3.060E+03	58	OC03I	2.283E+04
8	OC01H	3.060E+03	59	OC03J	2.283E+04
9	OC01I	2.474E+04	60	OC03K	4.567E+04
10	OC01J	2.474E+04	61	OC04A	1.878E+05
11	OC01K	4.947E+04	62	OC04B	9.390E+04
12	OB01D	3.672E+04	63	OC04C	9.134E+04
13	OB01E	3.672E+04	64	OC04I	9.134E+04
14	OB01F	3.672E+04	65	OC04J	9.134E+04
15	OB01G	3.672E+04	66	OC04K	1.827E+05
16	OB01H	3.672E+04	67	OB04D	1.469E+05
17	CR01A	2.347E+04	68	OB04E	1.469E+05
18	CR01B	1.174E+04	69	OB04F	1.469E+05
19	CR01C	1.142E+04	70	OB04G	1.469E+05
20	CR01D	1.836E+04	71	OB04H	1.469E+05
21	CR01E	1.836E+04	72	OC05A	1.643E+05
22	CR01F	1.836E+04	73	OC05B	8.216E+04
23	CR01G	1.836E+04	74	OC05C	7.992E+04
24	CR01H	1.836E+04	75	OC05D	1.285E+05
25	CR01I	1.142E+04	76	OC05E	1.285E+05
26	CR01J	1.142E+04	77	OC05F	1.285E+05
27	CR01K	2.283E+04	78	OC05G	1.285E+05
28	OC02A	1.408E+05	79	OC05H	1.285E+05
29	OC02B	7.042E+04	80	OC05I	7.992E+04
30	OC02C	6.850E+04	81	OC05J	7.992E+04
31	OC02D	1.102E+05	82	OC05K	1.598E+05
32	OC02E	1.102E+05	83	OC06A	1.878E+05
33	OC02F	1.102E+05	84	OC06B	9.390E+04
34	OC02G	1.102E+05	85	OC06C	9.134E+04
35	OC02H	1.102E+05	86	OC06D	1.285E+05
36	OC02I	6.850E+04	87	OC06E	1.285E+05
37	OC02J	6.850E+04	88	OC06F	1.285E+05
38	OC02K	1.370E+05	89	OC06G	1.285E+05
39	CR02A	2.347E+04	90	OC06H	1.285E+05
40	CR02B	1.174E+04	91	OC06I	9.134E+04
41	CR02C	1.142E+04	92	OC06J	9.134E+04
42	CR02D	1.836E+04	93	OC06K	1.827E+05
43	CR02E	1.836E+04	94	OB06D	1.836E+04
44	CR02F	1.836E+04	95	OB06E	1.836E+04
45	CR02G	1.836E+04	96	OB06F	1.836E+04
46	CR02H	1.836E+04	97	OB06G	1.836E+04
47	CR02I	1.142E+04	98	OB06H	1.836E+04
48	CR02J	1.142E+04	99	RR01	1.657E+06
49	CR02K	2.283E+04	100	RR02	1.841E+06
50	OC03A	4.695E+04	101	RR03	4.418E+06
51	OC03B	2.347E+04			

APPENDIX B

AUXILIARY TOOLS FOR ALM-FR ANALYSIS

PROGRAM card14_dopp
(Modification of nuclide identifiers and atomic densities to prepare input segments for use as part of the REBUS input for Doppler reactivity coefficients calculations)

```
      INTEGER CARD,K, METKA, ZADACHA, LASTLINE
      CHARACTER*5 ZONE
      CHARACTER*4 IST11, IST21, IST31, NOTCHANGE(5)
      CHARACTER*1 IST12, IST22, IST32, TMP12, TMP22, TMP32
      CHARACTER*1 IST13, IST23, IST33, TMP13, TMP23, TMP33
      CHARACTER*1 CORE
      CHARACTER*17 OUT
      REAL ATDENS1, ATDENS2, ATDENS3
      METKA=1
      ZADACHA=2
      LASTLINE=189
C     FOR eq1 LASTLINE=189
C     FOR others eq LASTLINE=419
C     METKA=1   FOR DOPPLER ICORE
C     METKA=2   FOR DOPPLER MCORE
C     METKA=3   FOR DOPPLER OCORE
C     METKA=4   FOR DOPPLER BLANKET
C     METKA=5   FOR DOPPLER WHOLE DRIVER CORE
C     METKA=6   FOR DOPPLER WHOLE CORE
C     ZADACHA=2    DO ALL 6 CALCULATIONS AND PUT INTO OUT1, OUT2,
      OUT3...
      NOTCHANGE(1)='B-10'
      NOTCHANGE(2)='B-11'
      NOTCHANGE(3)='C-12'
      NOTCHANGE(4)='N-15'
      NOTCHANGE(5)='PBPB'
      IF (ZADACHA.EQ.2) METKA=1
13    CONTINUE
      IF (METKA.EQ.1) THEN
        CORE='I'
        OUT='anip14.eq1_DDI'
      END IF
      IF (METKA.EQ.2) THEN
            CORE='M'
            OUT='anip14.eq1_DDM'
      END IF
      IF (METKA.EQ.3) THEN
            CORE='O'
            OUT='anip14.eq1_DDO'
      END IF
      IF (METKA.EQ.4) THEN
            CORE='B'
            OUT='anip14.eq1_DB'
```

```
      END IF
      IF (METKA.EQ.5) OUT='anip14.eq1_DDIOM'
      IF (METKA.EQ.6) OUT='anip14.eq1_DDBIOM'
!     CREATE CARD TYPE 14S FOR SELECTIVE SUFFIX MODIFICATION
      OPEN (UNIT=2, FILE='input', STATUS='OLD')
      OPEN (UNIT=3, FILE=OUT, STATUS='NEW')
      K=1
      DO K=1, LASTLINE
      READ (2,2) CARD,ZONE,IST11,IST12,IST13,ATDENS1,IST21,IST22,
     1      IST23,ATDENS2,IST31,IST32,IST33,ATDENS3
       IF (CARD.NE.14) GO TO 15
       TMP12=IST12
       TMP22=IST22
       TMP32=IST32
       TMP13=IST13
       TMP23=IST23
       TMP33=IST33
      IF (METKA.LT.5) THEN
      IF (IST12.EQ.CORE) IST13='T'
        IF (IST22.EQ.CORE) IST23='T'
        IF (IST32.EQ.CORE) IST33='T'
        GO TO 14
      END IF
       IF (METKA.EQ.5) THEN
      IF (IST12.EQ.'I') IST13='T'
         IF (IST22.EQ.'I') IST23='T'
         IF (IST32.EQ.'I') IST33='T'
      IF (IST12.EQ.'M') IST13='T'
         IF (IST22.EQ.'M') IST23='T'
         IF (IST32.EQ.'M') IST33='T'
         IF (IST12.EQ.'O') IST13='T'
         IF (IST22.EQ.'O') IST23='T'
         IF (IST32.EQ.'O') IST33='T'
       END IF
      IF (METKA.EQ.6) THEN
      IF (IST12.EQ.'I') IST13='T'
      IF (IST22.EQ.'I') IST23='T'
      IF (IST32.EQ.'I') IST33='T'
      IF (IST12.EQ.'M') IST13='T'
      IF (IST22.EQ.'M') IST23='T'
      IF (IST32.EQ.'M') IST33='T'
      IF (IST12.EQ.'O') IST13='T'
      IF (IST22.EQ.'O') IST23='T'
      IF (IST32.EQ.'O') IST33='T'
      IF (IST12.EQ.'O') IST13='T'
      IF (IST12.EQ.'B') IST13='T'
      IF (IST22.EQ.'B') IST23='T'
      IF (IST32.EQ.'B') IST33='T'
      END IF
14    CONTINUE
      DO I=1, 5
        IF (IST11.EQ.NOTCHANGE(I)) THEN
              IST12=TMP12
              IST13=TMP13
```

```
          END IF
          IF (IST21.EQ.NOTCHANGE(I)) IST23=TMP23
          IF (IST31.EQ.NOTCHANGE(I)) IST33=TMP33
        END DO
11      CONTINUE
         IF (ATDENS2.NE.0.0) GO TO 3
         IF (ATDENS3.NE.0.0) GO TO 3
        WRITE(3,2) CARD,ZONE,IST11,IST12,IST13,ATDENS1
         GO TO 4
3       WRITE(3,2) CARD,ZONE,IST11,IST12,IST13,ATDENS1,IST21,IST22,IST23,
   3          ATDENS2,IST31,IST32,IST33,ATDENS3
4       CONTINUE
2        FORMAT (I2,10X,A5,1X,A4,A1,A1,1X,ES11.5,2(A4,A1,A1,1X,ES11.5))
15      CONTINUE
        END DO
        CLOSE (UNIT=2)
        CLOSE (UNIT=3)
        IF (ZADACHA.EQ.1) GO TO 12
        IF (METKA.LT.6) THEN
          METKA=METKA+1
          GO TO 13
        END IF
12      CONTINUE
        STOP
        END
```

PROGRAM card14_Faex
(Modification of nuclide identifiers and atomic densities to prepare input segments for use as part of the REBUS input for core radial expansion and fuel axial expansion reactivity coefficients calculations)

```
        INTEGER CARD,K, METKA, ZADACHA, LASTLINE
        CHARACTER*5 ZONE, RR(2)
        CHARACTER*4 IST11, IST21, IST31, CROD(4), CLAD(2)
        CHARACTER*1 IST12, IST22, IST32
        CHARACTER*1 IST13, IST23, IST33
        CHARACTER*1 CORE
        CHARACTER*16 OUT
        REAL ATDENS1, ATDENS2, ATDENS3, REXPAN, AEXPAN
        REAL TMP1, TMP2, TMP3
        METKA=2
        ZADACHA=1
        LASTLINE=469
        REXPAN=1/(1.01*1.01)
        AEXPAN=1/(1.01)
C       METKA=1   FOR CORE RADIAL EXPANSION WHOLE CORE
C       METKA=2   FOR FUEL AXIAL EXPANSION WHOLE CORE
C       METKA=3   FOR FUEL AND CLADDING EXPANSION WHOLE CORE
C       ZADACHA=2  DO ALL 3 CALCULATIONS AND PUT INTO OUT1, OUT2, OUT3
        CROD(1)='PBPB'
```

```
      CROD(2)='B-10'
      CROD(3)='B-11'
      CROD(4)='C-12'
      RR(1)='RR01 '
      RR(2)='RR02 '
      CLAD(1)='CSIC'
      CLAD(2)='SISI'
!     CREATE CARD TYPE 14S FOR SELECTIVE SUFFIX MODIFICATION
      IF (ZADACHA.EQ.2) METKA=1
13    CONTINUE
      IF (METKA.EQ.1) OUT='anip14.eq4_Crex'
      IF (METKA.EQ.2) OUT='anip14.eq4_Faex'
      IF (METKA.EQ.3) OUT='anip14.eq4_FCaex'
      OPEN (UNIT=2, FILE='input', STATUS='OLD')
      OPEN (UNIT=3, FILE=OUT, STATUS='NEW')
      DO K=1, LASTLINE
      READ (2,2) CARD,ZONE,IST11,IST12,IST13,ATDENS1,IST21,IST22,
     1      IST23,ATDENS2,IST31,IST32,IST33,ATDENS3
      TMP1=ATDENS1
      TMP2=ATDENS2
      TMP3=ATDENS3
      IF (METKA.EQ.1) THEN
C     CORE RADIAL EXPANSION
      DO I=1, 2
      IF (ZONE.EQ.RR(I)) GO TO 11
      END DO
      ATDENS1=ATDENS1*REXPAN
      ATDENS2=ATDENS2*REXPAN
      ATDENS3=ATDENS3*REXPAN
      DO I=1, 4
            IF (IST11.EQ.CROD(I)) ATDENS1=TMP1
            IF (IST21.EQ.CROD(I)) ATDENS2=TMP2
            IF (IST31.EQ.CROD(I)) ATDENS3=TMP3
      END DO
      GO TO 11
      END IF
      IF (METKA.EQ.2) THEN
C     FUEL AXIAL EXPANSION
        DO I=1, 2
        IF (ZONE.EQ.RR(I)) GO TO 11
        END DO
      ATDENS1=ATDENS1*AEXPAN
        ATDENS2=ATDENS2*AEXPAN
        ATDENS3=ATDENS3*AEXPAN
        DO I=1, 4
          IF (IST11.EQ.CROD(I)) ATDENS1=TMP1
          IF (IST21.EQ.CROD(I)) ATDENS2=TMP2
          IF (IST31.EQ.CROD(I)) ATDENS3=TMP3
        END DO
      DO I=1, 2
      IF (IST11.EQ.CLAD(I)) ATDENS1=TMP1
      IF (IST21.EQ.CLAD(I)) ATDENS2=TMP2
      IF (IST31.EQ.CLAD(I)) ATDENS3=TMP3
      END DO
```

```
      END IF
      IF (METKA.EQ.3) THEN
C     FUEL AXIAL EXPANSION WITH CLADDING
      DO I=1, 2
      IF (ZONE.EQ.RR(I)) GO TO 11
      END DO
      ATDENS1=ATDENS1*AEXPAN
      ATDENS2=ATDENS2*AEXPAN
      ATDENS3=ATDENS3*AEXPAN
      DO I=1, 4
            IF (IST11.EQ.CROD(I)) ATDENS1=TMP1
            IF (IST21.EQ.CROD(I)) ATDENS2=TMP2
            IF (IST31.EQ.CROD(I)) ATDENS3=TMP3
      END DO
      END IF
 11   CONTINUE
      IF (ATDENS2.NE.0.0) GO TO 3
      IF (ATDENS3.NE.0.0) GO TO 3
      WRITE(3,2) CARD,ZONE,IST11,IST12,IST13,ATDENS1
      GO TO 4
3     WRITE(3,2) CARD,ZONE,IST11,IST12,IST13,ATDENS1,IST21,IST22,IST23,
   3        ATDENS2,IST31,IST32,IST33,ATDENS3
4     CONTINUE
2     FORMAT (I2,10X,A5,1X,A4,A1,A1,1X,ES11.5,2(A4,A1,A1,1X,ES11.5))
      END DO
      CLOSE (UNIT=2)
      CLOSE (UNIT=3)
      IF (ZADACHA.EQ.1) GO TO 12
      IF (METKA.LT.3) THEN
      METKA=METKA+1
      GO TO 13
      END IF
12    CONTINUE
      STOP
      END
```

PROGRAM card14_Void
(Modification of nuclide identifiers and atomic densities to prepare input segments for use as part of the REBUS input for void reactivity coefficients calculations)

```
    INTEGER CARD,K, METKA, ZADACHA, LASTLINE
      CHARACTER*5 ZONE, ICORE(5), MCORE(10), OCORE(10), IBLNK(5),
OBLNK(5)
      CHARACTER*5 TDRIV(25), TCORE(35)
      CHARACTER*4 IST11, IST21, IST31
      CHARACTER*1 IST12, IST22, IST32
      CHARACTER*1 IST13, IST23, IST33
      CHARACTER*1 CORE
      CHARACTER*17 OUT
      REAL ATDENS1, ATDENS2, ATDENS3, VOID
      METKA=6
```

```
      ZADACHA=2
      LASTLINE=469
c     LASTLINE=199
      VOID=8.21268E-1
C     METKA=1    FOR VOID ICORE
C     METKA=2    FOR VOID MCORE
C     METKA=3    FOR VOID OCORE
C     METKA=4    FOR VOID BLANKET
C     METKA=5    FOR VOID WHOLE DRIVER CORE
C     METKA=6    FOR VOID WHOLE CORE
C     ZADACHA=2   DO ALL 6 CALCULATIONS AND PUT INTO OUT1, OUT2, OUT3
C     LASTLINE=1 FOR eq1=199, =419 for others
            ICORE(1)='OC01D'
            ICORE(2)='OC01E'
            ICORE(3)='OC01F'
            ICORE(4)='OC01G'
            ICORE(5)='OC01H'
            MCORE(1)='OC02D'
            MCORE(2)='OC02E'
            MCORE(3)='OC02F'
            MCORE(4)='OC02G'
            MCORE(5)='OC02H'
            MCORE(6)='OC03D'
            MCORE(7)='OC03E'
            MCORE(8)='OC03F'
            MCORE(9)='OC03G'
            MCORE(10)='OC03H'
            OCORE(1)='OC05D'
            OCORE(2)='OC05E'
            OCORE(3)='OC05F'
            OCORE(4)='OC05G'
            OCORE(5)='OC05H'
            OCORE(6)='OC06D'
            OCORE(7)='OC06E'
            OCORE(8)='OC06F'
            OCORE(9)='OC06G'
            OCORE(10)='OC06H'
            IBLNK(1)='OB01D'
            IBLNK(2)='OB01E'
            IBLNK(3)='OB01F'
            IBLNK(4)='OB01G'
            IBLNK(5)='OB01H'
            OBLNK(1)='OB04D'
            OBLNK(2)='OB04E'
            OBLNK(3)='OB04F'
            OBLNK(4)='OB04G'
            OBLNK(5)='OB04H'
            DO I=1,5
             TDRIV(I)=ICORE(I)
            END DO
            DO I=1,10
             TDRIV(I+5)=MCORE(I)
            END DO
            DO I=1, 10
```

```
                TDRIV(I+15)=OCORE(I)
               END DO
               DO I=1,5
                TCORE(I)=ICORE(I)
               END DO
               DO I=1,10
                TCORE(I+5)=MCORE(I)
               END DO
               DO I=1, 10
                TCORE(I+15)=OCORE(I)
               END DO
               DO I=1, 5
               TCORE(I+25)=IBLNK(I)
               END DO
               DO I=1, 5
               TCORE(I+10)=OBLNK(I)
               END DO
      IF (ZADACHA.EQ.2) METKA=1
13    CONTINUE
      IF (METKA.EQ.1) THEN
               CORE='I'
               OUT='anip14.eq4_VDI'
      END IF
      IF (METKA.EQ.2) THEN
               CORE='M'
               OUT='anip14.eq4_VDM'
      END IF
      IF (METKA.EQ.3) THEN
               CORE='O'
               OUT='anip14.eq4_VDO'
      END IF
      IF (METKA.EQ.4) THEN
               CORE='B'
               OUT='anip14.eq4_VB'
      END IF
      IF (METKA.EQ.5) THEN
               CORE='D'
               OUT='anip14.eq4_VDIMO'
      END IF
      IF (METKA.EQ.6) THEN
               CORE='T'
               OUT='anip14.eq4_VDBIMO'
      END IF
!     CREATE CARD TYPE 14S FOR SELECTED SUFFIX MODIFICATION
      OPEN (UNIT=2, FILE='input', STATUS='OLD')
      OPEN (UNIT=3, FILE=OUT, STATUS='NEW')
      DO K=1, LASTLINE
      READ (2,2) CARD,ZONE,IST11,IST12,IST13,ATDENS1,IST21,IST22,
     1      IST23,ATDENS2,IST31,IST32,IST33,ATDENS3
      IF (METKA.EQ.1) THEN
        DO I=1, 5
      IF (ZONE.EQ.ICORE(I)) THEN
               IF (IST11.EQ.'PBPB') THEN
               ATDENS1=ATDENS1*VOID
```

```
END IF
IF (IST21.EQ.'PBPB') THEN
          ATDENS2=ATDENS2*VOID
          END IF
          IF (IST31.EQ.'PBPB') THEN
          ATDENS3=ATDENS3*VOID
          END IF
END IF
END DO
GO TO 11
END IF
IF (METKA.EQ.2) THEN
DO I=1, 10
IF (ZONE.EQ.MCORE(I)) THEN
IF (IST11.EQ.'PBPB') ATDENS1=ATDENS1*VOID
IF (IST21.EQ.'PBPB') ATDENS2=ATDENS2*VOID
IF (IST31.EQ.'PBPB') ATDENS3=ATDENS3*VOID
END IF
END DO
GO TO 11
END IF
IF (METKA.EQ.3) THEN
DO I=1, 10
IF (ZONE.EQ.OCORE(I)) THEN
IF (IST11.EQ.'PBPB') ATDENS1=ATDENS1*VOID
IF (IST21.EQ.'PBPB') ATDENS2=ATDENS2*VOID
IF (IST31.EQ.'PBPB') ATDENS3=ATDENS3*VOID
END IF
END DO
GO TO 11
END IF
IF (METKA.EQ.4) THEN
DO I=1, 5
IF (ZONE.EQ.IBLNK(I)) THEN
           IF (IST11.EQ.'PBPB') ATDENS1=ATDENS1*VOID
           IF (IST21.EQ.'PBPB') ATDENS2=ATDENS2*VOID
           IF (IST31.EQ.'PBPB') ATDENS3=ATDENS3*VOID
          END IF
          IF (ZONE.EQ.OBLNK(I)) THEN
           IF (IST11.EQ.'PBPB') ATDENS1=ATDENS1*VOID
           IF (IST21.EQ.'PBPB') ATDENS2=ATDENS2*VOID
           IF (IST31.EQ.'PBPB') ATDENS3=ATDENS3*VOID
END IF
END DO
GO TO 11
END IF
IF (METKA.EQ.5) THEN
DO I=1, 25
IF (ZONE.EQ.TDRIV(I)) THEN
           IF (IST11.EQ.'PBPB') ATDENS1=ATDENS1*VOID
           IF (IST21.EQ.'PBPB') ATDENS2=ATDENS2*VOID
           IF (IST31.EQ.'PBPB') ATDENS3=ATDENS3*VOID
END IF
END DO
```

```
            GO TO 11
            END IF
            IF (METKA.EQ.6) THEN
            DO I=1, 35
            IF (ZONE.EQ.TCORE(I)) THEN
                  IF (IST11.EQ.'PBPB') ATDENS1=ATDENS1*VOID
                  IF (IST21.EQ.'PBPB') ATDENS2=ATDENS2*VOID
                  IF (IST31.EQ.'PBPB') ATDENS3=ATDENS3*VOID
            END IF
            END DO
            GO TO 11
            END IF
11          CONTINUE
             IF (ATDENS2.NE.0.0) GO TO 3
             IF (ATDENS3.NE.0.0) GO TO 3
            WRITE(3,2) CARD,ZONE,IST11,IST12,IST13,ATDENS1
            GO TO 4
3           WRITE(3,2) CARD,ZONE,IST11,IST12,IST13,ATDENS1,IST21,IST22,IST23,
     3      ATDENS2,IST31,IST32,IST33,ATDENS3
4           CONTINUE
2           FORMAT (I2,10X,A5,1X,A4,A1,A1,1X,ES11.5,2(A4,A1,A1,1X,ES11.5))
            END DO
            CLOSE (UNIT=2)
            CLOSE (UNIT=3)
            IF (ZADACHA.EQ.1) GO TO 12
            IF (METKA.LT.6) THEN
            METKA=METKA+1
            GO TO 13
            END IF
12          CONTINUE
            STOP
            END
```

The given samples of the computer codes do not represent the complete input file set that is required for execution of the REBUS-3 computer code system. The actual input files are not provided because of the excessive file size.

VITA

Galina Valeryevna Tsvetkova
Dept. of Nuclear Engineering, Texas A&M University, College Station, TX 77843-3133
E-mail: tgalina@cedar.tamu.edu

Education

Ph.D. in Nuclear Engineering, Texas A&M University, December 2003

Dipl. in Molecular Physics and Physics of Kinetic Phenomena, Moscow State Engineering Physics Institute, Moscow, Russia, March 1995

Experience

Research Assistant, Department of Nuclear Engineering, Texas A&M University, College Station, TX (9/99 – present)

Scientific Researcher, Laboratory of Biophysical Fundamentals of Pathology, Pirogue Scientific Research Institute of Physics and Chemical Medicine Department, Interfaculty Reactor Institute, Moscow, Russia (9/95 – 1/97)

Research Assistant, Molecular Physics Department, Moscow State Engineering Physics Institute, Moscow, Russia (3/95 – 09/96)

Publications

G. V. Tsvetkova, W. S. Yang, D. C. Wade, K. L. Peddicord, "Reactor Physics Feasibility Analysis of Long-Lived STAR-H2 System", *Trans. Am. Nuc. Soc.,* **88**, 685 (2003).

D. C. Wade, K.L. Peddicord, M.H. Mendelsohn, A.V. Moisseytcev, J. Ruge, R.Doctor, L.Leibowitz, S.McDeavitt, S.Reynaud, J.Sienicki, G. V. Tsvetkova, W.S.Yang, "STAR-H2: A 400 MWth Lead-Cooled, Long Refueling Interval Reactor for Hydrogen Production". *Proc. 11th Intern. Conf. on Nucl. Eng. (ICONE 11),* Tokyi, JAPAN, April 20-23, 2003, ASME, Fairfield, New Jersey (2003)

G. V. Tsvetkova, K. L. Peddicord, "Utilization of Plutonium and Higher Actinides in the HTGR as Possibility to Maintain Long-Term Operation on One Fuel Loading". *Proc. 10th Intern. Conf. on Nucl. Eng. (ICONE 10),* Arlington, Virginia, April 14 - 18, 2002, ICONE10-22089, ASME, Fairfield, New Jersey (2002).

G. V. Tsvetkova, K. L. Peddicord, D. R. Liles, T. D. Knight, and J. P. Nelson, "Concept Analysis of a Modular 50 MW(Th), Pebble Bed High-Temperature Gas-Cooled Reactor for Process Heat", Los Alamos National Laboratory, LA-UR-01-5161, USA, (2001).

G. V. Tsvetkova, K. L. Peddicord, "A Long-Term Energy Source Based on an HTGR Concept". *Trans. Am. Nuc Soc.,* **84,** 115 (2001).

Honors and Awards

American Nuclear Society, Graduate Scholarship Award, 2003

2st Place, Physical Sciences, Grad., TAMU Student Research Week, 2002

American Nuclear Society, John and Muriel Landis Scholarship Award, 2001

TAMU, Dwight Look College of Eng., Willson Grad. Fellowship, 1999 – 2000